

# **From metagenomes to green algae – The biochemical variety of bilin biosynthesis enzymes**

vom Fachbereich Biologie der Universität Kaiserslautern  
zur Verleihung des akademischen Grades „Doktor der  
Naturwissenschaften“ genehmigte Dissertation

angefertigt im

**Fachbereich Biologie**

Abteilung Mikrobiologie

Wissenschaftliche Aussprache: Kaiserslautern, 26.01.2018

vorgelegt von

**Benjamin Ledermann**

**Referent:** Prof. Dr. Nicole Frankenberg-Dinkel  
**Korreferent:** Prof. Dr. Johannes Herrmann  
**Vorsitz:** Prof. Dr. Ekkehard Neuhaus

Kaiserslautern, 2018 – D 386

---

# Table of contents

<b>Table of contents</b> .....	<b>I</b>
<b>Abbreviations</b> .....	<b>V</b>
<b>1 Introduction</b> .....	<b>1</b>
1.1 The importance of tetrapyrroles in nature .....	1
1.2 The biosynthesis of bilins.....	1
1.2.1 The enzyme class of heme oxygenases .....	2
1.2.2 The enzyme class of ferredoxin-dependent bilin reductases.....	4
1.2.3 The structure of the ferredoxin-dependent bilin reductases.....	10
1.2.4 The reaction mechanisms of the FDBRs.....	11
1.3 The physiological functions of bilins .....	13
1.3.1 Light-harvesting .....	13
1.3.2 Light-sensing .....	15
1.4 Marine phages - Key players in aquatic ecosystems.....	17
1.4.1 Impact on the nutrient cycling and on the diversity.....	18
1.4.2 Auxiliary metabolic genes in marine phages .....	18
1.5 Marine metagenomes as a source for new enzymes .....	20
1.6 The discovery of new bilin biosynthesis enzymes .....	21
1.7 Objectives of this work.....	23
<b>2 Material and Methods</b> .....	<b>24</b>
2.1 Material and chemicals .....	24
2.1.1 Equipment .....	24
2.1.2 Special chemicals, material, enzymes, kits and antibodies .....	25
2.1.3 Bacterial strains .....	26
2.1.4 Plasmids.....	26
2.1.5 Oligonucleotides .....	28

---

2.2	Microbiological methods .....	29
2.2.1	Culture media and supplements .....	29
2.2.2	Storage of <i>E. coli</i> cells .....	30
2.2.3	Cultivation of <i>E. coli</i> cells .....	30
2.2.4	Determination of cell densities .....	30
2.2.5	Preparation of chemically competent <i>E. coli</i> cells .....	30
2.2.6	Transformation of chemically competent <i>E. coli</i> cells .....	31
2.3	Molecular biological techniques .....	31
2.3.1	Preparation of plasmid DNA .....	31
2.3.2	Determination of the concentration of DNA in aqueous solution .....	31
2.3.3	Agarose gel electrophoresis .....	31
2.3.4	Polymerase chain reaction.....	32
2.3.5	Purification of PCR products.....	32
2.3.6	Restriction of DNA .....	33
2.3.7	Gel extraction of DNA fragments .....	33
2.3.8	Ligation of DNA fragments.....	33
2.3.9	Construction of expression vectors .....	33
2.3.10	DNA sequence analysis.....	34
2.3.11	Site-directed mutagenesis .....	34
2.4	Protein biochemical and biophysical methods.....	34
2.4.1	Production of recombinant proteins in <i>E. coli</i> .....	34
2.4.2	Protein purification .....	35
2.4.3	SDS-polyacrylamide gel electrophoresis.....	37
2.4.4	Immuno-staining of immobilized proteins (Western Blot) .....	39
2.4.5	Determination of protein and bilin concentrations .....	40
2.4.6	Size exclusion chromatography .....	41
2.4.7	Heme oxygenase activity assays .....	41
2.4.8	Anaerobic FDBR activity assay.....	42
2.4.9	HPLC analyses.....	43
2.4.10	Coupled phytochrome assembly assay.....	44

---

2.4.11	Freeze-quench EPR experiments .....	45
2.4.12	Crystallization and X-ray crystallography .....	45
<b>3</b>	<b>Results.....</b>	<b>49</b>
3.1	Characterization of $\Phi$ HemO.....	49
3.1.1	$\Phi$ HemO catalyzes the reaction of heme to BV IX $\alpha$ .....	49
3.2	Characterization of the PcyX-family .....	51
3.2.1	Determination of the oligomeric state.....	51
3.2.2	Analysis of the $\Phi$ PcyX-activity .....	53
3.2.3	The reaction proceeds via a substrate radical.....	54
3.2.4	The reaction rate is highly dependent on the redox partner .....	55
3.2.5	Several side products occur under the chosen assay conditions .....	56
3.2.6	The molecular structure of $\Phi$ PcyX .....	59
3.2.7	Insights into the $\Phi$ PcyX reaction mechanism.....	64
3.2.8	Biochemical characterization of PcyX_actino and PcyA_Brady .....	69
3.3	Characterization of KflaHY2.....	72
3.3.1	Determination of the oligomerization state .....	73
3.3.2	KflaHY2 catalyzes the reduction of BV to PCB .....	74
3.3.3	Insights into the KflaHY2 reaction mechanism .....	75
<b>4</b>	<b>Discussion.....</b>	<b>79</b>
4.1	Characterization of the novel bilin biosynthesis enzymes.....	79
4.1.1	$\Phi$ HemO - A “classic” heme oxygenase .....	79
4.1.2	$\Phi$ PcyX - An enzyme with an unexpected activity .....	79
4.1.3	Comparison of essential, conserved amino acid residues.....	80
4.2	The biological function of $\Phi$ PcyX .....	86
4.3	KflaHY2 - A new type of HY2 enzyme.....	89
4.3.1	KflaHY2 – An enzyme with two pathways .....	91
<b>5</b>	<b>Summary.....</b>	<b>94</b>
<b>6</b>	<b>Zusammenfassung.....</b>	<b>95</b>
	<b>References .....</b>	<b>VII</b>

---

<b>Appendix .....</b>	<b>XXIV</b>
<b>Danksagung .....</b>	<b>XXVII</b>
<b>Curriculum Vitae .....</b>	<b>XXVIII</b>
<b>Eidesstattliche Erklärung .....</b>	<b>XXX</b>

---

## Abbreviations

Units of the International System of Units (SI) are not listed separately. The single letter or three-letter code is used for designation of amino acids. The single-letter code is used for designation of nucleic acids.

AMGs	auxiliary metabolic genes
APC	allophycocyanin
APS	ammonium persulfate
AU	absorbance units
BCIP	5-Bromo-4-chloro-3-indolyl phosphate
Bph	bacterial phytochrome
BR	bilirubin
BV	biliverdin
CBCR	cyanobacteriochrome
Chl	chlorophyll
Cph	cyanobacterial phytochrome
CV	column volume
DHBV	dihydrobiliverdin
DMF	dimethylformamide
EPR	electron paramagnetic resonance
Fd	ferredoxin
FDBR	ferredoxin-dependent bilin reductases
Fph	fungal phytochrome
FPLC	fast protein liquid chromatography
GAF	cGMP-specific phosphodiesterases, adenylyl cyclases and FhIA
GOS	Global Ocean Sampling Expedition
HK	histidine kinase
HO	heme oxygenase
HPLC	high performance liquid chromatography
LB	Lysogeny Broth
MW	molecular weight
MWCO	molecular weight cut off
NBT	nitro blue tetrazolium chloride
NRS	NADPH regenerating system
OD <sub>578nm</sub>	optical density at 578 nm
PΦB	phytochromobilin
PAS	Per-ARNT-Sim

---

PBP	phycobiliproteins
PC	phycocyanin
PCB	phycocyanobilin)
PCR	polymerase chain reaction
Pd	putidaredoxin
PDB	protein data bank
PdR	putidaredoxin reductase
PE	phycoerythrin
PEB	phycoerythrobin
PEC	phycoerythrocyanin
PEG MME 2000	poly(ethylene glycol) methyl ether average molecular weight 2000 Da
Pfr	far-red light absorbing form of phytochrome
PHY	phytochrome domain
PVB	phycoviolobin
PVDF	polyvinylidene fluoride
Pr	red light absorbing form of phytochrome
ROS	reactive oxygen species
SDS	sodium dodecyl sulfate
SDS-PAGE	sodium dodecyl sulfate polyacrylamide gel electrophoresis
TEMED	N,N,N',N'-Tetramethylethane-1,2-diamine
TES	N-[Tris(hydroxymethyl)methyl]-2-aminoethanesulfonic acid
TFA	trifluoroacetic acid
TMAO	trimethylamine N-oxide
UV/Vis	Ultra violet/Visible
v/v	volume per volume
w/v	weight per volume
WT	wild type

# 1 Introduction

## 1.1 The importance of tetrapyrroles in nature

The class of tetrapyrroles comprises various molecules that are involved in many important biological processes. For example, the light-harvesting chlorophylls of the photosystems employed by plants, cyanobacteria and algae are cyclic tetrapyrroles. Another prominent member belonging to the family of cyclic tetrapyrroles is heme. Heme functions as cofactor in proteins involved in the transport of diatomic gases, in proteins used for the transfer of electrons and is furthermore engaged in proteins linked to enzymatic catalysis. However, the cyclic state is not the only conformation in which tetrapyrroles occur. For instance, plants have developed a multistep pathway to breakdown chlorophyll during leaf senescence and fruit ripening, yielding fluorescent and non-fluorescent open-chain tetrapyrroles (Matile *et al.*, 1996; Hörtensteiner and Kräutler, 2011). This is most likely to avoid potential phototoxic effects, which include the formation of singlet oxygen (Foyer *et al.*, 1994; Hörtensteiner and Kräutler, 2011). Another important process that generates linear tetrapyrroles is the breakdown of heme. The heme synthesis needs to be tightly regulated due to its cytotoxicity in free form (Kumar and Bandyopadhyay, 2005). The toxic effects are caused by the formation of reactive oxygen species (ROS) upon the reaction of heme with oxygen (Larsen *et al.*, 2012). ROS are known to damage lipids as well as proteins (Tappel, 1955; Aft and Mueller, 1984). Vertebrates employ enzymes like heme oxygenases (HOs) for the catabolism of heme. HOs catalyze the ring-opening reaction of heme to the open-chain tetrapyrrole biliverdin IX $\alpha$  (BV IX $\alpha$ ). This compound is further reduced to bilirubin by biliverdin reductase and is then excreted in bile and urine (Kutty and Maines, 1981). The identification of the pigments found in the bile as linear tetrapyrroles led to the designation of these molecules as “bilins”. HO-dependent heme degradation is not only found in vertebrates. Moreover, different bacteria have developed a strategy of iron acquisition based on HO-activity (Ratliff *et al.*, 2001). Linear, open-chain tetrapyrroles are not only byproducts of catabolic pathways, they additionally play many important roles in nature. For instance, bilins act as the light-harvesting pigments of phycobiliproteins (PBPs) found in cyanobacteria, red algae, glaucophytes and cryptophytes. Furthermore, they serve as the light-sensing chromophores of the phytochrome-type photoreceptors in plants, algae, bacteria and fungi (Grombein *et al.*, 1975; Lagarias and Rapoport, 1980; Sharrock, 2008).

## 1.2 The biosynthesis of bilins

All open-chain tetrapyrroles involved in light-harvesting or light-sensing are derived from the cyclic precursor heme. Therefore, the first step in bilin biosynthesis is the ring-opening

reaction of the heme porphyrin macrocycle to the open-chain tetrapyrrole BV IX $\alpha$ , mediated by heme oxygenases (Cornejo and Beale, 1988; Rhie and Beale, 1992). BV IX $\alpha$  is then subsequently reduced to the specific light-harvesting or light-sensing pigments by ferredoxin-dependent bilin reductases (FDBRs). These enzymes catalyze site-specific reductions employing reduced ferredoxin as the electron donor (Beale and Cornejo, 1991b). FDBRs are versatile enzymes that catalyze the formation of a wide range of colorful pigments including phycocyanobilin (PCB), phycoerythrobilin (PEB), phytochromobilin (P $\Phi$ B), and phycourobilin (PUB).

### 1.2.1 The enzyme class of heme oxygenases

HOs are enzymes that catalyze a regiospecific cleavage of the heme macrocycle, yielding the open-chain tetrapyrrole biliverdin. The first member of the HO family was discovered in eukaryotes in the late 1960s (Tenhunen *et al.*, 1968, 1969). HOs play not only important roles in the biosynthesis of bilins, but are also key enzymes involved in iron metabolism, heme catabolism and oxidative stress response (Maines, 1988; Keyse and Tyrrell, 1989; Schmitt, 1997; Ratliff *et al.*, 2001; Frankenberg-Dinkel, 2004).

In organisms that use bilins as light-harvesting or light-sensing pigments, the main function of HOs is the synthesis of BV IX $\alpha$ , the substrate of almost all FDBRs. These HOs target the  $\alpha$ -meso carbon bridge of the heme macrocycle as the site for the ring opening reaction. In contrast, some HOs from *Pseudomonas aeruginosa* and other Pseudomonads were shown to yield BV IX $\beta$  and BV IX $\delta$  by targeting the respective meso carbon bridges of the heme molecule (Ratliff *et al.*, 2001; Gisk *et al.*, 2012). The HO mediated ring-opening reaction of heme requires three molecules of O<sub>2</sub> and seven electrons. It produces BV, free iron and CO (Figure 1).

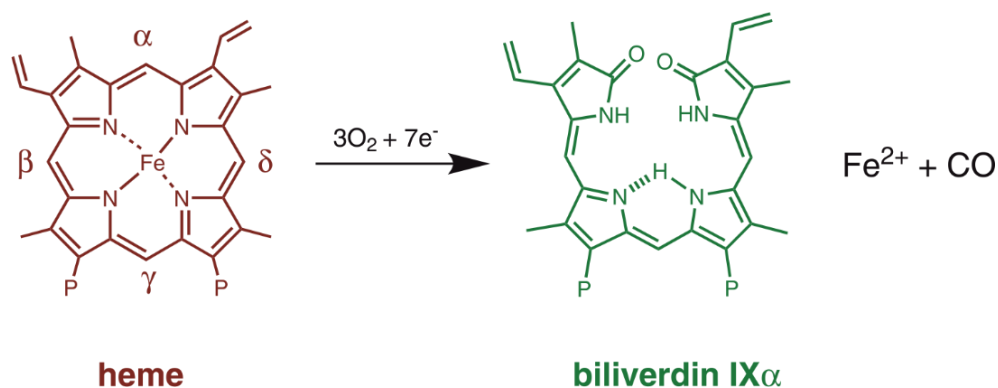


**Figure 1. The heme oxygenase reaction.** HO-mediated cleavage of the heme macrocycle (brown) at the  $\alpha$ -meso carbon bridge to yield biliverdin IX $\alpha$  (green). The reaction consumes three molecules of oxygen and seven electrons. The products are BV, Fe<sup>2+</sup> and CO. The meso carbons are labeled consecutively from  $\alpha$  to  $\delta$ . P = Propionate side chains.

The electron donors vary depending on the origin of the HO. In mammals, the electrons are provided by NADPH-cytochrome P450 reductase, whereas bacterial, algal and plant-derived HOs seem to prefer [2Fe-2S]-ferredoxins as the electron donor (Schacter *et al.*, 1972; Rhee and Beale, 1992; Wilks and Schmitt, 1998; Muramoto *et al.*, 1999). Moreover, ascorbate has also been described as a suitable electron donor for the HO reaction (Zhu *et al.*, 2000).

Even though the sequence identity between the HOs from different species is rather low, several solved crystal structures revealed that the overall fold is highly conserved among the family of HOs (Figure 2; Rivera and Zeng, 2005). All HOs harbor a single domain consisting mostly of conserved  $\alpha$ -helices (Wilks, 2002; Soldano *et al.*, 2017). The substrate is sandwiched between the distal and proximal helices, with the propionate groups coordinated by surface exposed lysine residues (Wilks and Heinzl, 2014). Heme is axially coordinated with a proximal His residue and a distal water molecule. This distal ligand changes several times during the reaction cycle (Rodriguez *et al.*, 2007).

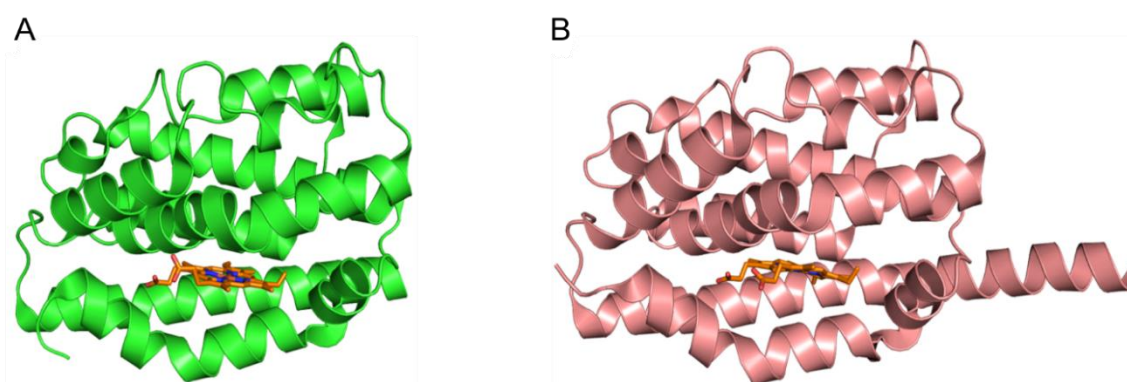


**Figure 2. Comparison of the crystal structures of an eukaryotic and a bacterial heme oxygenase.** **A.** HO1 of *Rattus norvegicus* (green; protein data bank (PDB) 1DVE; Sugishima *et al.*, 2000) with bound heme shown as brown sticks. **B.** HO1 from *Synechococcus* sp. PCC 6803 (salmon; PDB 1WE1; Sugishima *et al.*, 2004) in complex with heme (brown sticks).

The mechanism of the HOs is well characterized based on data of crystal structures, UV-Vis spectroscopy, electron paramagnetic resonance (EPR) measurements and Resonance Raman spectroscopy (Figure 3; Yoshida *et al.*, 1980; Sun *et al.*, 1993; Davydov *et al.*, 1999; Sugishima *et al.*, 2000; Sugishima *et al.*, 2004). The reaction starts with the reduction of the ferric  $\text{Fe}^{\text{III}}$ -heme-HO complex to the ferrous state. After that  $\text{Fe}^{\text{II}}$  forms a complex with  $\text{O}_2$  ( $\text{Fe}^{\text{II}}\text{-O}_2$ ) which is reduced to an activated, reactive  $\text{Fe}^{\text{III}}$ -peroxo species. Thus, heme acts both as the substrate and the cofactor in its own degradation (Wilks and Heinzl, 2014). The next step is the conversion of the activated intermediate to  $\alpha$ -meso-hydroxy-heme. The subsequent binding of a second molecule of  $\text{O}_2$  followed by the release of CO leads to the formation of  $\text{Fe}^{\text{III}}$ -verdoheme. Finally,  $\text{Fe}^{\text{III}}$ -verdoheme is converted to biliverdin. This is the least well understood part of the reaction mechanism and involves five electrons and one oxygen molecule. In many HOs, the final product is ( $\text{Fe}^{\text{III}}$ )-BV, whereas in some HOs the ferric iron is further reduced to allow the release of BV (Chu *et al.*, 1999; Wilks, 2002).

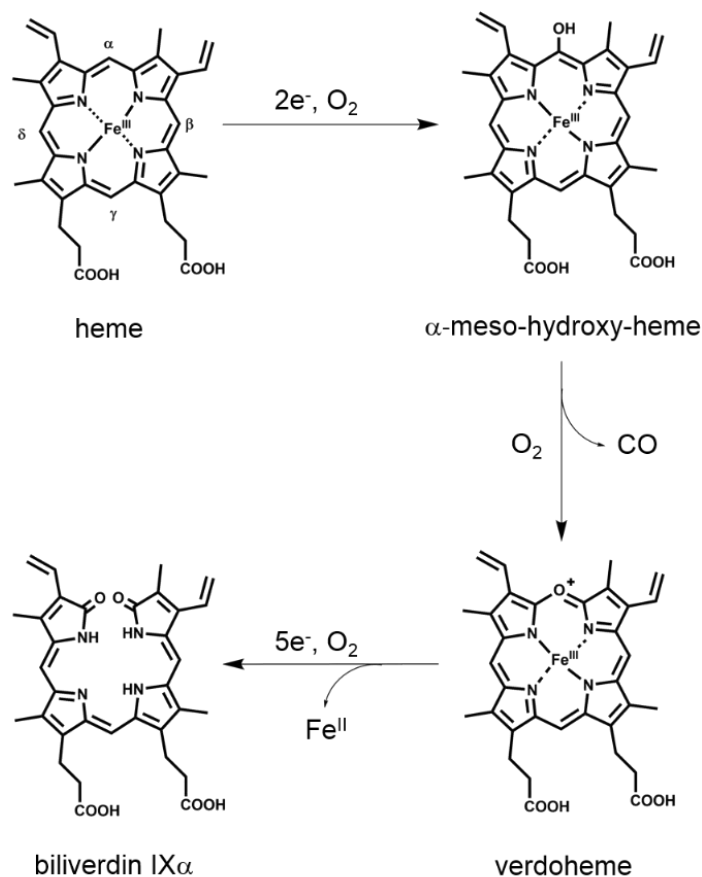


**Figure 3. Simplified scheme of the heme oxygenase reaction.** Most HO catalyze the regiospecific ring-opening of the heme macrocycle at the  $\alpha$ -meso carbon bridge, employing seven electrons and three molecules of oxygen. The reaction proceeds via the intermediates  $\alpha$ -meso-hydroxy-heme and verdoheme to yield the open-chain tetrapyrrole biliverdin IX $\alpha$ .

BV can either be used as the light-sensing chromophore of phytochromes found in heterotrophic bacteria (BphPs) and fungi (Fphs) or it serves as the precursor for several other pigments involved in light-harvesting or light-sensing.

### 1.2.2 The enzyme class of ferredoxin-dependent bilin reductases

BV IX $\alpha$ , the product of the HO reaction, serves as the substrate for a class of enzymes called ferredoxin-dependent bilin reductases. These enzymes catalyze the site specific reduction to the light-harvesting or light-sensing pigments employed by several phytochromes and PBPs. The first FDBR-related activity was described by Beale and Cornejo in 1984, when they reported the transformation of BV to PCB by cell-free extracts of the red alga *Cyanidium caldarium* (Beale and Cornejo, 1984a). These extracts also showed HO-activity, a circumstance that led to the association of HO and FDBR activity in the formation of phycobilins (Beale and Cornejo, 1984b). It took seven more years until the small iron-sulfur protein ferredoxin was identified as the electron donor employed in the reduction (Beale and Cornejo, 1991b). In the early 2000s, the FDBR phytychromobilin synthase was purified from *Avena sativa* L. cv Garry (McDowell and Lagarias, 2001). It was

shown to catalyze the reduction of BV to PΦB, the chromophore of plant-type phytochromes. Moreover, the gene product of *HY2* (phytochromobilin:ferredoxin oxidoreductase; EC: 1.3.7.4) from *Arabidopsis thaliana* was characterized as an enzyme catalyzing the same reaction (Kohchi *et al.*, 2001). The identification of this enzyme as a FDBR opened the door for a functional genomic approach that led to the identification of several other members of the FDBR-family in cyanobacteria, oxyphotobacteria and plants (Frankenberg *et al.*, 2001). To date, the FDBR-family comprises six members. All FDBRs, except phycoerythrobilin:ferredoxin oxidoreductase (PebB; EC: 1.3.7.3), employ BV as their substrate and catalyze site specific double-bond reductions. FDBRs can be classified into two different groups, depending on the number of electrons they transfer during the reaction. The reductases 15,16-dihydrobiliverdin:ferredoxin oxidoreductase (PebA; EC: 1.3.7.2), PebB and HY2 from higher plants catalyze two-electron reductions. In contrast, phycocyanobilin:ferredoxin oxidoreductase (PcyA; EC: 1.3.7.5), phycoerythrobilin synthase (PebS; EC: 1.3.7.6) and phycourobilin synthase (PUBS; EC: not designated yet) are capable to catalyze two subsequent two-electron reductions. In this process, the reductases first transfer two electrons onto the substrate BV, yielding a dihydrobiliverdin (DHBV) intermediate. In a following second two-electron reduction, the intermediate is reduced to a tetrahydrobiliverdin product (Figure 4).

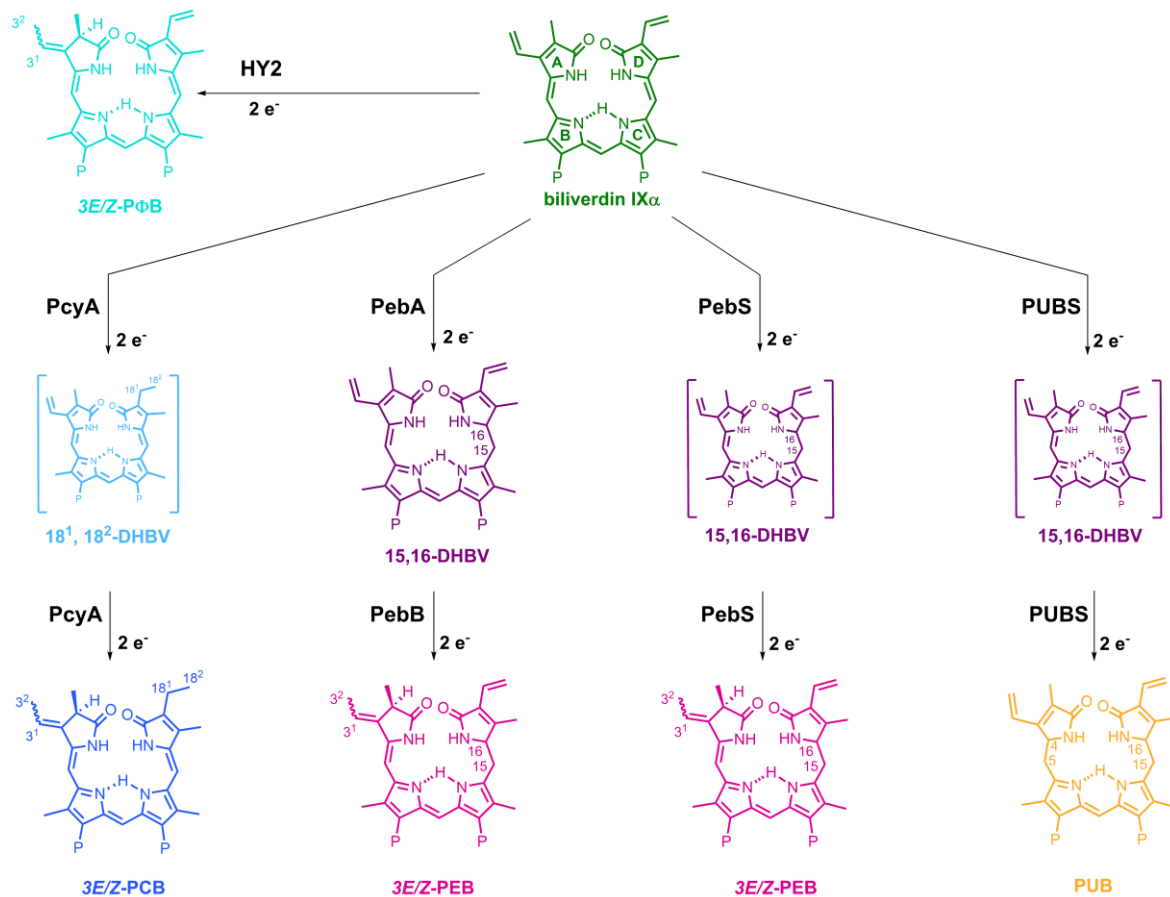


**Figure 4. Overview of the reactions catalyzed by the FDBR-family.** Biliverdin IX $\alpha$  is the substrate for all FDBRs except for PebB. It is shown in green color with the pyrrole rings lettered from A to D. "P" symbolizes propionate side chains. 3E/Z = the respective 3(E)- and 3(Z)-isomers. The molecules in brackets represent dihydrobiliverdin intermediates that are not released from the active site during the reaction. The coloration represents the approximate color of the different compounds. The reductase HY2 from higher plants catalyzes the two-electron reduction of BV to PΦB. The blue pigment PCB is formed via a PcyA-mediated four-electron reduction of BV. The reductase PebA catalyzes the reduction of BV to 15,16-DHBV, which acts as the substrate for PebB. In a second two-electron reduction, PebB reduces 15,16-DHBV to the pink pigment PEB. The second way to yield PEB is the four-electron reduction of BV catalyzed by the reductase PebS. The enzyme PUBS catalyzes the four-electron reduction of BV to the yellow pigment PUB.

PΦB is the chromophore of the phytochrome-type photoreceptors employed by higher plants (Terry *et al.*, 1993; Terry, 1997). The biosynthesis of PΦB is mediated by the FDBR HY2. The first HY2-related effects were described in *A. thaliana*, where the deletion of the gene *LONG HYPOCOTYL 2* led to nonfunctional phytochromes and therefore, impaired photomorphogenesis (Koornneef *et al.*, 1980; Chory *et al.*, 1989; Parks and Quail, 1991). The recombinant production of the protein in *E. coli* resulted in the identification of HY2 as a ferredoxin-dependent bilin reductase involved in the formation of PΦB out of BV (Kohchi *et al.*, 2001). Studies with native protein purified from *Avena sativa* confirmed this result (McDowell and Lagarias, 2001). HY2 catalyzes the two-electron reduction of BV at the A-ring 2,3,3<sup>1</sup>,3<sup>2</sup>-diene system to yield PΦB via a radical mechanism (Figure 5; Kohchi *et al.*, 2001; Tu *et al.*, 2008).

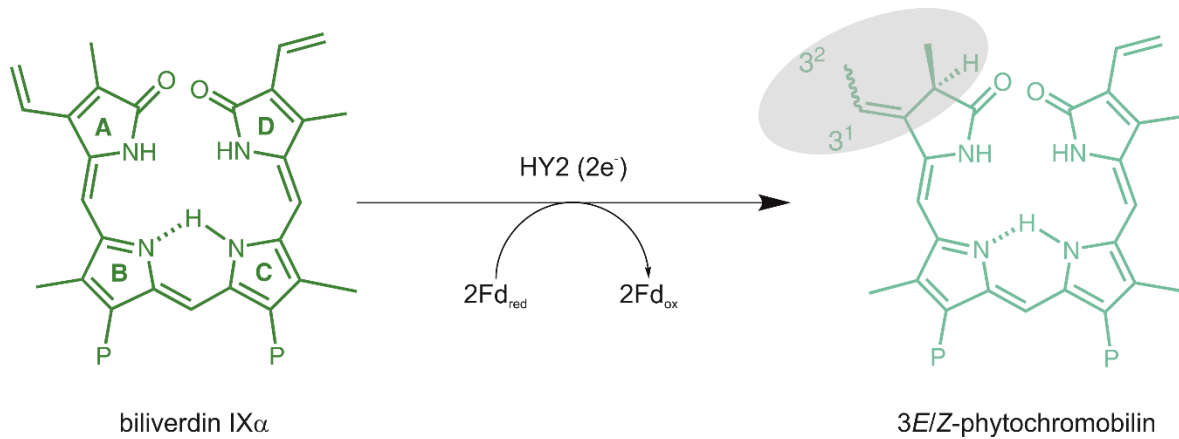


**Figure 5. Biosynthesis of phytochromobilin.** The FDBR HY2 catalyzes the two-electron reduction at the A-ring 2,3,3',3<sup>2</sup>-diene system of biliverdin IX  $\alpha$  (green; pyrrole rings lettered from A to D) to yield phytochromobilin (light blue). The site of the reduction is highlighted light-grey P = Propionate side chains. 3E/Z-phytochromobilin = 3(E)- and 3(Z)-phytochromobilin isomers.

This reduction generates the ethylidene group, which is necessary for the linkage of the chromophore to the apophytochrome (Lagarias and Rapoport, 1980).

#### *The biosynthesis of phycocyanobilin*

The blue colored phycocyanobilin is one of the most abundant bilins in nature. It plays an important role as the light-harvesting pigment employed in PBPs found in cyanobacteria, red algae, glaucophytes and cryptophytes. Furthermore, it acts as the light-sensing chromophore of phytochrome-type photoreceptors of cyanobacteria and streptophyte algae (Lamparter *et al.*, 2001; Rockwell *et al.*, 2017). The biosynthesis of PCB is mediated by two different enzymes. In cyanobacteria and cyanophages PcyA reductases catalyze the formal four-electron reduction of BV to PCB via a radical mechanism (Figure 6; Frankenberg and Lagarias, 2003; Tu *et al.*, 2007). In the first part of the reaction, PcyA mediates the two-electron reduction at the D-ring exo-vinyl group, yielding the intermediate 18<sup>1</sup>,18<sup>2</sup>-dihydrobiliverdin (18<sup>1</sup>,18<sup>2</sup>-DHBV). In a second two-electron reduction at the A-ring 2,3,3',3<sup>2</sup>-diene system, PcyA catalyzes the reaction of 18<sup>1</sup>18<sup>2</sup>-DHBV to yield PCB.

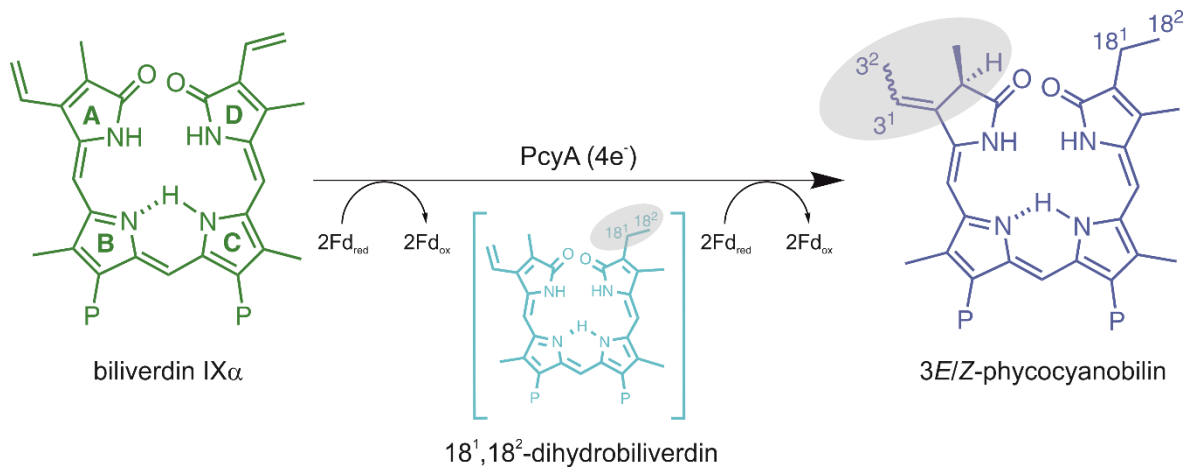


**Figure 6. Biosynthesis of phycocyanobilin in cyanobacteria.** PcyA catalyzes the four-electron reduction of BV (green, pyrrole rings lettered from A to D) to PCB (blue). The reduction proceeds in two coupled steps via the intermediate 18<sup>1</sup>,18<sup>2</sup>-DHBV (light blue). The sites of the respective reductions are highlighted light-grey. P = Propionate side chains. 3E/Z-phycocyanobilin = 3(E)- and 3(Z)-phycocyanobilin isomers.

In contrast, it was recently described that streptophyte algae synthesize PCB employing a HY2 reductase (Rockwell *et al.*, 2017). The reconstitution of the bilin biosynthesis pathway of the alga *Klebsormidium flaccidum* in *E. coli* showed that the coexpression of a HY2-type reductase (i.e. KflaHY2) with the corresponding HO (i.e. KflaHY1) and different phytochromes produces functional holophytochromes with PCB as the chromophore (Rockwell *et al.*, 2017). However, the course of this reaction is not fully understood and the direct proof that purified KflaHY2 itself catalyzes the reaction of BV to PCB is still missing.

#### The biosynthesis of phycoerythrobilin

The pink open-chain tetrapyrrole PEB is an important light-harvesting pigment in PBPs of cyanobacteria, red algae, glaucophytes and cryptomonads. Interestingly, there are different ways to synthesize PEB, depending on the origin of the FDBR. In cyanobacteria, the reductase pair PebA and PebB is involved in the formation of PEB (Figure 7; Frankenberg *et al.*, 2001; Dammeyer and Frankenberg-Dinkel, 2006).

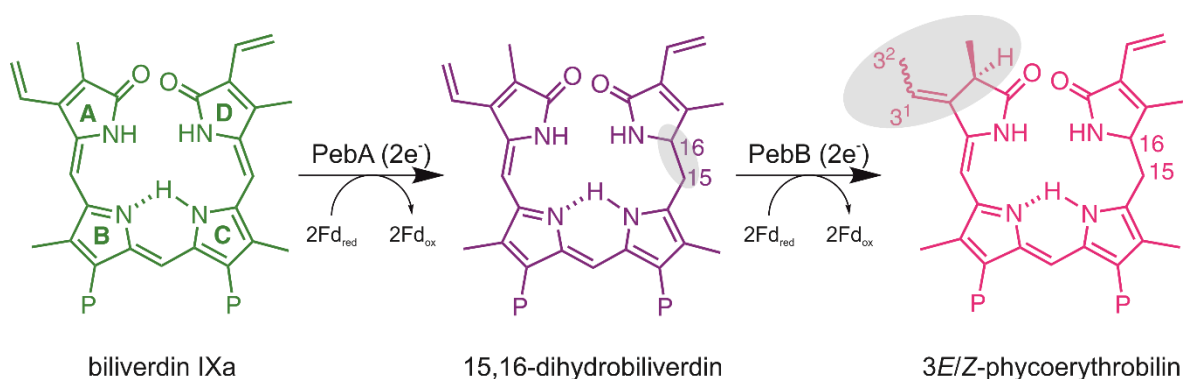


**Figure 7. Biosynthesis of phycoerythrobilin in cyanobacteria.** PebA catalyzes the two-electron reduction of BV (green; pyrrole rings lettered from A to D) to 15,16-DHBV (purple) at the C15 methine bridge. 15,16-DHBV is the substrate for PebB, which catalyzes the reduction at the A-ring 2,3,3<sup>1</sup>,3<sup>2</sup>-diene system to yield PEB (pink). The sites of the respective reductions are highlighted light-grey. P = Propionate side chains. 3E/Z-phycoerythrobilin = 3(E)- and 3(Z)-phycoerythrobilin.

In the first part of this reaction, PebA mediates a two-electron reduction of BV at the C15 methine bridge between the C- and D-ring, yielding 15,16-DHBV. Subsequently, 15,16-DHBV is reduced by PebB to PEB in a two-electron reduction at the A-ring 2,3,3<sup>1</sup>,3<sup>2</sup>-diene system. As 15,16-DHBV is very unstable, a substrate channeling between the two reductases has been postulated (Dammeyer and Frankenberg-Dinkel, 2006). The reduction at the A-ring is the most common reaction found in FDBRs and only PebA and PUBS do not catalyze this reaction. Furthermore, PebB is the only known member of the FDBR family that does not accept BV as its substrate.

Additionally, PEB can also be synthesized by another member of the FDBR family: The PebS reductases. PebS shares a high homology to PebA and was discovered in the myovirus P-SSM2, a virus infecting marine *Prochlorococcus* species (Dammeyer *et al.*, 2008a). Compared to the coupled reduction of the PebA and PebB reductases, PebS is capable of catalyzing the formal four-electron reduction of BV to PEB via the intermediate 15,16-DHBV (Figure 8).

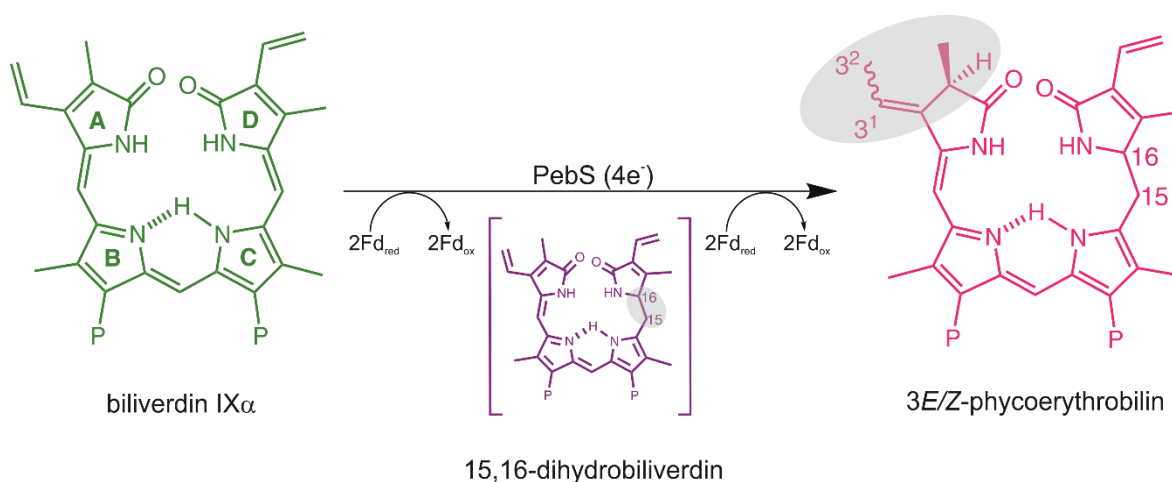


**Figure 8. Phage-related biosynthesis of phycoerythrobilin.** PebS catalyzes the formal four-electron reduction of BV (green; pyrrole rings lettered from A to D) to PEB (pink) via the intermediate 15,16-DHBV (purple). The sites of the respective reductions are highlighted light-grey. P = Propionate side chains. 3E/Z-phycoerythrobilin = 3(E)- and 3(Z)-phycoerythrobilin.

PebS combines the activities of both PebA and PebB. A possible advantage for the phage could lie in the reduction of the genetic material required for the formation of PEB, as the size of the capsid strictly limits the available space for the packaging of DNA (Dammeyer *et al.*, 2008a). Interestingly, PebS sequences have thus far only been discovered in DNA originating from phages and not from cyanobacteria.

#### *The biosynthesis of phycourobilin*

The yellow pigment phycourobilin can be found as one of the light-harvesting chromophores in the phycobiliproteins of cyanobacteria and red algae (Bryant *et al.*, 1981; Yu *et al.*, 1981). PUB was also found in the moss *Physcomitrella patens* where it was described to play a role in phytochrome-related light sensing (Chen *et al.*, 2012). In this plant, PUB is formed in

a four-electron reduction mediated by the FDBR PUBS. In the first part of the reaction, PUBS catalyzes the reduction of BV at the C15 methine bridge to produce the intermediate 15,16-DHBV. In a second reduction, 15,16-DHBV is reduced at the C5 methine bridge between the A- and the B-ring to yield PUB (Figure 9).

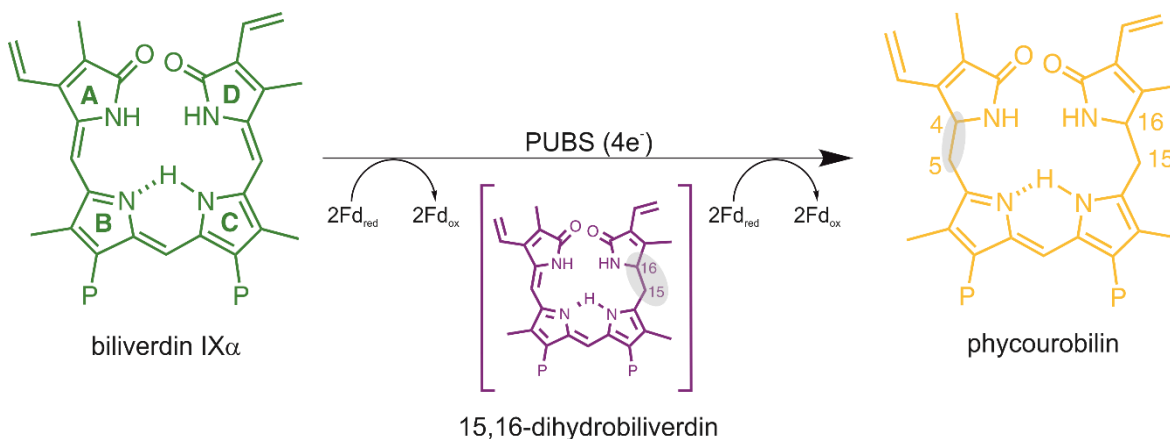


**Figure 9. Biosynthesis of phycourobilin catalyzed by PUBS.** The FDBR PUBS catalyzes the four-electron reduction of BV (green; pyrrole rings lettered from A to D) to PUB (yellow) via the intermediate 15,16-DHBV (purple). The sites of the respective reductions are highlighted light-grey. P = Propionate side chains.

In contrast, in cyanobacteria PUB is synthesized by an isomerization of PEB during the attachment to phycobiliproteins mediated by enzymes possessing lyase-isomerase activity (Blot *et al.*, 2009; Shukla *et al.*, 2012). PUBS along with PebA is one of the two FDBR-members that is not capable of catalyzing a reduction at the A-ring 2,3,3 $^1$ ,3 $^2$ -diene system.

### 1.2.3 The structure of the ferredoxin-dependent bilin reductases

To date, several crystal structures of FDBRs, including PcyA, PebA and PebS, have been solved (Hagiwara *et al.*, 2006a; Dammeyer *et al.*, 2008b; Busch *et al.*, 2011a). This revealed that all FDBRs possess the same structure, although their overall sequence identity is rather low. The reductases are globular single-domain proteins that all employ an  $\alpha/\beta/\alpha$ -sandwich fold with a central  $\beta$ -sheet flanked by  $\alpha$ -helices (Figure 10 A-C).

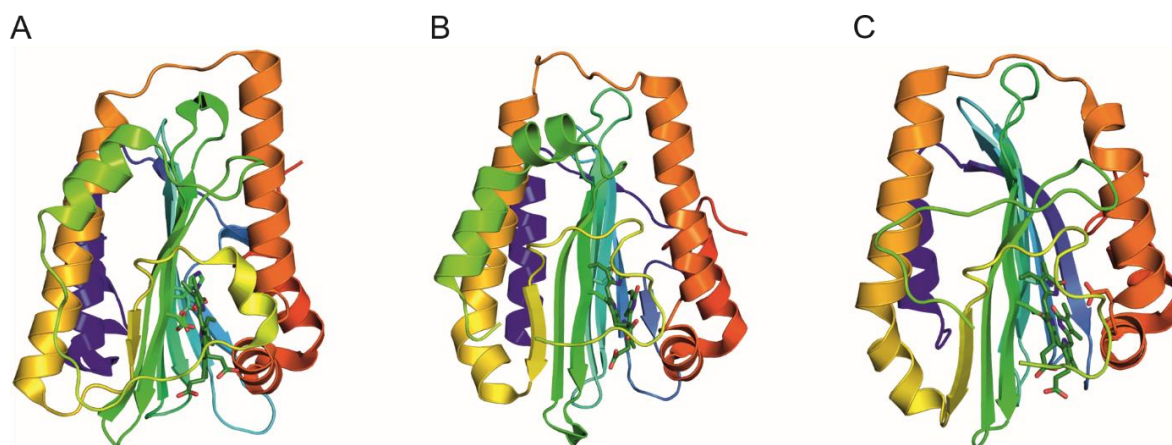


**Figure 10. Overview of the crystal structures of three different FDBRs.** Important catalytic residues are shown as sticks. The structures are colored from blue to red, starting with the N-terminus. The substrate BV is shown as green sticks. **A.** Crystal structure of PcyA with bound BV shown in cartoon representation (PDB 2D1E; Hagiwara *et al.*, 2006a). **B.** Cartoon representation of the crystal structure of PebA with bound BV (PDB 2X9Q; Busch *et al.*, 2011a). **C.** Crystal structure of PebS with bound substrate shown in cartoon representation (PDB 2VCK; Dammeyer *et al.*, 2008b).

The active site of the reductases is formed by a cavity located between the central  $\beta$ -sheet (proximal side) and the C-terminal  $\alpha$ -helices (distal side). BV is bound in the active site of the enzyme with its propionate groups facing the solvent. The electrostatic potential on the surface of the BV-binding site is typically positively charged (Hagiwara *et al.*, 2006b; Tu *et al.*, 2007; Dammeyer *et al.*, 2008b). Therefore, this is most likely the region where the FDBR and the acidic, negatively charged, electron donor ferredoxin interact.

Despite the fact that all FDBRs show a similar overall structure and certain conserved features, they are able to catalyze a variety of reactions, yielding different products. In conclusion, the FDBRs must catalyze these reactions using slightly different mechanisms.

#### 1.2.4 The reaction mechanisms of the FDBRs

Several studies including X-ray crystallography, EPR measurements, as well as site-directed mutagenesis experiments have been performed to gain insights into the reaction mechanism employed by the different FDBRs (Tu *et al.*, 2004; Hagiwara *et al.*, 2006a; Tu *et al.*, 2006; Tu *et al.*, 2007; Stoll *et al.*, 2009; Kohler *et al.*, 2010; Busch *et al.*, 2011a; Busch *et al.*, 2011b; Unno *et al.*, 2015). All FDBRs use the small iron-sulfur protein ferredoxin as the electron donor in their reactions. As ferredoxin is only capable of transferring one electron at a time and the FDBRs lack metallic or organic cofactors, it has been speculated that the reactions catalyzed by FDBRs proceed via a substrate radical mechanism (Frankenberg and Lagarias, 2003). EPR studies confirmed this hypothesis (Tu *et al.*, 2004; Tu *et al.*, 2008; Busch *et al.*, 2011a; Busch *et al.*, 2011b). To date, all FDBR reactions are thought to act via substrate radical mechanisms involving protonations followed by the transfer of one electron at a time. The protonation raises the midpoint potential of the

protonated BV or the protonated intermediate, facilitating the transfer of electrons from reduced ferredoxin onto the bilin, creating a substrate radical (Tu *et al.*, 2006).

The most thoroughly studied member of the FDBR family is PcyA. Several X-ray structures, neutron-crystallography, site-directed mutagenesis, as well as EPR experiments resulted in a detailed understanding of the PcyA reaction mechanism. These studies identified Glu76, His88 and Asp105 (PcyA from *Synechocystis* sp. PCC 6803 numbering) as catalytically essential residues located in the active site of PcyA (Figure 11 A Hagiwara *et al.*, 2006a; Tu *et al.*, 2006; Tu *et al.*, 2007). Site-directed mutagenesis experiments, exchanging His88 with Gln and Asp105 with Asn led to PcyA variants that have lost almost all of their catalytic activity. Both His88 and Asp105 function as proton donors during the course of the reaction, with Asp105 being the initial proton donor responsible for the formation of a protonated BV (BVH<sup>+</sup>). Interestingly, the exchange of Glu76 with Gln creates an enzyme that catalyzes the formation of PΦB resembling HY2-activity. This PcyA variant is not able to form the intermediate 18<sup>1</sup>,18<sup>2</sup>-DHBV, but is still able to catalyze the reduction at the A-ring. Hence, Glu76 must act as a proton donor in the reduction of the D-ring exovinyl group. Furthermore, the solution of PcyA crystal structures identified another feature of this member of the FDBR family: A proton shuttle reaching from His88 over several basic amino acid residues to the solvent. This proton channel is proposed to be involved in the reprotonation of His88 during the course of the reaction (Tu *et al.*, 2007).

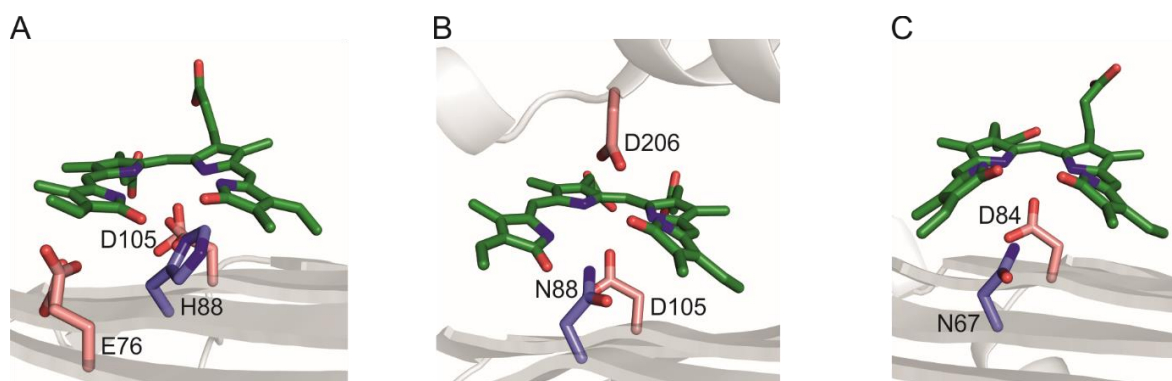


**Figure 11. Overview of catalytically important residues and the substrate binding in the active sites of different FDBRs.** The substrate BV is shown as green sticks. Acidic amino acid residues are shown as red sticks, other important amino acid residues are shown as blue sticks. The corresponding secondary structure elements are indicated in a light-grey cartoon representation **A**. Close-up of the active site of PcyA from *Synechocystis* sp. PCC 6803 (PDB 2D1E; Hagiwara *et al.*, 2006a). **B**. Close-up of the active site of PebS from the cyanophage P-SSM2 (PDB 2VCK; Dammeyer *et al.*, 2008b). **C**. Close-up of the active site of PebA from *Synechococcus* sp. WH 8020 (PDB 2X9O; Busch *et al.*, 2011a).

The reaction mechanisms of the other members of the FDBR family are not as well understood as the reaction mechanism of the PcyA reductases. A common feature of all FDBRs except HY2 is a conserved Asp (i.e. Asp105 of PcyA) residue located on the central  $\beta$ -sheet close to the binding site of the substrate (Figure 11 A - C). This conserved acidic residue is thought to be involved in the protonation of BV and/or radical intermediates and has been shown to be essential for the catalytic activity not only for PcyA, but also for PebA,

PebB and PebS (Tu *et al.*, 2006; Busch *et al.*, 2011a; Busch *et al.*, 2011b). Interestingly, in PebA, PebB and PebS the PcyA His88 is replaced with an Asn residue which cannot function as a proton donor (PebS and PebA –Figure 11 B & C). Moreover, these reductases, as well as HY2, possess a conserved Asp (i.e. Asp206 – PebS from P-SSM2 numbering) residue located on one of the distal  $\alpha$ -helices (PebS –Figure 11 B). This residue was shown to be critical for the A-ring reduction in PebS, PebB and HY2, whereas in PebA it points away from the active site (Tu *et al.*, 2008; Busch *et al.*, 2011a; Busch *et al.*, 2011b). For this reason, it seems that FDBRs achieve their A-ring reductions in two different ways. PcyA reductases employ His88 located on the central  $\beta$ -sheet as a proton donor for this reaction. On the other hand, PebS, PebB and HY2 reduce the A-ring by employing Asp206 located on the distal  $\alpha$ -helices as protonating residue.

The studies on the reaction mechanisms of the FDBRs not only revealed different essential amino acid residues, but the solution of several crystal structures also showed that the substrate adopts different conformations depending on the type of reductase. For example in the PcyA reductases, BV adopts a cyclic conformation where the pyrrole rings are almost located in one plane (Figure 11 A; Hagiwara *et al.*, 2006a). In PebS, the substrate can be found in two different conformations, a planar and a more helical conformation, in which the A-ring is shifted towards the D-ring (Figure 11 B; Dammeyer *et al.*, 2008b). In contrast, in PebA the BV is bound in a roof-like conformation with the A- and D-ring tilted by approximately 40° out of plane (Figure 11 C; Busch *et al.*, 2011a).

In conclusion, this suggests that not only the conserved catalytically active residues contribute to the different regiospecificities of the reductases. Moreover, also the conformation and orientation of the substrate in the active site seems to play an important role in the FDBR-mediated reactions to the specific pigments.

## 1.3 The physiological functions of bilins

### 1.3.1 Light-harvesting

Photosynthesis is characterized as the conversion of light energy into chemical energy by the reduction of CO<sub>2</sub> to carbohydrates, making it one of the key processes in nature. Most photosynthetically active organisms harvest light by employing the cyclic tetrapyrrole chlorophyll (Chl) in antenna complexes. Hence, Chls are the most abundant light-harvesting pigments on earth. Nevertheless, Chls absorb primarily blue and red light, leaving a considerable amount of light-energy unused, also known as the “green gap” between ~ 500 nm and 600 nm. Therefore, many organisms like cyanobacteria, red algae and cryptomonads have developed strategies to overcome the limitations of their chlorophyll-related light-harvesting machinery. They employ proteins with attached open-chain, linear tetrapyrroles that allow efficient light-harvesting in regions of the spectrum where their Chls

only poorly absorb light. These proteins are called phycobiliproteins. Some organisms like cyanobacteria and red algae assemble these PBPs into large protein complexes called phycobilisomes that form rod-shaped antennae which are directly attached to the photosystem II and act like an energy funnel (Glazer, 1977; Zilinskas and Greenwald, 1986). Several solved crystal structures revealed that the PBPs obtain a globin-like fold, but possess additional helices (Schirmer *et al.*, 1986). The PBPs form heterodimers consisting of homologous  $\alpha$ - and  $\beta$ -subunits that are thought to have coevolved from a common ancestor (Apt *et al.*, 1995). The heterodimers are capable to form higher oligomeric states and assemble into ring-shaped  $(\alpha\beta)_3$ -trimers or  $(\alpha\beta)_6$ -hexamers that are the building blocks for the phycobilisome (Figure 12).

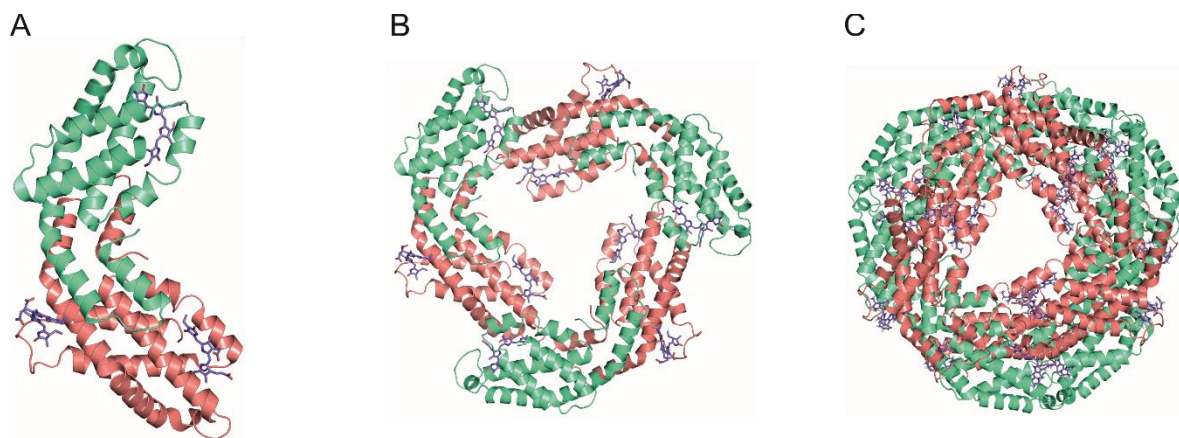


**Figure 12. Crystal structures of phycocyanin in different oligomerization states.** The proteins are shown in cartoon representation.  $\alpha$ -subunits are colored in green,  $\beta$ -subunits are colored in salmon. The phycocyanobilin chromophores are shown as blue sticks. A.  $(\alpha\beta)$ -monomer of phycocyanin from *Synechocystis* sp. PCC 6803 (PDB 4F0T; Marx and Adir, 2013). B.  $(\alpha\beta)_3$ -trimer of phycocyanin from *Synechocystis* sp. PCC 6803 (PDB 4F0T). C.  $(\alpha\beta)_6$ -hexamer of phycocyanin from *Thermosynechococcus elongatus* (PDB 4ZIZ; Fromme *et al.*, 2015). Figure modified after Ledermann *et al.*, 2017a.

The structure of the phycobilisome is divided into two parts: The core and the peripheral rods. The core of the phycobilisome is formed by allophycocyanin (APC) which is made up out of six  $(\alpha\beta)_3$ -trimers. The rod-shaped antennae are composed of  $(\alpha\beta)_3$ -trimers or  $(\alpha\beta)_6$ -hexamers which are held together by linker proteins that connect the single building blocks. Four different types of PBPs with different chromophore compositions exist in cyanobacteria: APC, phycocyanin (PC), phycoerythrocyanin (PEC) and phycoerythrin (PE). The differences in the chromophore composition also lead to different absorbance characteristics, which are given in the table below.

**Table 1. Absorbance characteristics and colors of the different phycobiliproteins in cyanobacteria.**

Phycobiliprotein	Absorbance range [nm]	Color
Allophycocyanin	650 – 655	Green-blue
Phycocyanin	610 – 620	Blue
Phycoerythrocyanin	570 – 590	Purple
Phycoerythrin	540 – 570	Orange-red

The differences in the absorbance ranges of the PBPs is mostly caused by their bilin chromophores. To date, four different bilins are known to occur as the light-harvesting pigments in PBPs: The blue PCB ( $\lambda_{\max} = 620$  nm), the violet phycoviolobilin (PVB;  $\lambda_{\max} = 590$  nm), the pink PEB ( $\lambda_{\max} = 540$  nm) and the yellow PUB ( $\lambda_{\max} = 500$  nm). These chromophores are attached to the apoproteins via thioether bonds to conserved cysteine residues. This attachment was shown to happen spontaneously *in vitro*, leading to a mixture of different products due to a low fidelity of the process (Fairchild and Glazer, 1994; Scheer and Zhao, 2008). Therefore, in nature the chromophores are site- and stereospecifically attached to the apoproteins by a class of enzymes called phycobiliprotein lyases. These enzymes promote the formation of a thioether bond from the conserved cysteine residue of the PBP to the A-ring of the bilin chromophore. In most cases the chromophore is linked to the protein by a single thioether bond via the C3<sup>1</sup> atom, but there are cases where a second bond is formed between the C18<sup>1</sup> atom of the D-ring and another cysteine residue (Scheer and Zhao, 2008).

### 1.3.2 Light-sensing

Bilins are not only found as the light-harvesting chromophores in PBPs, but also act as the light-sensing pigments in phytochrome-type photoreceptors. Photoreceptors are used by many organisms, allowing them to sense the quality, intensity and the direction of the ambient light. This enables these organisms to adapt their metabolism according to the different light conditions. Phytochromes are the most extensively studied members of the photoreceptors and were first discovered in the late 1950s in plants (Butler *et al.*, 1959). Phytochromes have been found in several other organisms like cyanobacteria (cyanobacterial phytochromes, Cphs; Yeh *et al.*, 1997), heterotrophic bacteria (bacterial phytochromes, Bphs; Bhoo *et al.*, 2001) and fungi (fungal phytochromes, Fphs; Blumenstein *et al.*, 2005). Furthermore, the family of phytochromes comprises atypical, phytochrome-like proteins discovered in cyanobacteria. Consequently they are termed as cyanobacteriochromes (CBCRs) (Ikeuchi and Ishizuka, 2008).

Phytochromes employ a covalently bound bilin chromophore (P $\Phi$ B in plants, PCB in streptophyte algae and cyanobacteria, BV in heterotrophic bacteria and fungi) to sense red and far-red light. The chromophore is autocatalytically attached to a conserved cysteine of the apoprotein and triggers a reversible photoconversion of the holoprotein between a red-absorbing (Pr) and a far-red absorbing (Pfr) state upon the absorption of light. This mechanism qualifies phytochromes as tools to measure the ratio of red and far-red light, enabling for example plants to perceive shading caused by neighboring vegetation (Holmes and Smith, 1975). The perception of changing light conditions then allows the response by the activation of shade-avoidance reactions (Smith and Whitelam, 1990). Furthermore,

phytochromes induce reactions including seed germination, chloroplast movement, photoperiodic time measurement and photomorphogenesis (Mathews, 2006; Sharrock, 2008). The molecular mechanism behind the change between the Pr- and Pfr-form of the phytochromes is a reversible *Z/E* isomerization between the C- and the D-ring of the bilin chromophore. This isomerization leads to conformational changes in the protein and triggers the initiation of the response reactions.

The typical architecture of a phytochrome is divided into two parts: An N-terminal photosensory module and a C-terminal signaling domain (Figure 13).

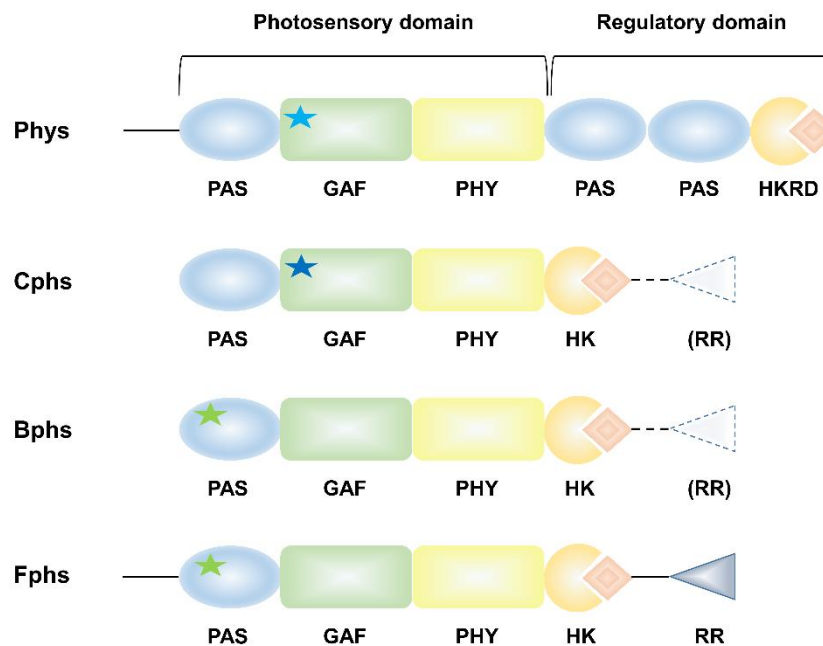


**Figure 13. Overview of the typical architectures of phytochromes from different species.** Phytochromes consist of a photosensory and a regulatory domain. The photosensory part of the phytochrome carries the chromophore and typically contains a PAS domain (blue circle), a GAF domain (green box) and a PHY domain (yellow box). Furthermore, plant-type (Phys) and fungal phytochromes (Fphs) possess N-terminal extensions (black lines N-terminal to the PAS domains). In plant-type phytochromes, the chromophore PΦB (light blue star) is bound within the GAF domain. Cyanobacterial phytochromes (Cphs) employ PCB (blue star) as the light-sensing chromophore that is also attached to the GAF domain. In contrast, bacterial (Bphs) and fungal Fphs use BV (green star) as the chromophore bound to their PAS domains. The composition of the regulatory domain differs depending on the origin of the phytochrome. The regulatory region of Phys usually consists of two PAS domains and a histidine kinase-related domain (orange circle with sector and red rhombus). The other phytochromes show typical histidine kinase domains (HK) and lack the PAS domains. Fphs usually harbor a response regulator domain (blue triangle), whereas only a minority of the Cphs and Bphs possess this feature (indicated as dashed triangles).

The structure of the photosensory module is conserved among the different phytochromes and comprises PAS (**P**er-**A**RNT-**S**im), GAF (**c**GMP-specific phosphodiesterases, **a**denylyl cyclases and **F**h1A) and PHY (**p**hytochrome) domains. In addition to the conserved domains, Phys and Fphs also possess N-terminal extensions which seem to influence the dark reversion of the phytochrome (Brandt *et al.*, 2008; Sharrock, 2008; Burgie *et al.*, 2014). In bacterial and fungal phytochromes, the light-sensing bilin is usually bound to a cysteine residue in the PAS domain preceding the GAF domain, whereas in cyanobacterial and plant-type phytochromes the bilin is bound within the GAF domain (Nagano, 2016). The composition of the signaling domain differs depending on the origin of the phytochrome.

Prokaryotic phytochromes typically employ a histidine kinase (HK) domain, while plant-type phytochromes retain a histidine kinase-related domain, lacking the conserved histidine involved in the acceptance of the phosphoryl group (Yeh *et al.*, 1997; Yeh and Lagarias, 1998). Even though the histidine kinase-related domain inhabits serine/threonine kinase activity, it has been shown that it is not essential for the function of plant-type phytochromes (Krall and Reed, 2000). In contrast, prokaryotic phytochromes function as light-regulated histidine kinases in two-component systems (Yeh *et al.*, 1997). Interestingly, in fungal phytochromes it is common that the signaling domain is directly fused to a response regulator domain. On the other hand, in Bphs and Cphs most of the members do not possess this C-terminal fusion (Sharrock, 2008).

The family of phytochromes also comprises the atypical CBCRs. These photoreceptor proteins are found in cyanobacteria where they are related to processes like the regulation of phototaxis, light-dependent cell aggregation and complementary chromatic adaptation (Savakis *et al.*, 2012; Hirose *et al.*, 2013; Narikawa *et al.*, 2015). CBCRs only need a GAF domain to form photoactive adducts with a bilin chromophore and function as light-sensors in near-UV/visible lights between 330 nm and 680 nm (Hirose *et al.*, 2013; Enomoto *et al.*, 2014). They employ PCB and PVB as light-sensing chromophores, whereas PVB is formed via an intrinsic isomerase activity (Ishizuka *et al.*, 2011). CBCRs show diverse photocycles which include for example, photoconversions from blue to green absorbing species as well as conversions from green to red absorbing forms (Narikawa *et al.*, 2013). The spectral properties of the CBCRs are not only determined by their chromophore. Moreover, there are several mechanisms that tune the absorption characteristics. These are for instance the formation of a covalent bond from a second Cys residue to C10 of the chromophore and protonation/deprotonation cycles (Rockwell *et al.*, 2008; Hirose *et al.*, 2013; Narikawa *et al.*, 2015). Another interesting characteristic of the CBCRs are the related output domains. The physiological roles are not fully understood nevertheless, there are several output domains associated with the CBCR GAF domain (Enomoto *et al.*, 2014). These include histidine kinase domains, as well as methyl-accepting chemotaxis domains and GGDEF/EAL domains (Yoshihara *et al.*, 2004; Hirose *et al.*, 2010; Savakis *et al.*, 2012). GGDEF domains possess diguanylate cyclase activity and are therefore, involved in the formation of the second messenger cyclic di-GMP. The EAL domain typically is the corresponding phosphodiesterase that degrades cyclic di-GMP (Römling *et al.*, 2013; Enomoto *et al.*, 2014).

#### **1.4 Marine phages - Key players in aquatic ecosystems**

Some of the enzymes involved in the biosynthesis of the light-sensing and light-harvesting bilins are not only present in organisms like cyanobacteria, but were also discovered in marine phages. With an estimated number of  $10^{30}$ , viruses represent by far the most

abundant biological entity in the oceans (Breitbart *et al.*, 2002; Suttle, 2007; Perez Sepulveda *et al.*, 2016). Furthermore, it is thought that in every second  $10^{23}$  infection events take place (Suttle, 2007). This highlights the importance of the understanding of the mechanisms underlying the phage-host interactions, as every infection has the potential to transfer genetic information. Hence, viruses are one of the major driving forces that increase genetic diversity. They also play an important role in the nutrition cycles and have a direct impact on the diversity of the bacterial communities (Middelboe *et al.*, 2003).

#### **1.4.1 Impact on the nutrient cycling and on the diversity of the bacterial community**

The lysis of the host cell is often the final step in the “life cycle” of a phage. As a result phages contribute not only to the controlling of the host population, but also liberate large amounts of organic matter into the dissolved state. This is extremely important, as the lysis of the host yields substrates which are usable as an energy source for other prokaryotes. This withdrawal of nutrients from the “classic” food chain involving eukaryotic grazers is termed the “viral shunt” and is thought to free up to 26% of the photosynthetically fixed carbon (Wilhelm and Suttle, 1999).

The lysis of the specific hosts not only yields soluble organic compounds, but also has an impact on the composition of bacterial communities (Weinbauer and Rassoulzadegan, 2004). An increase of the abundance of the host is most likely followed by an increase of the number of its phages. Thus, marine phages play an important role in keeping the composition of bacterial communities in check.

#### **1.4.2 Auxiliary metabolic genes in marine phages**

Despite the first DNA-based genome ever to be sequenced was that of bacteriophage  $\Phi$ X174, published in 1977 by Frederick Sanger and coworkers, it took more than 20 years until the first genome of a marine phage was sequenced (Sanger *et al.*, 1977; Mannisto *et al.*, 1999). Since then, the number of available genomes rapidly increased. The classic approach of sequencing a phage genome is limited by the requirement to cultivate the host bacterium. A technique to overcome this limitations was found in metagenomics-based methods. The first metagenomics study on marine viral communities was conducted by Breitbart and coworkers in the early 2000s (Breitbart *et al.*, 2002). Until now several other studies applying metagenomics approaches have been performed to specifically shed light onto the diverse viral genomes (Angly *et al.*, 2006; Sharon *et al.*, 2011; McDaniel *et al.*, 2014).

The intensive studies of the genetic composition of marine viruses revealed that a common feature in phages that infect cyanobacteria (i.e. cyanophages) is the occurrence of auxiliary metabolic genes (AMGs). AMGs are homologs to bacterial genes involved in the

metabolism and are thought to improve phage fitness during the infection (Breitbart *et al.*, 2002; Dammeyer *et al.*, 2008a; Gao *et al.*, 2016). For instance, cyanophages often carry AMGs related to photosynthesis (Puxty *et al.*, 2015). These processes include pigment biosynthesis, formation of reaction centers, electron transport and carbon fixation (Mann *et al.*, 2003; Dammeyer *et al.*, 2008a; Millard *et al.*, 2009).

The AMGs related to light-harvesting pigments comprise FDBRs, HOs and PBP-lyases. The FDBRs found in cyanophages are members of the PcyA and PebS reductases enabling the synthesis of both PCB and PEB (Dammeyer *et al.*, 2008a). Viral HOs target the  $\alpha$ -meso carbon of the heme macrocycle yielding BV IX $\alpha$ , the substrate of PcyA and PebS. The fact that PebS, as well as other genes involved in pigment biosynthesis have been described to be transcribed during infection events, highlight their importance for the phages (Dammeyer *et al.*, 2008a). In addition, Shan and coworkers reported in *Synechococcus* sp. WH7803 an increase of the amount of phycoerythrin per cell upon infection with phage S-PM2. A result that supports the theory that cyanophages modify the cyanobacterial light-harvesting machinery upon infection (Shan *et al.*, 2008). Another class of genes involved in the bilin-related light-harvesting encode for PBP-lyases, proteins that are involved in the specific attachment of bilins onto phycobiliproteins. The PBP-lyases found in cyanophages belong to the class of T-type lyases which are ubiquitous among cyanobacteria (Shen *et al.*, 2006; Gasper *et al.*, 2017). A recently characterized viral T-type lyase (i.e.  $\Phi$ CpeT), originating from cyanophage P-HM1 revealed that it adopts the same overall  $\beta$ -barrel fold as the T-type lyase found in *Nostoc* sp. PCC7120, but is more compact and smaller (Zhou *et al.*, 2014; Gasper *et al.*, 2017). Accordingly, most AMGs have a reduced gene length compared to the homologs found in bacteria, as the limited space of a viral capsid increases the pressure to reduce the genetic information as efficiently as possible (Puxty *et al.*, 2015).

AMGs are not only restricted to the field of pigment biosynthesis and attachment. For instance, *psbA* and *psbD*, genes encoding for the proteins D1 and D2 which form the core of the reaction center of photosystem II, are widespread among cyanophages (Zouni *et al.*, 2001; Mann *et al.*, 2003; Lindell *et al.*, 2004; Sullivan *et al.*, 2006; Zheng *et al.*, 2013). As the *psbA* and *psbD* genes found in the phages share a high homology to the genes found in the hosts, it is likely that they serve the same functions. Therefore, the contribution of *psbA* and *psbD* to phage fitness is thought to be in the limitation of photo-inhibition in the host cells during infection (Mann *et al.*, 2003).

Furthermore, phages carry genes like *petF* and *petE* which encode for ferredoxin and plastocyanin, respectively (Dammeyer *et al.*, 2008b; Millard *et al.*, 2009). PetF functions as electron donor for the FDBRs involved in the pigment biosynthesis, whereas plastocyanin is a small copper protein engaged in the electron transfer from the cytochrome b6f complex and photosystem I.

Phages also possess AMGs related to carbon fixation and metabolism. Genes that are quite common among cyanophages for example, are *cp12* and *talC* (Sullivan *et al.*, 2010). In the hosts, the gene product of *cp12* is a small redox protein that is linked to the termination of the Calvin-cycle (Tamoi *et al.*, 2005). The host homolog to *talC* is *talB*, which encodes for a transaldolase of the pentose phosphate pathway. In conclusion, it seems that cyanophages redirect the carbon cycles during the infection, resulting in a decreased Calvin-cycle activity and an increased pentose phosphate pathway activity. As a result, the NADPH over NADP ratio is raised during the infection. A possible contribution to phage fitness could be the promotion of the synthesis of dNTPs required for the replication of the phages (Thompson *et al.*, 2011).

### **1.5 Marine metagenomes as a source for new enzymes**

As most of the viruses and organism in the ocean are to date not cultivable under laboratory conditions, the gathering and analysis of marine metagenomics data has become a precious tool to access the majority of genetic information present in the oceans. Metagenomics bypass the cultivation of organisms in the laboratory by isolating DNA directly out of environmental samples. To exploit this rich source of genetic information, several expeditions took place that include sampling activities in the Sargasso Sea (Venter *et al.*, 2004), as well as expeditions that collected samples at several sites across the world's oceans. One of the first ventures that was undertaken was the "Global Ocean Sampling Expedition (GOS)" that started as a cruise from the North Atlantic through the Panama Canal to the South Pacific Ocean. The data gathered through that part of the expedition comprise about 6.3 billion base pairs of DNA (Rusch *et al.*, 2007). A major limitation of this expedition was that all samples of this expedition were collected within a few meters from the surface. Furthermore, they were filtered to yield a fraction only comprising a range between 0.2 and 0.8  $\mu\text{m}$ . Therefore, the genetic information gained during this study was limited to the near surface planktonic niche (Nealson and Venter, 2007). Consequently, the next parts of the expedition also comprised sampling from extreme environments like saline ponds or thermal vents. An expedition with a focus on the collection of samples from the ocean's surface and the bathypelagic layer (depths > 1000 m) was the Malaspina expedition that took place between 2010 and 2011 (Duarte, 2015). Samples were taken in the Atlantic Ocean, the Indian Ocean and the South Pacific. Another expedition that span the world's oceans was the *Tara* Oceans expedition that was started in 2009 and finished in 2013. This expedition included the collection of 35,000 samples at 210 sites focusing on planktonic organisms from the surface (0 - 200 m) and the mesopelagic zone (200 - 1000 m), complementing the GOS and the Malaspina expedition (Pesant *et al.*, 2015).

## 1.6 The discovery of new bilin biosynthesis enzymes

A “problem” of the expeditions mentioned in the previous paragraph is the sheer amount of genetic information that is gathered in the metagenomic-approaches. For that reason, the identification of interesting genes is mostly dependent on the bioinformatic processing of these datasets. In order to identify new AMGs in the metagenomic data collected during the GOS expedition, the VirMic project was created (Sharon *et al.*, 2011). This comprises a dataset that is enriched with viral scaffolds that carry genes with a microbial origin. The screening of this data led to the identification of several FDBR and phycobiliprotein lyase genes (Ledermann *et al.*, 2016). Interestingly, in phylogenetic analyses one of the discovered FDBRs showed that it did not cluster within the already characterized FDBRs. As it shares the most homology to the group of PcyA reductases (~ 30%) and the biochemical properties were unknown at this point, it was termed PcyX. Further analyses using the sequence of the discovered *pcyX* gene against the **C**ommunity cyberinfrastructure for **A**dvanced **M**icrobial **E**cology **R**esearch and **A**nalysis (CAMERA) server (Sun *et al.*, 2011) led to the identification of several other *pcyX* genes on GOS scaffolds which were predicted to be of viral origin (Ledermann *et al.*, 2016). Upstream to some of the discovered *pcyX* sequences, genes encoding for heme oxygenases were identified (*hemO*; Figure 14). This HO and FDBR “mini-cassette” was also discovered in two fosmid from uncultured Mediterranean Sea phages.

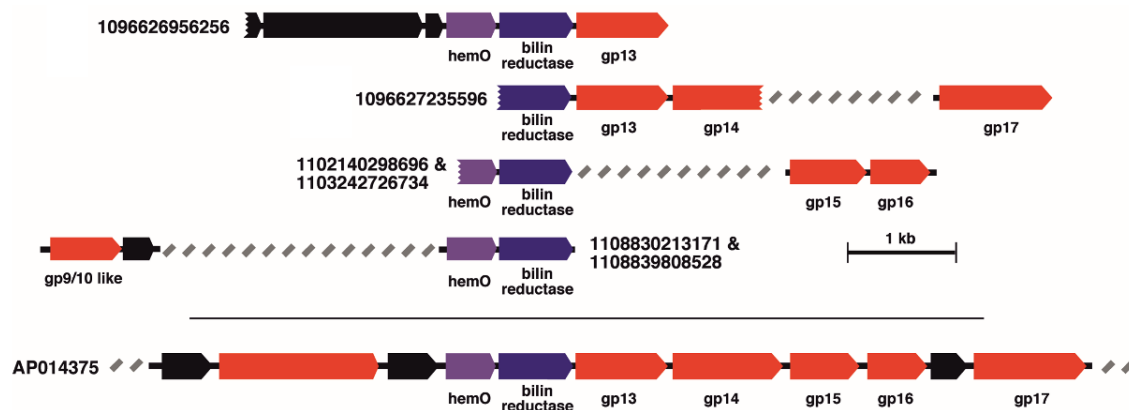


**Figure 14. Schematic maps of the GOS-scaffolds and a Mediterranean Sea fosmid on which the new bilin biosynthesis genes were discovered.** For reasons of clarity only a part of the AP014375 Mediterranean Sea fosmid map is shown. Dashed lines symbolize non-sequenced areas of the GOS clones. The predicted *hemO* ORFs are marked in purple and the predicted *pcyX* ORFs are marked in blue. ORFs with no homology to cultured microorganisms and viruses are marked in black and ORFs with a viral origin are colored red. Adapted from Ledermann *et al.*, 2016.

Phylogenetic comparison of the newly discovered HOs and FDBRs showed that both form distinct clusters in phylogenetic trees when compared to other members of the enzyme families (FDBRs - Figure 15).

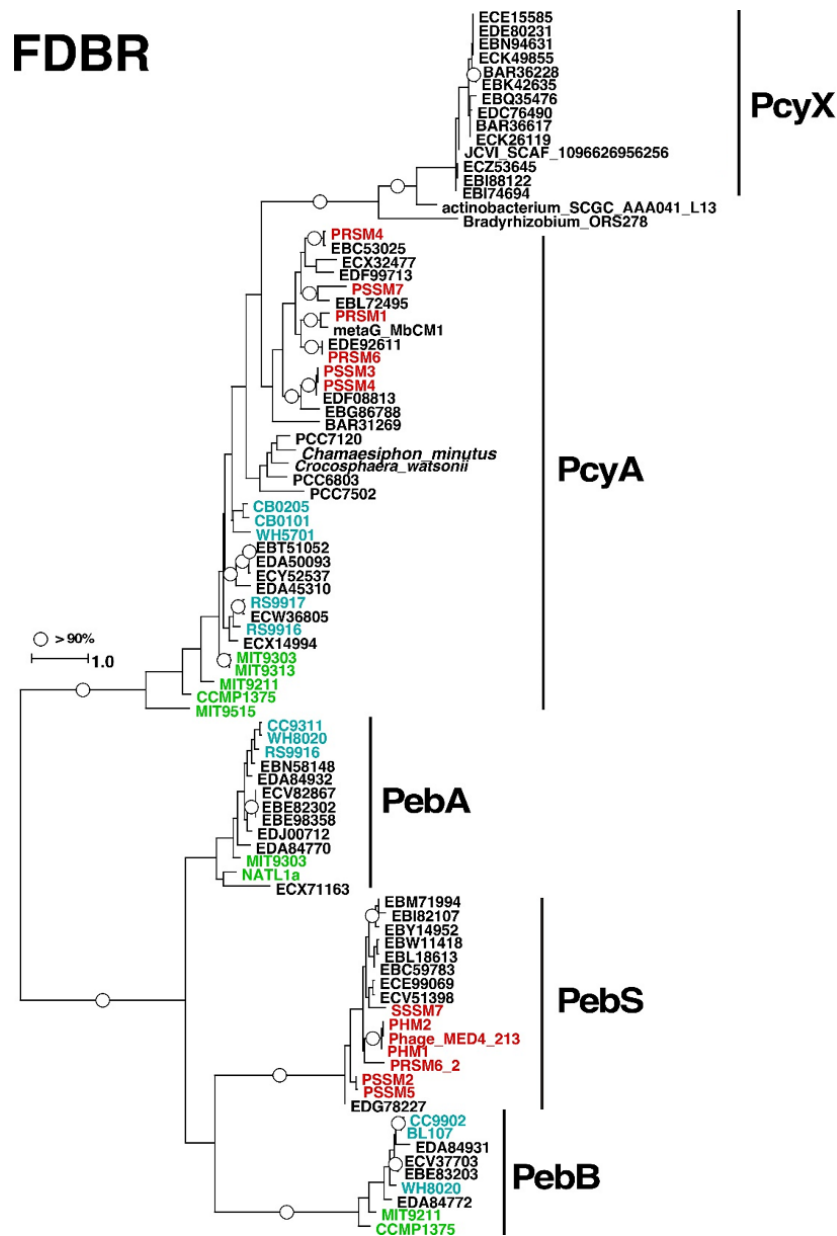


**Figure 15. Phylogenetic tree displaying the relationship between the members of the FDBR family.** FDBR sequences from cultured phages are shown in red. Sequences from *Synechococcus* sp. are shown in blue and sequences from *Prochlorococcus* sp. in green. The circles symbolize bootstrap values > 90%. Adapted from Ledermann *et al.*, 2016.

In order to identify the origin of the new bilin biosynthesis genes, the neighboring viral genes were examined. The phylogenetic comparison of the gp13 myophage neck protein that was discovered on some of the scaffolds (see Figure 14) revealed that they are most likely not derived from cyanophages, but could originate from phages that rather infect alphaproteobacteria (Ledermann *et al.*, 2016).

## 1.7 Objectives of this work

The discovery of novel, viral members of the HO- and FDBR-families raised the question, whether these sequences encode for active enzymes. Moreover, the characterization of the FDBR PebS revealed that the activity of enzymes cannot reliably be predicted based on phylogenetic analyses (Dammeyer *et al.*, 2008a). The objective of this work was to biochemically and biophysically investigate the recombinantly produced gene products of *hemO* and *pcyX*. A special focus was set on the characterization of the mechanisms underlying the reaction catalyzed by the PcyX FDBR group.

Another part of this project was to investigate the activity of the FDBR KflaHY2. This reductase was shown to catalyze the reduction of BV to PCB in indirect *in vivo* approaches reconstituting the bilin biosynthesis of the alga in *E. coli* (Rockwell *et al.*, 2017). To identify the reaction products in direct *in vitro* assays and to gain further insights into the reaction mechanism, the recombinant KflaHY2 reductase was biochemically characterized.

## 2 Material and Methods

### 2.1 Material and chemicals

All chemicals and reagents used in this study were ACS grade or better and were purchased from AppliChem (Darmstadt), Carl Roth (Karlsruhe), Merck (Darmstadt) and Sigma Aldrich (Munich) unless stated otherwise. For buffers, solutions and cultivation media ultra-pure water was used at a resistance of 18 M $\Omega$ . For the cultivation of bacteria all solutions were autoclaved or filter sterilized prior to use. The glass ware was sterilized by dry heat.

#### 2.1.1 Equipment

**Table 2. Instruments.**

Type of instrument	Name	Manufacturer
Agarose gel electrophoresis	Com Phor L Mini	Biozym
	Com Phor L Midi	
Autoclave	VX 150	Systec
Blotting equipment	Semidry Blot	Bio-Rad
	Trans-Blot® SD	
Centrifuges and rotors	Centrifuge 54115D	Eppendorf
	Rotor F-45-24-11	
	Z32HK	HERMLE
	Rotor 12/032	Thermo Fisher
	Sorvall LYNX 6000	
	Rotor T29	
EPR spectrometer	Rotor F9	Bruker
	Elexsys E580	
	Pulsed Microwave Bridge E580-1010	
	Cavity 4122SHQE-W1/1017	
FPLC	ÄktaPure	GE Healthcare
FPLC columns	HiLoad™ 16/600 Superdex™ 75	GE Healthcare
	pg	
	HisTrap™ FF 1 ml	
	HiTrap™ DEAE FF 5 ml	
	Superdex™ 75 10/300 GL	
Gel documentation	GeliX20 Imager	Intas
High pressure homogenizer	LM 10 Microfluidizer	Microfluidics
HPLC	1100 series	Agilent
HPLC column	Luna 5 $\mu$ m C18 (2) 100 A, 250 x	Phenomenex
	4,6 mm	
pH meter	Basic pH Meter P-11	Sartorius

Photometers	8453 UV visible System	Agilent
	NanoDrop™ Lite	Thermo Fisher
	Novaspec III	Amersham Bioscience
Power supply	PowerPac 300	Bio-Rad
Scales	AccuLab	Sartorius
	Research	Sartorius
SDS-PAGE	Mini-Protean® Tetra cell System	Bio-Rad
Thermocycler	T1 Thermocycler	Biometra
Ultrasonic homogenizer	UW 2200 with tip KE 76	Bandelin
Ultra-pure water system	MilliQ® Integral Water Purification System	Merck Millipore

### 2.1.2 Special chemicals, material, enzymes, kits and antibodies

**Table 3. Special chemicals and material.**

Type of material	Name	Manufacturer
Column material for affinity chromatography	Protino® Glutathione Agarose 4B	Macherey-Nagel
	Strep-Tactin® Sepharose®	IBA
Centrifugal concentrator	Vivaspin 6 10.000 MWCO PES	Sartorius
	Vivaspin 6 3.000 MWCO PES	
Crystallization plates 96 well	3550	Corning
Crystallization plates 24 well	XRL plates	Molecular Dimensions
Dialysis tubing	Visking MWCO 10,000	Carl Roth
DNA loading dye	DNA Gel Loading Dye Purple (6x)	New England Biolabs
DNA size standard	GeneRuler™ DNA Ladder Mix	Thermo Fisher
DNA stain	GelRed™	Biotium
Filter	PTFE, 0.2 µm/0.45 µm ø 4 mm	Phenex
Protein size standard	PageRuler™ prestained protein ladder	Thermo Fisher
PVDF membrane	Roti®-PVDF-Membrane	Carl Roth
Solid phase extraction	Sep-Pak®-light C18	Waters
Sterile filter	Rotilabo® 0.2 µm/0.45 µm ø 30 mm	Carl Roth

**Table 4. Enzymes and kits.**

Type of material	Name	Manufacturer
DNA ligase	T4 DNA Ligase	Thermo Fisher
DNA polymerase	Phusion High-Fidelity DNA Polymerase	Thermo Fisher
PCR clean-up kit	NucleoSpin® Gel and PCR Clean-up	Macherey-Nagel
Plasmid DNA miniprep kit	NucleoSpin® Plasmid EasyPure	Macherey-Nagel
Protease	PreScission Protease	GE Healthcare

Restriction Endonucleases	FastDigest line	Thermo Fisher
Site-Directed Mutagenesis	QuikChange Lightning	Agilent

**Table 5. Antibodies for Western Blot analyses.**

Antibody	Dilution	Antigen	Manufacturer
Goat anti-GST antibody	1:20000	GST-tag	Pharmacia Biotech
Rabbit anti-goat IgG-alkaline phosphatase conjugate	1:2000	Goat IgG	ImmunoResearch

### 2.1.3 Bacterial strains

**Table 6. Bacterial strains.**

Strain	Genotype	Reference
<i>E. coli</i> BL21 (DE3)	<i>F<sup>-ompT gal dcm lon hsdS<math>\beta</math>(r<sub>B</sub>-m<sub>B</sub>-)</sup></i> $\lambda$ (DE3 [lacI lacUV5-T7p07 ind1 sam7 nin5]) [malB+]K-12( $\lambda$ S)	Studier and Moffatt, 1986
<i>E. coli</i> JM83	<i>rpsL ara <math>\Delta</math>lac-proAB strA thi</i> [ $\Phi$ 80dlacZ $\Delta$ M15]	Vieira and Messing, 1982
<i>E. coli</i> XL10-Gold	endA1 glnV44 recA1 thi-1 gyrA96 relA1 lac Hte $\Delta$ (mcrA)183 $\Delta$ (mcrCB-hsdSMR-mrr)173 tet <sup>R</sup> F'[proAB lacI <sup>q</sup> Z $\Delta$ M15 Tn10(Tet <sup>R</sup> Amy Cm <sup>R</sup> )]	Agilent

### 2.1.4 Plasmids

**Table 7. Plasmids.**

Plasmid	Features	Affinity tag	Reference
pASK-IBA3- <i>bphP</i>	pASK-IBA3 derivate containing the <i>bphP</i> (PA 4117) gene from <i>Pseudomonas aeruginosa</i>	C-terminal Strep tag II	Tasler <i>et al.</i> , 2005
pASK- <i><math>\Phi</math>pcyX</i>	pASK-IBA-45(+) derivate containing a synthetic gene of <i><math>\Phi</math>pcyX</i> from marine metagenome	N-terminal Strep tag II	This study
pCWori- <i>pd</i>	pCWori derivate containing a gene encoding for putidaredoxin from <i>Pseudomonas putida</i> .		Donation of P. Ortiz de Montellano, UC SF
pET23a- <i>pdR</i>	pET-23a(+) derivate containing a gene encoding for putidaredoxin reductase from <i>Pseudomonas putida</i>	N-terminal T7 tag	Donation of P. Ortiz de Montellano, UC SF

pET28a-KflaHY2	pET-28a(+) derivate carrying a synthetic gene comprising the catalytic core region of KflaHY2 without the predicted chloroplast transit peptide	N-terminal His <sub>6</sub> tag	Donation of J. Clark Lagarias, UC Davis; unpublished
pET- <i>cph1</i>	pET derivate carrying the <i>cph1</i> gene from <i>Synechocystis</i> sp. PCC6803	C-terminal His <sub>6</sub> tag	Donation of J. Clark Lagarias, UC Davis
pGEX_ <i>ΦhemO_optimizer</i>	pGEX-6P-1 derivate containing a synthetic gene of <i>ΦhemO</i> from marine metagenome optimized for the codon usage of <i>E. coli</i> using the “Optimizer” web server ΦHemO = EBK42634 from GOS scaffold JCVI_SCAF_1101668336406	N-terminal GST tag	Donation of Oded Béjà, Technion Israel Institute of Technology Ledermann <i>et al.</i> , 2016
pGEX_ <i>mHY2</i>	pGEX-6P-1 derivate with mature <i>HY2</i> gene from <i>Arabidopsis thaliana</i>	N-terminal GST tag	Kohchi <i>et al.</i> , 2001
pGEX_ <i>pcyA</i>	pGEX-6P-1 derivate with <i>pcyA</i> from <i>Nostoc</i> sp. PCC7120	N-terminal GST tag	Frankenberg and Lagarias, 2003
pGEX_ <i>pcyA_Brady</i>	pGEX-6P-1 derivate containing a synthetic gene of <i>pcyA</i> from <i>Bradyrhizobium</i> sp. ORS 278	N-terminal GST tag	This study
pGEX_ <i>pcyX_actino</i>	pGEX-6P-1 derivate containing a synthetic gene of <i>pcyX</i> from the uncultured actinobacterium SCGC AAA041-L13 obtained by single cell genomics	N-terminal GST tag	This study
pGEX_ <i>ΦpcyX</i>	pGEX-6P-1 derivate containing a synthetic gene of <i>ΦpcyX</i> from marine metagenome (ΦPcyX = EBK 42635 from GOS scaffold JCVI_SCAF_1101668336406)	N-terminal GST tag	Donation of Oded Béjà, Technion Israel Institute of Technology Ledermann <i>et al.</i> , 2016
pGEX_ <i>ΦpcyX_optimizer</i>	pGEX-6P-1 derivate containing a synthetic gene of <i>ΦpcyX</i> from marine metagenome ( <i>ΦpcyX</i> = EBK 42635 from GOS scaffold JCVI_SCAF_1101668336406; adapted to the codon usage of <i>E. coli</i> ).	N-terminal GST tag	Donation of Oded Béjà, Technion Israel Institute of Technology Ledermann <i>et al.</i> , 2016
pGEX_ <i>ΦpcyX_D55E</i>	Derivate of pGEX_ <i>ΦpcyX</i> obtained by site-directed mutagenesis.	N-terminal GST tag	This study
pGEX_ <i>ΦpcyX_D55N</i>	Derivate of pGEX_ <i>ΦpcyX</i> obtained by site-directed mutagenesis	N-terminal GST tag	This study
pGEX_ <i>ΦpcyX_M67I</i>	Derivate of pGEX_ <i>ΦpcyX</i> obtained by site-directed mutagenesis	N-terminal GST tag	This study

pGEX_ <i>φ</i> pcyX_H69Q	Derivate of pGEX_ <i>φ</i> pcyX obtained by site-directed mutagenesis	N-terminal GST tag	This study
pGEX_ <i>φ</i> pcyX_C71A	Derivate of pGEX_ <i>φ</i> pcyX obtained by site-directed mutagenesis	N-terminal GST tag	This study
pGEX_ <i>φ</i> pcyX_D86N	Derivate of pGEX_ <i>φ</i> pcyX obtained by site-directed mutagenesis	N-terminal GST tag	This study
pGEX_ <i>φ</i> pcyX_N198D	Derivate of pGEX_ <i>φ</i> pcyX obtained by site-directed mutagenesis	N-terminal GST tag	This study
pGEX_ <i>φ</i> pcyX_H200Q	Derivate of pGEX_ <i>φ</i> pcyX obtained by site-directed mutagenesis	N-terminal GST tag	This study
pGEX_ <i>pebS</i>	pGEX-6P-3 derivate with a synthetic gene of <i>pebS</i> from P-SSM2	N-terminal GST tag	Dammeyer <i>et al.</i> , 2008a
pGEX- <i>petF</i> -P-SSM2	pGEX-6P-3 derivate carrying a synthetic gene of the ferredoxin <i>petF</i> from the cyanophage P-SSM2	N-terminal GST tag	Dammeyer <i>et al.</i> , 2008a
pGEX- <i>petH</i>	pGEX derivate carrying a gene of <i>petH</i> from <i>Synechococcus</i> sp. PCC 7002	N-terminal GST tag	Lab stock Frankenberg-Dinkel
pGro7	Chaperone plasmid carrying the genes encoding for <i>groEL/groES</i>		TaKaRa

### 2.1.5 Oligonucleotides

#### *Oligonucleotides for the construction of expression vectors*

**Table 8. Oligonucleotides for the construction of expression vectors.**

No.	Primer	Sequence 5' – 3'	Construction of plasmid
1	PcyX 45plus fwd	GCG AAT TCA ATG ATT TGG GAA AGA C	pASK_ <i>φ</i> pcyX
2	PcyX 45plus rev	GCC TCG AGT TAT TTC AAG TAG GG	pASK_ <i>φ</i> pcyX
3	ActPcyXEcofwd	GTT TAC GAA TTC ATG AAT AGT GTG TGG GAT AG	pGEX_ <i>pcyX_actino</i>
4	ActPcyXXhorev	GAT ATC CTC GAG TTA CTT AAT TTC TGG AAA CAA AC	pGEX_ <i>pcyX_actino</i>
5	BraPcyXEcofwd	GTT TAC GAA TTC ATG AGT GAT GGG GAC G	pGEX_ <i>pcyA_Brady</i>
6	BraPcyXXhorev	GAT ATC CTC GAG TCA ATC GAC ATG CGC	pGEX_ <i>pcyA_Brady</i>

*Oligonucleotides used for site-directed mutagenesis*

For reasons of clarity, only the forward primers are listed, as the reverse primers are complementary to them. The sites where the mutations were introduced are underlined.

**Table 9. Oligonucleotides used for site-directed mutagenesis generating different variants of pGEX\_φpcyX.**

No.	Primer	Sequence 5' – 3'	Construction of plasmid
1	PcyX D55E fwd	GAA GAG CTC ATC TTG <u>AGG</u> TAG TTG ATG TTA GAG	pGEX_φpcyX_D55E
2	PcyX D55N fwd	GAA GAG CTC ATC TTA <u>ACG</u> TAG TTG ATG	pGEX_φpcyX_D55N
3	PcyX M67I fwd	GAA TCT AAA GGT CTT TGG ATA <u>GCT</u> CAT CTA TGT TTA TTT C	pGEX_φpcyX_M67I
4	PcyX H69Q fwd	CTA AAG GTC TTT GGA TGG CTC <u>AAC</u> TAT GTT TAT TTC CTA TGT TGA	pGEX_φpcyX_H69Q
5	PcyX C71A fwd	CTT TGG ATG GCT CAT CTA <u>GCT</u> TTA TTT CCT ATG TTG AC	pGEX_φpcyX_C71A
6	PcyX D86N fwd	CGA TTT ACG GTT TTA <u>ATA</u> TTA TTG CAG GTG	pGEX_φpcyX_D86N
8	PcyX N198D fwd	GAA CAT CAA CAA AAG <u>GAT</u> CCT CAC ACG CCT AG	pGEX_φpcyX_N198D
10	PcyX H200Q fwd	CAA AAG AAT CCT CAA <u>ACG</u> CCT AGA GTT ATG	pGEX_φpcyX_H200Q

## 2.2 Microbiological methods

### 2.2.1 Culture media and supplements

For the cultivation of *E. coli* Lysogeny Broth (LB)- and 2YT-medium with appropriate antibiotics and supplements was used. Solid media were prepared by the addition of 1.5 % (w/v) Agar Agar prior to sterilization.

#### LB-medium (Lennox)

Tryptone 10 g/l  
Yeast extract 5 g/l  
NaCl 5 g/l

#### 2YT-medium

Tryptone 16 g/l  
Yeast extract 10 g/l  
NaCl 5 g/l

**Table 10. Media supplements.**

Supplement	Stock concentration	Final concentration
Ammonium ferric citrate	12 mg/ml	12 mg/l
Ampicillin (Amp)	100 mg/ml	100 mg/l
Anhydrotetracycline (AHT)	2 mg/ml	200 µg/l
L(+)-Arabinose	100 mg/ml	1 g/l
Chloramphenicol (Cm)	34 mg/ml	34 mg/l
Riboflavin	400 µg/ml	10 µg/l
Isopropyl-β-D-thiogalactopyranoside (IPTG)	1 M	0.5 – 1 mM

### 2.2.2 Storage of *E. coli* cells

*E. coli* cells were stored for longer periods as 40% (v/v) glycerol stocks at -80°C.

### 2.2.3 Cultivation of *E. coli* cells

For the preparation of pre-cultures 5 ml of LB-medium supplemented with the respective antibiotic (Table 10) was inoculated either with a single colony of a freshly transformed *E. coli* culture or with a glycerol stock. The pre-culture was incubated overnight under constant shaking at 170 rpm and 37°C (SM 30 CONTROL, Edmund Buehler). On the next day, the main-cultures were prepared by inoculating LB- or 2YT-medium containing the appropriate antibiotic 1:100 with the pre-culture. The cultures were incubated at 37°C and 90 rpm (Innova®44, New Brunswick Scientific) to an OD<sub>578nm</sub> of ~ 0.4 – 0.6. Gene expression was induced after a construct specific reduction of the temperature.

### 2.2.4 Determination of cell densities

Cell densities in liquid cultures were determined by measuring the optical density at 578 nm using the cultivation medium as reference.

### 2.2.5 Preparation of chemically competent *E. coli* cells

For the preparation of chemically competent *E. coli* cells 70 ml LB-medium, supplemented with 5 mM MgCl<sub>2</sub> and 5 mM MgSO<sub>4</sub>, were inoculated 1:100 with an overnight culture of the respective *E. coli* strain. The culture was grown at 37°C and 160 rpm to an OD<sub>578nm</sub> of ~ 0.4 – 0.6. Then, 25 ml of the culture were pelleted by centrifugation for 10 min at 4000 rpm (Z32HK Hermle, rotor 12/032). The pellet was resuspended in 12.5 ml ice-cold TMF buffer and was incubated on ice for 1 h. After another centrifugation step (10 min, 4000 rpm, Z32HK Hermle, rotor 12/032), the cells were resuspended in a mixture of 2.5 ml TMF buffer and 750 µl glycerol. Afterwards, the cells were transferred in 200 µl aliquots into reaction tubes and were stored at -80°C prior to use.

### TMF buffer

CaCl<sub>2</sub> 100 mM

MnCl<sub>2</sub> 40 mM

RbCl<sub>2</sub> 50 mM

### **2.2.6 Transformation of chemically competent *E. coli* cells**

For the transformation of chemically competent *E. coli*, the cells were thawed on ice and subsequently, 1 µl of plasmid DNA or 10 µl of a ligation reaction were added. Afterwards, the cells were incubated on ice for 30 min, followed by a heat shock for 2 min at 42°C. After the cells were chilled on ice for 2 min, 700 µl LB-medium were added and the cells were incubated for 1 h at 37°C and 180 rpm (SM 30 CONTROL, Edmund Buehler). Lastly, the cells were plated on selective LB-agar plates followed by an incubation overnight at 37°C. To create *E. coli* strains that carry two different plasmids, the cells were first transformed with one plasmid and chemically competent cells were prepared using the transformed cells. Then, the second plasmid was transferred into the cells by transformation.

## **2.3 Molecular biological techniques**

### **2.3.1 Preparation of plasmid DNA**

Plasmid DNA was prepared from *E. coli* JM83. Therefore, a single colony of a freshly transformed *E. coli* culture was used to inoculate 5 ml LB medium containing the appropriate antibiotic. The culture was incubated overnight at 37°C and 180 rpm (SM 30 CONTROL, Edmund Buehler). The plasmid DNA was prepared using the NucleoSpin® Plasmid EasyPure Kit (Macherey Nagel) according to the manufacturer's instructions.

### **2.3.2 Determination of the concentration of DNA in aqueous solution**

The concentration of DNA in aqueous solutions was determined by measuring the absorbance at 260 nm using a NanoDrop™ Lite photometer (Thermo Fisher) and the corresponding software. The purity of the samples was determined by the comparison of the absorbance at 260 nm ( $A_{260}$ ) and 280 nm ( $A_{280}$ ). For double-stranded DNA an  $A_{260}/A_{280}$  ratio of ~ 1.8 – 2.0 was accepted as sufficiently pure.

### **2.3.3 Agarose gel electrophoresis**

The separation of DNA fragments according to their size was achieved by agarose gel electrophoresis (Aaij and Borst, 1972). All agarose gels were prepared by dissolving 1% (w/v) of agarose in boiling 1x TAE buffer. After the solution had cooled down to ~ 60°C, the DNA stain GelRed™ was added to the solution (1:20000 (v/v)). The samples were mixed with 6x loading dye before loading. The separation was performed in 1x TAE buffer at a

constant current of 100 V. The DNA fragments were visualized by the fluorescence of the DNA-GelRed complex after excitation with UV light (312 nm). The size of the fragments was estimated by comparison with the GeneRuler™ DNA Ladder Mix (Thermo Fisher).

#### TAE buffer (50x)

Tris/acetate pH 8.0 2 M

EDTA 50 mM

#### **2.3.4 Polymerase chain reaction**

The polymerase chain reaction (PCR) was used for the amplification of DNA fragments and for the specific introduction of restriction sites (Mullis and Faloona, 1987). To avoid mutations during the amplification process, all PCR reaction were carried out using the Phusion High-Fidelity DNA Polymerase (Thermo Fisher), as it possesses a 3'-5' exonuclease proofreading activity.

#### PCR-reaction

Template	10 ng
5x Phusion HF Buffer	10 µl
dNTPs	0.2 mM each
Forward Primer	0.5 µM
Reverse Primer	0.5 µM
Phusion HF DNA Polymerase	1 U
H <sub>2</sub> O	ad 50 µl

**Table 11. PCR thermal-cycling program.**

Cycle step	Temperature	Duration	
Initial Denaturation	98°C	30 s	
Denaturation	98°C	10 s	} 30 cycles
Annealing	Primer specific	20 s	
Elongation	72°C	30 s/kb	
Final Elongation	72°C	420 s	

#### **2.3.5 Purification of PCR products**

PCR products were purified using the NucleoSpin® Gel and PCR Clean-up Kit (Macherey Nagel) according to manufacturer's instructions.

### 2.3.6 Restriction of DNA

Restriction of DNA was carried out using FastDigest enzymes (Thermo Fisher) in FD Green Buffer according to manufacturer's instructions. Test restrictions were performed in a total volume of 10 µl for 20 min at 37°C. Preparative DNA digestion was achieved in bigger approaches up to a total volume of 50 µl with an incubation at 37°C for 45 min. If two different enzymes were needed for the restriction, the digestion was performed stepwise with a thermal inactivation for 5 min at 80°C in between.

### 2.3.7 Gel extraction of DNA fragments

Digested DNA was purified in an agarose gel electrophoresis and the corresponding band was cut out from the gel. The DNA was extracted using the NucleoSpin® Gel and PCR Clean-up Kit (Macherey Nagel) according to manufacturer's instructions.

### 2.3.8 Ligation of DNA fragments

The ligation of DNA fragments was carried out by using T4 DNA Ligase (Thermo Fisher). For the ligation reaction 100 ng of vector DNA was incubated with a 3-fold molar excess of insert DNA. The reaction was performed in a total volume of 20 µl for 1 h at room temperature. The T4 DNA Ligase was inactivated for 5 min at 70°C prior to the transformation of the ligation product into chemically competent *E. coli* JM83 cells.

#### Ligation reaction

Vector DNA	100 ng
Insert DNA	3-fold molar excess to vector
10x T4 DNA Ligase buffer	2 µl
T4 DNA Ligase	5 U
H <sub>2</sub> O	ad 20 µl

### 2.3.9 Construction of expression vectors

For the expression of genes derived from metagenomics data, synthetic genes were cloned into vectors suitable for the overexpression in *E. coli*. The synthetic genes were obtained by ATUM (Newark, California). The appropriate restriction sites for the cloning of the genes into the vectors were introduced by PCR via the primers listed in Table 8. The obtained PCR products were cut with the corresponding restriction enzymes and ligated into the similarly cut vector. The ligation products were transformed into *E. coli* JM83. The cells were plated on selective agar plates and the obtained colonies were used for the inoculation of 5 ml overnight cultures prepared in LB medium containing the respective antibiotic. The

overnight cultures were used for the preparation of plasmid DNA. The isolated plasmids were verified by DNA sequence analyses.

### 2.3.10 DNA sequence analysis

The sequences of isolated plasmid DNA were analyzed either at Eurofins Genomics (Ebersberg) or GATC Biotech (Konstanz).

### 2.3.11 Site-directed mutagenesis

Different variants of GST-tagged  $\Phi$ PcyX protein were created by site-directed mutagenesis. The introduction of specific mutations was performed via specific primers harboring either single or double base exchanges (Table 9). The corresponding plasmids were generated using the QuikChange Lightning Kit (Agilent) according to manufacturer's instructions. The obtained constructs were sequenced prior to use.

## 2.4 Protein biochemical and biophysical methods

### 2.4.1 Production of recombinant proteins in *E. coli*

The proteins used in this study were produced in *E. coli* BL21 (DE3). For the production of GST- $\Phi$ PcyX and the corresponding variants, the cells were grown in 2YT-medium containing 100 mg/l ampicillin. For the production of all other proteins, the cells were grown in LB-medium containing appropriate selection markers (Table 10). For the expression of pGEX-*petH* or pET23a-*pdR* the medium was supplemented with 10  $\mu$ g/l riboflavin. The main culture was inoculated 1:100 with an overnight culture of *E. coli* BL21 (DE3) carrying the respective plasmid. The cells were grown at 37°C under constant shaking at 90 rpm (Innova®44, New Brunswick Scientific) to an OD<sub>578nm</sub> of ~ 0.4 – 0.6. Before the induction, the cells carrying pCWori-*pd* were supplemented with 12 mg/l ammonium ferric citrate. After a temperature switch to 17°C (all pGEX- and pASK-derived constructs), or 20 °C (pET23a-*pdR* and pCWori-*pd*) or 24°C (pET-*cph1*), the protein expression was induced by the addition of either IPTG (0.5 mM for all pGEX-derived constructs and pET23a-*pdR* or 1 mM pET-*cph1*, pET28a-*KflaHY2* and pCWori-*pd*) or AHT (200  $\mu$ g/l for all pASK constructs). After the induction, the cells were incubated overnight under constant shaking at 90 rpm. On the next morning the cells were harvested by centrifugation for 8 min at 17000 x g (Sorvall LYNX 6000 Centrifuge) and stored at -20°C.

To improve the solubility of the PcyA\_Brady protein, pGEX-*pcyA*\_Brady was coexpressed with the chaperone plasmid pGro7. Therefore, the medium was supplemented with 60 mg/l ampicillin, 20 mg/l chloramphenicol and 1 g/l L-(+)-arabinose. Otherwise the expression conditions were similar to standard pGEX-derived constructs.

The ferredoxin PetF (i.e. Fd<sub>P-SSM2</sub>) from the cyanophage P-SSM2 was produced as described previously (Dammeyer *et al.*, 2008a).

#### 2.4.2 Protein purification

##### *Affinity chromatography of GST- and Strep-tagged proteins*

Prior to purification the cells containing the overproduced proteins were thawed overnight on ice. On the next morning, cells were resuspended either in ice-cold PBS (GST-tagged proteins) or in ice-cold Buffer W (Strep-tagged proteins). After the addition of a spatula tip of lysozyme and DNaseI, the suspension was chilled on ice for 30 min. The cells were lysed using a microfluidizer for three rounds at 18000 psi or by sonication using an ultrasonic homogenizer for 3x 2.5 min (cycle 6/10; ~ 60% power output; Bandelin UW 2200 with tip KE 76). To separate the soluble parts from the debris, the lysate was centrifuged for 45 min at 50000 x g (Sorvall™ LYNX™ 6000 centrifuge) and filtered afterwards through a 0.45 µm syringe filter. The filtered lysate was passed through gravity flow columns packed with Protino® Glutathione Agarose 4B (equilibrated with PBS; GST-tagged proteins) or StrepTactin® sepharose® (equilibrated with Buffer W; Strep-tagged proteins). The columns were washed with 10 column volumes (CV) of ice-cold PBS (GST-tagged proteins) or ice-cold Buffer W (Strep-tagged proteins). In the next step, the proteins were eluted with 3 CV of GST-elution buffer (GST-tagged proteins) or Buffer E (Strep-tagged proteins). After the success of the purification had been verified by SDS-PAGE, the protein containing fractions of Strep-tagged proteins were dialyzed overnight against the desired assay buffer.

To rule out any influence of the tag on the activity of the protein, all GST-tagged proteins were treated with PreScission Protease before they were used in biochemical or biophysical experiments. The protease cleaves the fusion protein at a recognition sequence in the linker region between the GST tag and the protein of interest. Therefore, 5 µl PreScission Protease were added to 15 ml of eluted protein solution obtained by affinity chromatography. After a dialysis overnight against PreScission Protease cleavage buffer at 4°C, the dialysate was transferred onto a second column packed with Protino® Glutathione Agarose 4B. The flow-through was collected and the protein was dialyzed against the desired assay buffer.

The dialysate was concentrated using Vivaspin® 6 concentrators with a molecular weight cut off (MWCO) of 3000 Da or 10000 Da, depending on the size of the protein. The concentration of the purified protein was determined based on its absorbance at 280 nm. Extinction coefficients were calculated as described by Gill and von Hippel (Gill and von Hippel, 1989).

<u>10x PBS buffer</u>		<u>GST-elution buffer</u>	
NaCl	1.4 M	Tris/HCl pH 8.0	50 mM
KCl	27 mM	Glutathione	10 mM
Na <sub>2</sub> HPO <sub>4</sub>	100 mM		
KH <sub>2</sub> PO <sub>4</sub>	18 mM		
pH 7.4			

<u>Buffer W</u>		<u>Buffer E</u>	
Tris/HCl pH 8.0	100 mM	Buffer W with 2.5 mM desthiobiotin	
NaCl	150 mM		
EDTA	1 mM		

#### PreScission Protease cleavage buffer

Tris/HCl pH 7.5	50 mM
NaCl	150 mM
EDTA	1 mM
DTT	1 mM

For the protease treatment of proteins carrying [2Fe-2S]-clusters the buffer was prepared without EDTA.

#### *Affinity chromatography of His-tagged KflaHY2*

The His<sub>6</sub>-tagged KflaHY2 protein was purified by affinity chromatography using an Äkta pure system with a 1 ml HisTrap<sup>TM</sup> FF column. The pellets were thawed on ice and resuspended in “binding buffer”. After the addition of a spatula tip of DNaseI and lysozyme the suspension was kept on ice for 30 min. Afterwards, the cells were disrupted by sonication for 2 x 2.5 min (Bandelin Sonopuls HD 2200; tip KE76; cycle 6/10; ≈ 60% power output) and centrifuged for 45 min at 50000 x g (Sorvall<sup>TM</sup> LYNX<sup>TM</sup> 6000 centrifuge) and 4°C. The lysate was filtered using a 0.45 µm syringe filter and loaded onto a 1 ml HisTrap<sup>TM</sup> FF column at a flow rate of 1 ml/min. The column was washed with 10 CV of binding buffer and the protein was eluted applying a gradient from 0 – 100% “elution buffer” in 10 CV at a flow rate of 1 ml/min. Protein containing fractions were pooled and dialyzed overnight against TES-KCl buffer. The dialysate was concentrated using Vivaspin® 6 concentrators with a MWCO of 10000 Da. The concentration of the purified protein was determined based on its absorbance at 280 nm (Gill and von Hippel, 1989).

<u>Binding buffer</u>		<u>Elution buffer</u>	
NaH <sub>2</sub> PO <sub>4</sub> pH 7.4	20 mM	NaH <sub>2</sub> PO <sub>4</sub> pH 7.4	20 mM
Imidazole	30 mM	Imidazole	500 mM
NaCl	500 mM	NaCl	500 mM

TES-KCl buffer

TES/KOH pH 7.5	25 mM
KCl	100 mM

*Purification by anion exchange chromatography*

Putidaredoxin (Pd) and the corresponding putida redoxin reductase (PdR) were purified by anion exchange chromatography. Therefore, the cells overexpressing the respective constructs were thawed overnight on ice and were afterwards resuspended in “low salt buffer”. After the addition of a spatula tip of DNaseI and lysozyme, the cells were disrupted using a microfluidizer at 15000 psi. After a centrifugation step for 1 h at 50000 x g and 4°C (Sorvall™ LYNX™ 6000 centrifuge), the lysate was filtered and applied to a 5 ml HiTrap™ DEAE FF column. The column was washed with 8 CV of “low salt buffer”. The protein of interest was eluted with a linear gradient to 50% “high salt buffer” in 20 CV. The fractions containing Pd or PdR were pooled and concentrated using Vivaspin® 6 concentrators with a MWCO of either 10000 Da (PdR) or 3000 Da (Pd). To improve the purity, the proteins were further purified by size exclusion chromatography (SEC) using a Superdex75™ 10/300 GL column. Prior to use the column was equilibrated with TES-KCl buffer containing 15% (v/v) glycerol. The SEC was performed at a constant flow rate of 1 ml/min. The fractions containing the respective proteins were pooled and concentrated. The concentration of the proteins was determined based on the absorbance of their cofactors.

Low salt buffer

Tris/HCl pH 7.8	20 mM
NaCl	10 mM

High salt buffer

Tris/HCl pH 7.8	20 mM
NaCl	1 M

TES-KCl (15% glycerol)

TES/KOH pH 7.5	25 mM
KCl	100 mM
Glycerol	15% (v/v)

**2.4.3 SDS-polyacrylamide gel electrophoresis**

Proteins were separated and analyzed according to their molecular weight by SDS-polyacrylamide gel electrophoresis (SDS-PAGE) under reducing conditions in a discontinuous system according to Laemmli (Laemmli, 1970). This system comprises a stacking gel with an acrylamide concentration of 5.25% (pH 6.8) and a separation gel with an acrylamide concentration of 12.5% or 15% (pH 8.8). The negatively charged, denaturing detergent sodium dodecyl sulfate (SDS) binds proteins in a specific ratio of 1.4 g SDS/1 g

of protein. This leads to an almost constant mass:charge ratio and allows the separation of proteins in the electric field depending on their molecular weight. The samples were prepared by the addition of 4x loading dye and incubation for 5 min at 95°C prior to loading onto the gel. The electrophoresis was performed by applying a constant current of 200 V until the tracking dye reached the bottom of the gel. Afterwards, the proteins were visualized by incubation for 5 min under constant shaking with staining solution containing Coomassie Brilliant Blue G250. To enhance the contrast, the gels were discolored by shaking in destaining solution for additional 5 min.

4x Stacking gel buffer

Tris/HCl pH 6.8	0.5 M
SDS	0.4% (w/v)

4x Separation gel buffer

Tris/HCl pH 8.8	1.5 M
SDS	0.4% (w/v)

4x Loading dye

Tris	100 mM
SDS	8% (w/v)
Glycerol	40% (v/v)
β-Mercaptoethanol	10% (v/v)
Bromphenol blue	1% (w/v)

10x SDS-PAGE running buffer

Tris/HCl pH 8.8	250 mM
Glycine	1,92 M
SDS	1% (w/v)

Stacking gel 5.25% (4 mini gels)

Rotiphorese Gel 30 (30 % acrylamide, 0.8 % bis-acrylamide)	1.4 ml
4x Stacking gel buffer	2 ml
H <sub>2</sub> O	4.6 ml
APS (10% w/v)	30 µl
TEMED	20 µl

Separating gel 12.5% (4 mini gels)

Rotiphorese Gel 30 (30 % acrylamide, 0.8% bis-acrylamide)	6.7 ml
4x Separating gel buffer	4 ml
H <sub>2</sub> O	5.3 ml
APS (10% w/v)	80 µl
TEMED	8 µl

Staining solution

Acetic acid	10% (v/v)
Ethanol	30% (v/v)
Coomassie brilliant blue G250	0.25% (w/v)

Destaining solution

Acetic acid	10% (v/v)
Ethanol	30% (v/v)

#### 2.4.4 Immuno-staining of immobilized proteins (Western Blot)

Western Blot analysis uses antibodies to specifically detect proteins in a sample after SDS-PAGE and a transfer of the proteins onto a membrane (Towbin *et al.*, 1979). Therefore, the protein samples were separated according to their molecular weight by SDS-PAGE and subsequently transferred onto a PVDF membrane using the semi-dry technique. Before the proteins were transferred, the gel was equilibrated for 5 min in Towbin transfer buffer and the membrane was activated by wetting with methanol. After the activation, the membrane was equilibrated in Towbin transfer buffer together with the gel and two blotting papers (Whatman; 3 mm). The blotting construction was set up as follows: The equilibrated gel and the membrane were placed between the two blotting papers and the sandwich was placed between the anode and the cathode of the blotting machine. The electroblotting was performed for 20 min at a constant current of 15 V. To saturate non-specific binding sites, the membrane was incubated under constant shaking in blocking solution overnight at 4°C. For the detection of GST-tagged proteins, the membrane was incubated with the primary antibody (diluted 1:20000 in blocking solution) for at least 1 h under constant shaking. In the next step, the membrane was washed three times for 5 min with PBS-T buffer, followed by the incubation with the second antibody (diluted 1:2000 in blocking solution) under constant shaking for 1 h. Subsequently, the membrane was washed three times with PBS-T buffer and three times with PBS buffer. Afterwards, the secondary antibody-AP conjugate was detected by incubation with a BCIP/NBT detection solution in AP buffer.

##### Towbin transfer buffer

Tris-base	25 mM
Glycine	192 mM

##### 10x PBS buffer

NaCl	1.4 M
KCl	27 mM
Na <sub>2</sub> HPO <sub>4</sub>	100 mM
KH <sub>2</sub> PO <sub>4</sub>	18 mM
pH 7.4	

##### PBS-T buffer

1x PBS buffer	
Tween-20	0.1% (v/v)

##### Blocking solution

1x PBS-T buffer	
Albumin fraction V	3% (w/v)

##### AP buffer

Tris/HCl pH 9.5	100 mM
NaCl	100 mM
MgCl <sub>2</sub>	5 mM

##### NBT solution

NBT	10% (w/v) in 70% DMF
-----	----------------------

##### BCIP solution

BCIP	5% (w/v) in DMF
------	-----------------

Detection solution

1x AP buffer	
NBT solution	0.33% (v/v)
BCIP solution	0.66% (v/v)

**2.4.5 Determination of protein and bilin concentrations**

The concentration of proteins purified by affinity chromatography was determined by their absorbance at 280 nm. The amino acids that contribute to the absorption at 280 nm are cysteine, tryptophan and tyrosine and therefore, the molar extinction coefficients of proteins can be calculated depending on their content of these amino acids as described by Gill and von Hippel according to the following formula (Gill and von Hippel, 1989):

$$\epsilon_{280} = (n_{\text{Trp}} \cdot 5690 + n_{\text{Tyr}} \cdot 1280 + n_{\text{Cys}} \cdot 120) \text{M}^{-1} \text{cm}^{-1}$$

$n_x$  = number of the amino acid per molecule of protein

The concentration of the protein is then calculated in accordance to Lambert-Beer's law:

$$c = \frac{A_{280}}{\epsilon_{280}} \cdot d$$

$$c = \text{concentration in } \frac{\text{mol}}{\text{l}}$$

$$A_{280} = \text{absorption at 280 nm}$$

$$\epsilon_{280} = \text{molar extinction coefficient at 280 nm}$$

$$d = \text{light path in the cuvette in cm}$$

The calculated extinction coefficients of the proteins examined in this study are given in the table below. The extinction coefficients of GST-tagged constructs were calculated for the proteins after protease treatment.

**Table 12. Molar extinction coefficients of the proteins examined in this study.**

Protein	Extinction coefficient $\epsilon_{280}$ [ $\text{M}^{-1} \text{cm}^{-1}$ ]
$\Phi$ HemO	35820
$\Phi$ PcyX	54600
His <sub>6</sub> -KflaHY2	36116
HY2	33418
PcyA	27305
PcyA_Brady	26720
PcyX_actino	46470
PebS	37485

Moreover, the concentrations of proteins carrying either [2Fe-2S]-clusters or flavin adenine dinucleotide (FAD) cofactors were determined using the corresponding extinction coefficients.

$\epsilon_{420}$  [2Fe-2S]-cluster:  $9.7 \text{ mM}^{-1}\text{cm}^{-1}$  (Shin and Oshino, 1978)

$\epsilon_{455}$  FAD cofactor:  $10.4 \text{ mM}^{-1}\text{cm}^{-1}$  (Gunsalus and Wagner, 1978)

The concentrations of BV and PΦB were determined by their absorption using the following extinction coefficients:

$\epsilon_{698}$  BV in 2.5% HCl in MeOH:  $32.6 \text{ mM}^{-1}\text{cm}^{-1}$  (Heirwegh *et al.*, 1991)

$\epsilon_{386}$  PΦB in 2% HCl in MeOH:  $64.6 \text{ mM}^{-1}\text{cm}^{-1}$  (Terry *et al.*, 1995)

#### 2.4.6 Size exclusion chromatography

To determine the oligomerization state of affinity purified proteins, they were analyzed by size exclusion chromatography (Moore, 1964). SEC is a method that separates the analytes based on their hydrodynamic radius. For globular proteins, the hydrodynamic radius is directly related to their size. This allows a size determination by comparison of the elution volume of the protein of interest with the elution volumes of standard proteins. The SEC experiments were performed using an Äkta Pure FPLC-system with a Superdex™ 75 10/300 GL column. The column was equilibrated with TES-KCL buffer prior to use and the flow rate was set to 1 ml/min. The samples were transferred onto the column using a 500  $\mu\text{l}$  loop.

The calibration curve for the size determination was created by plotting the log of the MW of standard proteins against the quotient of the elution volume ( $V_e$ ) and the void volume ( $V_0$ ). The calibration curve was calculated using a linear regression in Origin.

The standards used for the calibration were: Conalbumin (MW = 75 kDa), albumin (MW = 66 kDa), carbonic anhydrase (MW = 29 kDa) and cytochrome C (MW = 12.4 kDa). The void volume of the column was determined by the elution volume of Blue Dextran 2000 (MW ~ 2000 kDa). All standards were obtained from Sigma-Aldrich.

#### 2.4.7 Heme oxygenase activity assays

The activity of purified HOs was assayed in a HO activity test employing equimolar amounts of HO and hemin as the substrate. The electrons required for the reaction were supplied by an NADPH-regenerating system (NRS) based on glucose-6-phosphat (G6P) and glucose-6-phosphate dehydrogenase (G6PDH). In this reaction, the oxidation of G6P to 6-phosphogluconolactone simultaneously leads to a reduction of NADP<sup>+</sup> to NADPH. NADPH itself is employed as cofactor by the enzyme ferredoxin-NADP<sup>+</sup> reductase (FNR) that

catalyzes the reduction of oxidized ferredoxin ( $Fd_{ox}$ ) to reduced ferredoxin ( $Fd_{red}$ ).  $Fd_{red}$  serves as the electron donor for the HOs. In all assays ferredoxin from the cyanophage P-SSM2 ( $Fd_{P-SSM2}$ ) was used as the electron donor. The employed FNR was PetH from *Synechococcus* sp. PCC 7002.

Initially, all components of the reaction mixture except for the HO:heme complex and the NRS were transferred into a quartz cuvette. After the HO:heme complex was added to the reaction mixture, the reaction was started by the addition of the NRS. The turnover was monitored by UV-Vis spectroscopy and spectra were recorded every 30 s. The total reaction time was 1.5 min and the reaction was stopped by the addition of 10 volumes of ice cold 0.1% TFA. Afterwards, the samples were prepared for HPLC analyses.

#### Standard reaction mix

HO:heme complex	10 $\mu$ M each
BSA	0.15 mg/ml
Ferredoxin	4.6 $\mu$ M
FNR	0.01 $\mu$ M
Ascorbate	5 mM
Catalase	10 $\mu$ M
NRS	7.1 $\mu$ l
KPi buffer	ad 500 $\mu$ l

#### NADPH-regenerating system (NRS)

Glucose-6-phosphate	50 mM
Glucose-6-phosphate dehydrogenase	250 U/ml
NADP <sup>+</sup>	12.5 mM

#### KPi buffer

$K_2HPO_4$ pH 7.2	100 mM
-------------------	--------

#### **2.4.8 Anaerobic FDBR activity assay**

The activity of purified FDBRs was tested under anaerobic conditions to stabilize and detect substrate radicals. The assays were performed employing equimolar amounts of FDBR and substrate. Residual oxygen in the reaction mixture was removed using an oxygen scavenging system employing glucose and glucose oxidase. The electrons for the reduction were supplied by an NADPH-regenerating system (NRS) based on glucose 6-phosphate and glucose 6-phosphate dehydrogenase. For assays with defined electron equivalents the NRS was replaced with a NADPH solution. For the transfer of electrons to the reductase, ferredoxin from cyanophage P-SSM2 ( $Fd_{P-SSM2}$ ), ferredoxin from spinach ( $Fd_{spinach}$ ; Sigma-Aldrich) or a ferredoxin from *Pseudomonas putida* (Pd) was employed.  $Fd_{spinach}$  and  $Fd_{P-SSM2}$  were reduced by the FNR PetH from *Synechococcus* sp. PCC 7002, Pd was reduced by the corresponding Putidaredoxin reductase (PdR) from *P. putida*.

Firstly, all components of the reaction mixture, except for the FDBR:BV-complex and the NRS, were transferred into a gas-tight cuvette. To remove the oxygen from the reaction vessel, the mixture was incubated under constant stirring and a continuous nitrogen flow for 20 min. In the next step, the FDBR:BV-complex was added to the cuvette and the mixture was incubated for 5 min. The reaction was started by the addition of the NRS. The total reaction time varied between 2 and 30 min depending on the type of experiment. The reaction was monitored via UV-Vis spectroscopy and spectra were recorded every 30 s. The reaction was stopped by the addition of 10 volumes of ice-cold 0.1% TFA and the samples were prepared for subsequent HPLC analyses.

#### Standard reaction mixture

BSA	10 $\mu$ M
Glucose	100 mM
Glucose oxidase	50 U/ml
Catalase	5 $\mu$ M
Ferredoxin	1 - 20 $\mu$ M
FNR	0.01 – 0.02 $\mu$ M
FDBR:BV complex	10 $\mu$ M each
NRS	100 $\mu$ l
TES-KCl buffer	ad 2 ml

#### NADPH regenerating system

NADP <sup>+</sup>	8.2 mM
Glucose 6-phosphate	65 mM
Glucose 6-phosphate dehydrogenase	11 U/ml

#### TES-KCl buffer

TES/KOH pH 7.5	25 mM
KCl	100 mM

### 2.4.9 HPLC analyses

High performance liquid chromatography (HPLC) is a technique that separates analytes in a mixture depending on their polarity. A HPLC system comprises a stationary and a mobile phase that both possess different polarities. This causes a different partitioning of each analyte between the two phases. As a result, each compound of a mixture has a specific retention time on the stationary phase, leading to a separation.

#### *Sample preparation*

To separate the bilins from the non-polar components of the crude reaction mixture of the HO- and FDBR-assays, a solid phase extraction with Sep-Pak<sup>®</sup> C18 light cartridges was performed. Before the samples were loaded, the cartridges were conditioned by flushing them two times with the following solvents:

Acetonitrile	3 ml
H <sub>2</sub> O	3 ml
0.1% (v/v) TFA	3 ml
10% (v/v) MeOH in 0.1% TFA	3 ml

After the samples had been loaded, the cartridges were washed with 5 ml of 0.1% TFA, 5 ml 20% MeOH in 0.1% TFA and 5 ml 20% acetonitrile in 0.1% TFA. The bilins were eluted with 1 ml acetonitrile and subsequently frozen at -80°C. In the next step, the samples were desiccated by lyophilization (Alpha 2-4 LSC plus, Martin Christ GmbH) for approximately 24 h. After the samples had been dried, they were dissolved in 15 µl of DMSO and mixed with 200 µl of the mobile phase. After a filtration through a 0.2 µm PTFE filter the samples were ready for the application to the HPLC system.

#### *HPLC analyses of different bilins*

To identify the reaction products of the anaerobic bilin reductase, HPLC analyses were carried out with the reaction products of already characterized reductases employed as standards. Furthermore, separation by HPLC was used to purify bilins designated for further biochemical experiments. For the analyses an Agilent 1100 series HPLC system with a reversed-phase column (Phenomenex - Luna 5 µm C18 (2) 100A) as stationary phase was used. The mobile phase consisted of a mixture of 50% (v/v) 20 mM formic acid and 50% (v/v) acetone. The samples were applied to the system using a 200 µl sample loop. The elution was isocratic with a constant flow rate of 0.6 ml/min. The analytes were monitored using an UV-Vis detector at 380, 560 and 680 nm, as most bilins possess absorbance maxima at ~ 380 nm and in a range between 540 and 680 nm. To further characterize the separated compounds, peak absorbance spectra were recorded between 350 nm and 800 nm. Compounds designated for further examinations were collected directly after the outlet of the UV-Vis detector, immediately frozen at -80°C, freeze-dried and stored at -80°C prior to use.

#### HPLC mobile phase

Acetone	50% (v/v)
Formic acid (20 mM)	50% (v/v)

#### **2.4.10 Coupled phytochrome assembly assay**

Coupled phytochrome assembly assays were performed to characterize unknown bilins. The incubation of phytochromes with suitable chromophores leads to the formation of photoactive adducts (Terry and Lagarias, 1991). These adducts reveal characteristic difference spectra upon irradiation with red and far-red light. The comparison of the spectra

obtained with unknown bilins and the spectra obtained with known standards allow the identification of the unknown compounds.

In vitro chromophore assembly of the phytochromes Cph1 and BphP with different bilins was carried out using the lysate of a pET-*cph1* or a pASK-*bphP* overexpression after centrifugation and filtration. The assembly was tested employing 50  $\mu$ l lysate incubated either with 40  $\mu$ M P $\Phi$ B or with 4  $\mu$ l of bilin solutions of unknown concentration for 30 min at room temperature in the dark. Afterwards, the volume was adjusted to 500  $\mu$ l with PBS. Absorbance spectra were recorded after incubation for 3 min with red light (636 nm – Pfr spectrum) and after incubation for 3 min with far red light (730 nm for Cph1; 750 nm for BphP – Pr spectrum). Difference spectra were calculated by the subtraction of the Pfr from the Pr spectrum.

#### 2.4.11 Freeze-quench EPR experiments

The EPR-experiments were carried out in a cooperation with Antonio Pierik and Dominique Bechtel (Biochemistry group, TU Kaiserslautern).

EPR is a technique to detect the presence of unpaired electrons in a sample. In an externally applied magnetic field, unpaired electrons can adopt two states with different energy levels. The difference in energy between these states is dependent on the strength of the applied magnetic field. The electrons can switch between these two states by either absorbing or emitting a photon that matches the energy difference between these two states. In the EPR spectrometer these photons are supplied by a microwave source. The frequency of the microwave source is typically kept constant during the experiments, while the strength of the magnetic field is varied. When the variable magnetic field leads to a difference between the two states equivalent to the supplied energy by the microwave, the electrons can absorb these photons, yielding a detectable signal.

To investigate, whether substrate radical intermediates occur during the course of FDBR-mediated reactions, freeze-quenched EPR experiments were conducted. Therefore, a 3 ml reaction mixture of an anaerobic FDBR-assay was set up. Samples with a volume of 200  $\mu$ l were taken before and 2, 6 and 8 min after the start of the reaction. They were immediately transferred into a quartz EPR-tube and flash frozen in liquid nitrogen. The samples were analyzed using a Bruker Elexsys E580 spectrometer. The EPR measurements were carried out at a constant temperature of 77 K with a microwave frequency of 9.43 GHz, a field modulation amplitude of 10 G and a power of 20  $\mu$ W.

#### 2.4.12 Crystallization and X-ray crystallography

For the crystallization experiments, the GST-tagged  $\Phi$ PcyX protein was produced as described in section 2.4.1. Crystallization experiments require extra-pure samples of the

respective proteins. Therefore, the purification process was slightly different compared to the purification of proteins employed in biochemical experiments. The cells were thawed overnight on ice and resuspended in ice-cold PBS buffer. After the addition of a spatula tip of lysozyme and DNaseI, the cells were lysed using a microfluidizer at 18000 psi. Subsequently, the lysate was centrifuged for 1 h at 50000 x g. To remove residual cell debris, the supernatant was filtered using a 0.45  $\mu\text{m}$  syringe filter. Then, it was loaded onto a freshly prepared gravity flow column, packed with Protino® Glutathione Agarose 4B. The column was washed using 10 CV of ice cold PBS and 5 CV ice cold PreScission Protease cleavage buffer. In the next step, the column material was resuspended in 3 CV PreScission Protease cleavage buffer. After the addition of 30  $\mu\text{l}$  PreScission Protease, the sample was digested under constant shaking for 20 h at 4°C. The suspension was transferred into a new gravity flow column and the flow-through was collected. To remove all residual GST tag, the flow-through was run through a freshly prepared gravity flow column packed with Protino® Glutathione Agarose 4B. The flow-through was collected and dialyzed overnight against “crystallization buffer”. The obtained dialysate was concentrated using Vivaspin® 6 concentrators (MWCO = 10000 Da). To further purify the  $\Phi\text{PcyX}$  protein, a size exclusion chromatography using a Superdex™ 75 16/600 pg column was performed. The column was equilibrated with crystallization buffer prior to use. Fractions containing only  $\Phi\text{PcyX}$  protein were pooled and concentrated to 10 mg/ml in crystallization buffer. For the screening of  $\Phi\text{PcyX}$  crystallization conditions with bound substrate, the concentrated protein was supplemented with a 2-fold molar excess of BV.

#### Crystallization buffer

TES/KOH pH7.5	20 mM
KCl	20 mM

#### *Screening for crystallization conditions*

The screening for crystallization conditions was performed in a collaboration with Eckhard Hoffmann and Johannes Sommerkamp (Protein Crystallography Group, Ruhr University Bochum) at the Ruhr University Bochum.

Initial crystallization conditions were screened using the sitting drop vapor diffusion method. For the screening the following commercially available crystallization suites were employed: Cryos (Qiagen), JCSG Core I – IV (Qiagen), JCSG+ (Qiagen), MbClass (Qiagen), MemGold I & II (Molecular Dimensions), Morpheus (Molecular Dimensions), PACT (Qiagen), PEGs & PEGs II (Qiagen), Pi-PEG (Jena Bioscience). First, 100/100 nl mixtures of protein and reservoir solution were prepared in 96-well crystallization plates (Corning - 3550) using a liquid handling robot (Phoenix, ArtRobins). The corresponding reservoir

contained 70  $\mu\text{l}$  of the respective solution. The samples were incubated at either 18°C or 4°C.

Initial crystals were obtained in a 1/1 mixture of protein and reservoir containing 0.1 M Tris/HCl pH 8.5, 0.2 M Trimethylamine N-oxide (TMAO) and 20% (w/v) PEG MME 2000 (JCSG+, G4, Qiagen) at 4°C. At 18°C no crystal growth was observed. The condition yielding the initial crystals served as the starting point for manual refinement screens. In these experiments the concentration of one component was kept stable, while the concentrations of the other two components were varied gradually. This led to the identification of 0.1 M Tris/HCl pH 8.5, 0.05 M TMAO and 15% (w/v) PEG MME 2000 as the best reservoir solution to grow  $\Phi\text{PcyX}$  crystals.

The final crystals were grown using the “hanging drop method” with 1/1  $\mu\text{l}$  mixtures of protein (10 mg/ml) and reservoir at 4°C in 24-well XRL plates. The wells were filled with 700  $\mu\text{l}$  reservoir solution. Before the crystals were frozen in liquid  $\text{N}_2$ , they had been soaked in reservoir solution containing 20% (v/v) PEG 400 for cryoprotection.

#### *Data collection and structure determination*

The data collection was performed by Eckhard Hofmann and Johannes Sommerkamp (Protein Crystallography Group, Ruhr University Bochum). The structure was determined in a collaboration with Eckhard Hofmann and Johannes Sommerkamp.

Oscillation data of the obtained  $\Phi\text{PcyX}$  crystals were recorded at a constant temperature of 100 K on beamline ID30B at the European Synchrotron Radiation Facility (Grenoble, France) using a PILATUS 6M detector (DECTRIS) and a MiniKappa goniometer head (ARINAX).

The X-rays that are diffracted by a protein crystal contain all information about the three dimensional organization of the atoms in the crystal lattice. They are defined by their amplitude and phase. As the information concerning the phase is lost during the detection, it needs to be recovered afterwards. There are multiple techniques to solve this problem. The most convenient is the determination of the phase by molecular replacement. This method uses already solved crystal structures of structurally similar proteins to solve the phase problem (Rossmann and Blow, 1962). This was not the suitable approach for the solution of the  $\Phi\text{PcyX}$  structure. Several attempts employing molecular replacement with PcyA and other FDBRs failed. For that reason, 15 low-dose datasets with different kappa orientations ( $0^\circ$  -  $140^\circ$ ) were collected at a long wavelength of 2.0664 Å. This wavelength is appropriate for experimental phasing by single-wavelength anomalous dispersion of sulfur atoms. The anomalous dispersions allows the localization of the sulfur atoms and based on this information, the phase can be calculated.

The collected diffraction data were processed and scaled employing XDS and XSCALE (Kabsch, 2010). The phase problem was solved based on the experimental data using

Phenix.autosol (Adams *et al.*, 2010). An initial model was built using Phenix.autobuild (Adams *et al.*, 2010). The model was subsequently refined using Phenix.refine and Coot (Emsley and Cowtan, 2004; Adams *et al.*, 2010).

The final model was deposited in the PDB with the accession code 5OWG.

## 3 Results

Metagenomics are a powerful tool for the discovery of novel enzymes. Yet, sequence analyses can only deliver hints regarding the activity of the putative enzymes. For this reason, the biochemical and biophysical properties of the gene products are characterized in the following paragraph.

### 3.1 Characterization of $\Phi$ HemO

To analyze whether the *hemO* genes discovered on metagenomic scaffolds encode for functional enzymes, one member (termed  $\Phi$ HemO thereafter) was overproduced as GST-fusion protein in *E. coli*. After purification by affinity chromatography, HO-activity tests were conducted with equimolar amounts of  $\Phi$ HemO and heme. Subsequently, the reaction products were analyzed via HPLC.

The recombinant production of GST- $\Phi$ HemO and the purification by affinity chromatography resulted in a protein with good purity but moderate yields (Figure 16).

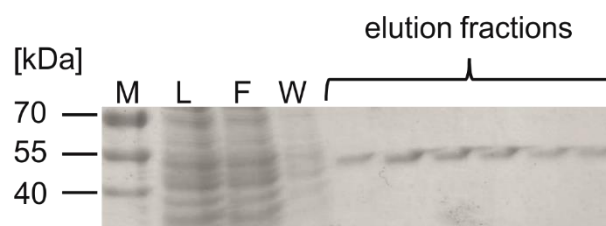


**Figure 16. SDS-PAGE of a purification of GST- $\Phi$ HemO by affinity chromatography.** M = Size marker – PageRuler™ Prestained (Thermo Fisher); L = Lysate; F = Flow-through fraction; W = Washing fraction. The elution fractions contain mostly GST- $\Phi$ HemO (MW = 50.6 kDa).

#### 3.1.1 $\Phi$ HemO catalyzes the reaction of heme to BV IX $\alpha$

The purified  $\Phi$ HemO protein was used in activity tests, employing heme as the substrate and Fd<sub>P-SSM2</sub> as the electron donor (Figure 17). Upon incubation with the substrate  $\Phi$ HemO formed a heme:heme oxygenase complex with a characteristic absorbance spectrum showing a clear Soret band at ~ 410 nm (designated as “heme” in Figure 17). The absorbance of the Soret band decreased immediately after the reaction was started, suggesting a turnover of heme. At the same time, the formation of biliverdin was indicated by an increase of the absorbance at ~ 350 nm and ~ 680 nm. Moreover, an absorbance maximum at ~ 645 nm became visible. After a total reaction time of 1.5 min no more changes in the absorbance were detected and thus, the reaction was stopped.

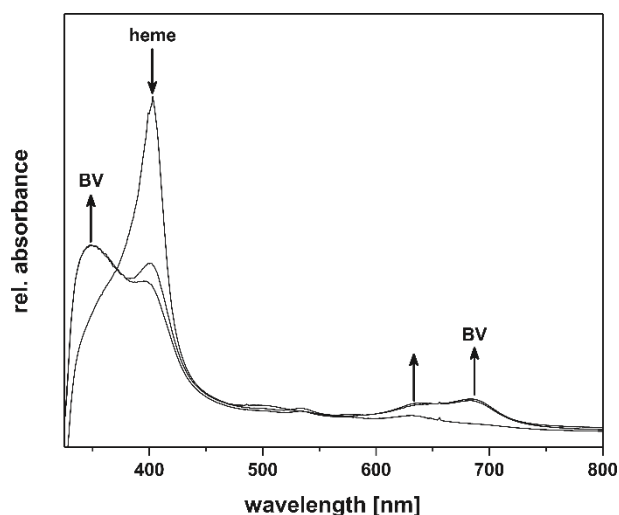


**Figure 17. Time resolved UV-Vis spectroscopy of an *in vitro* turnover of heme mediated by  $\Phi$ HemO.** The increment between the spectra is 30 s, the total reaction time is 1.5 min. The arrows indicate the course of the absorbance over the time. Heme = Soret band of heme. BV = Absorbance maxima related to the formation of biliverdin.

The crude reaction mixture was then loaded onto a pre-conditioned Sep-Pak C18 cartridge which immediately turned green. This observation implies that the green pigment BV was formed out of heme during the course of the reaction. To identify the reaction product and to gain information about the regioselectivity of  $\Phi$ HemO, HPLC analyses were performed. The reaction products of HO3 from *A. thaliana* (BV IX $\alpha$ ) and HemO from *P. aeruginosa* (BV IX $\beta$  and BV IX $\delta$ ) were used as standards. The comparison of the chromatograms showed that the  $\Phi$ HemO reaction product possesses the same retention time as the reaction product of HO3 from *A. thaliana* (~ 22.5 min Figure 18 A). Furthermore, the spectrum recorded at the peak maximum is typical for BV with absorbance maxima at approximately ~ 380 nm and ~ 665 nm (Figure 18 B).

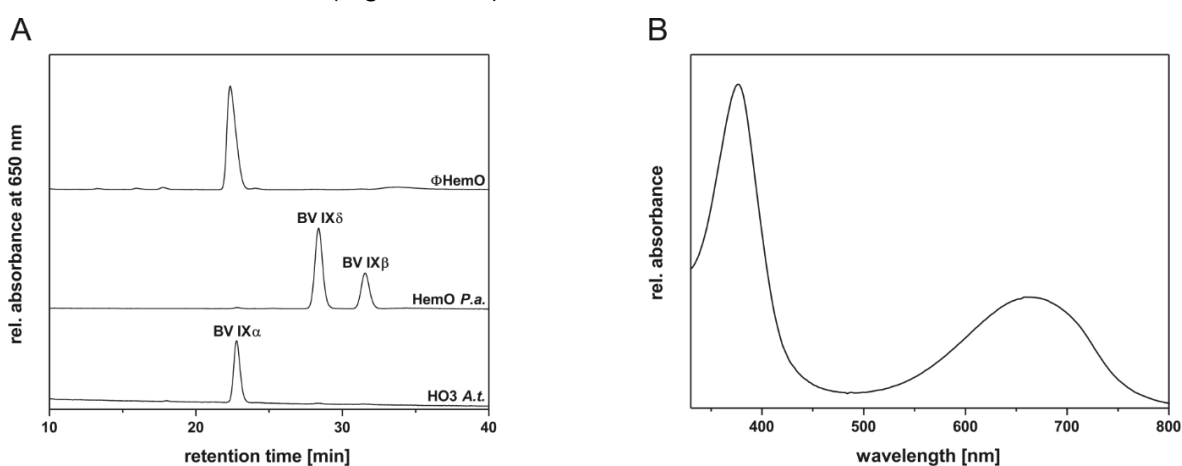


**Figure 18. Characterization of the  $\Phi$ HemO reaction products.** **A.** HPLC analyses of the  $\Phi$ HemO reaction product employing the products of HO3 from *A. thaliana* (HO3 A. t.; BV IX $\alpha$ ) and HemO from *P. aeruginosa* (HemO P.a.; BV IX $\beta$  and BV IX $\delta$ ) as standards. The products were analyzed using a reversed-phase 5  $\mu$ m C18 Luna column (Phenomenex) as stationary phase. The mobile phase consisted of 50% (v/v) acetone and 50% (v/v) 20 mM formic acid. The products were detected using their absorbance at 650 nm. **B.** Peak absorbance spectrum of the  $\Phi$ HemO reaction product with a retention time of ~ 22.5 min.

Hence,  $\Phi$ HemO cleaves heme at the  $\alpha$ -methine bridge yielding BV IX $\alpha$ . Based on these results  $\Phi$ HemO possesses the typical activity of most of the characterized HOs and is involved in the formation of the substrate for the majority of the FDBRs. As a consequence, in the next part of the project a member of the newly discovered reductases was examined.

### 3.2 Characterization of the PcyX-family

To investigate, if the newly discovered *pcyX* sequences encode for functional FDBRs, one of the genes (termed  $\Phi$ *pcyX* thereafter) was heterologously expressed in *E. coli* BL21 (DE3). The recombinant production of the protein was started with a pGEX-6P-1 construct harboring a  $\Phi$ *pcyX* sequence optimized for the codon-usage of *E. coli* using the “Optimizer” tool (Puigbo *et al.*, 2007). The yield of soluble GST- $\Phi$ PcyX fusion protein (MW = 54.7 kDa) after purification by affinity chromatography was low (Figure 19 A). Moreover, the protein did not show any activity in anaerobic FDBR-activity tests (data not shown). Several experiments were performed to optimize the production conditions. All of these approaches were carried out with  $\Phi$ *pcyX* sequences that were adapted to the *E. coli* codon usage. Unfortunately, all experiments failed to significantly improve the yield and the activity of the putative FDBR (optimization experiments conducted by Maximilian Klosowski, Master Thesis 2013, unpublished). These results led to the generation of a construct that employs the native DNA sequence obtained from the metagenomic dataset in the expression vector pGEX-6P-1. Interestingly, when this construct was used for the production of the GST- $\Phi$ PcyX fusion protein, the yield of soluble protein increased drastically compared to the vectors carrying the adapted genes (Figure 19).

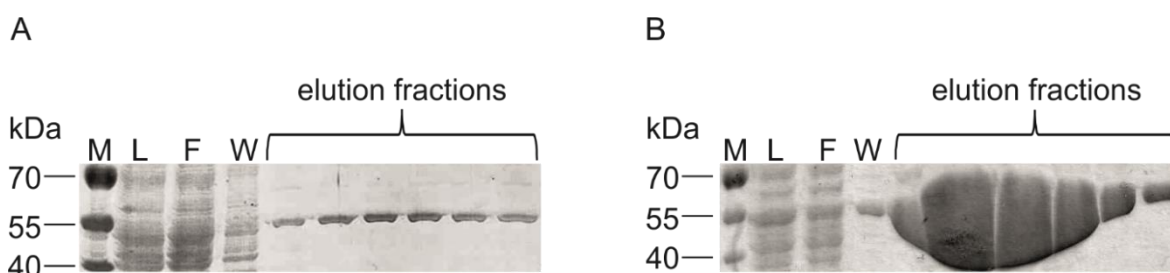


**Figure 19. Comparison of the outcome of two overproduction and purification approaches of GST-tagged  $\Phi$ PcyX.** Both constructs were overexpressed in *E. coli* BL21 (DE3) in 9 I 2YT medium. Purification and sampling were performed in the same way in both experiments. M = Size marker – PageRuler™ Prestained (Thermo Fisher); L = Lysate; F = Flow-through; W = Washing fraction **A.** SDS-PAGE of the purification of GST- $\Phi$ PcyX recombinantly produced in 9 I 2YT medium using a sequence optimized for the *E. coli* codon-usage. **B.** SDS-PAGE of the purification of GST- $\Phi$ PcyX recombinantly produced in 9 I 2YT medium using the native sequence.

#### 3.2.1 Determination of the oligomeric state

All investigated members of the FDBR-family were shown to act as monomeric enzymes. To investigate whether this is also true for the new PcyX reductases, analytical size exclusion chromatography experiments were performed. Before the protein was employed

in these experiments, the GST-tag was removed by protease treatment and the product was further purified employing a second glutathione affinity chromatography (Figure 20 A; lane 1, lane 2 and lane 3). The purified protein was analyzed on a Superdex® 75 10/300 GL column (GE Healthcare) and showed an elution volume of ~ 11.65 ml (Figure 20 B). Based on the calibration curve, (Figure 20 C) this corresponds to a relative MW of ~ 32.9 kDa. The calculated molecular weight of the protein is ~ 28.3 kDa. Hence, the purified  $\Phi$ PcyX is also present as a monomer and the minor peaks eluting at smaller volumes are most likely caused by impurities of the sample (see Figure 20 A, lane 3).

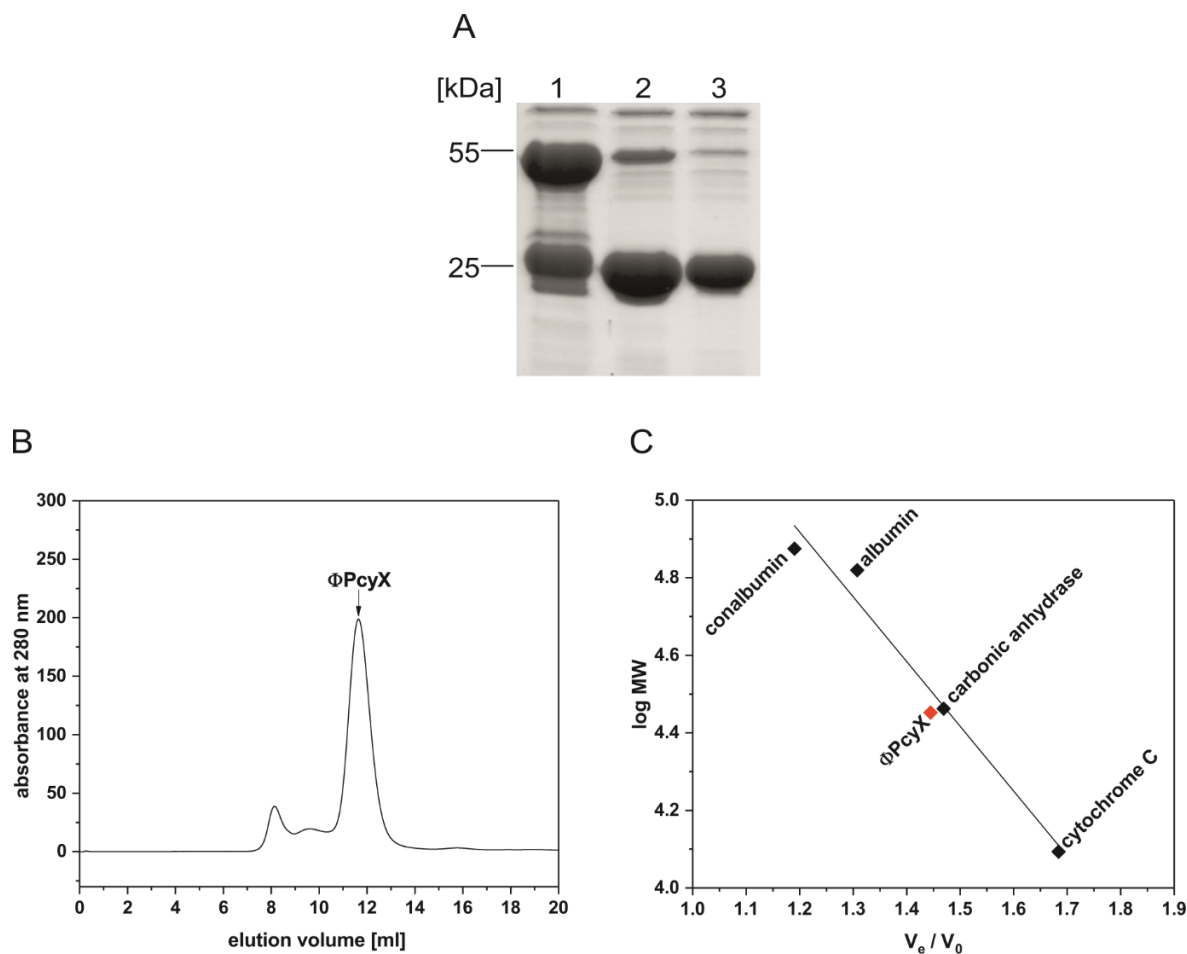


**Figure 20. Protease digest and determination of the oligomeric state of  $\Phi$ PcyX.** **A.** SDS-PAGE showing the digestion of the purified GST- $\Phi$ PcyX fusion protein with PreScission Protease and the subsequent purification by a second affinity chromatography. 1 = Elution fraction of a purification by affinity chromatography of GST- $\Phi$ PcyX (MW = 54.7 kDa). 2 = Sample shown in lane 1 after protease digest. 3 = Sample shown in lane 2 after additional purification using glutathione agarose to remove the cleaved GST-tag and undigested fusion protein. **B.** Size exclusion chromatography with purified  $\Phi$ PcyX protein. The experiment was performed with a Superdex® 75 10/300 GL column equilibrated with TES-KCl buffer pH 7.5 and purified  $\Phi$ PcyX after protease digest and purification with a second affinity chromatography. Eluting proteins were detected using their absorbance at 280 nm. **C.** Calibration curve of the Superdex® 75 10/300 GL column. The standards used for calibration were: Conalbumin (MW = 75 kDa), albumin (MW = 66 kDa), carbonic anhydrase (MW = 29 kDa) and cytochrome C (MW = 12.4 kDa). The void volume of the column was determined using Blue Dextran 2000. The column was calibrated by plotting (black squares) the log of the MW (log MW) of the standards against the quotient of the elution volume and the void volume ( $V_e/V_0$ ). The calibration curve was calculated using a linear regression in Origin. The red square shows the position of  $\Phi$ PcyX in the calibration plot.

### 3.2.2 Analysis of the $\Phi$ PcyX-activity and characterization of the reaction products

To gain insights into the catalytic activity of  $\Phi$ PcyX, anaerobic FBDR-assays were performed using equimolar amounts of  $\Phi$ PcyX and BV.

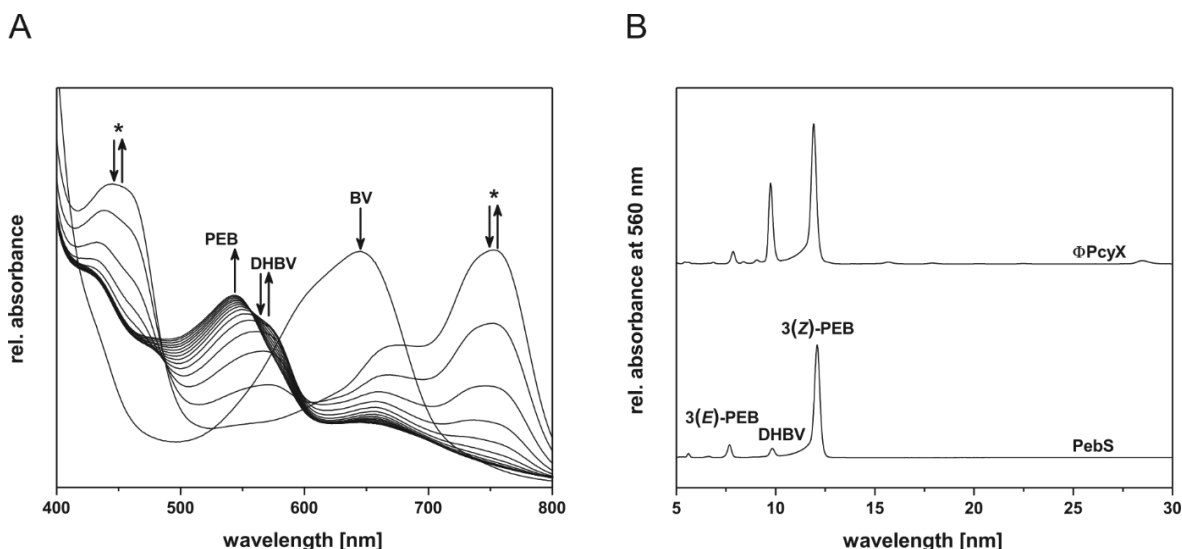


**Figure 21. Activity testing and characterization of the  $\Phi$ PcyX reaction products.** **A.** Time-resolved UV-Vis spectroscopy of an anaerobic activity test employing  $\Phi$ PcyX and BV IX $\alpha$  as the substrate. The total reaction time was 30 min. Spectra were recorded every 30 s. For reasons of clarity the increment between the shown spectra is 2 min. The arrows indicate the course of the absorbance during the reaction. BV = Initial spectrum of the  $\Phi$ PcyX:BV complex before the reaction was started. Asterisks indicate the formation of radical intermediates. DHBV and PEB mark absorbance maxima related to the formation of 15,16-DHBV and PEB. **B.** HPLC analyses of the reaction products of  $\Phi$ PcyX. The analyses were carried out using a Luna 5  $\mu$ m reversed phase C18 column (Phenomenex) as stationary phase. The mobile phase consisted of a mixture of 50% (v/v) acetone and 50% (v/v) 20 mM formic acid. The  $\Phi$ PcyX products were identified at a wavelength of 560 nm employing the products of PebS as standards.

The incubation of  $\Phi$ PcyX with the substrate led to the formation of a stable, turquoise  $\Phi$ PcyX:BV complex with an absorbance maximum at  $\sim$  645 nm (see initial spectrum designated as “BV” in Figure 21 A). After the reaction was started by the addition of a NADPH-regenerating system (i.e. electrons from NADPH), the absorbance of the complex declined rapidly. Simultaneously, the absorbance at  $\sim$  560 nm increased which can be linked to the formation of 15,16-DHBV from BV. During later stages of the reaction, a shift of the absorbance from 560 nm to 540 nm was observed which is most likely due to the formation of PEB from 15,16-DHBV. Moreover, a rapid increase of the absorbance at 450 nm and 750 nm was visible during the initial phases of the activity test. These absorbance maxima subsequently disappeared and can be linked to the presence of substrate radical intermediates, as it was described for other FDBRs (Tu *et al.*, 2008; Busch *et al.*, 2011b). Based on the time-resolved UV-Vis spectroscopy,  $\Phi$ PcyX seems to catalyze the reaction of BV to PEB via the intermediate 15,16-DHBV employing a radical mechanism. To verify the nature of the compounds, HPLC analyses were performed with the reaction products of the anaerobic activity tests (Figure 21 B). The PebS reaction products 15,16-DHBV as well as 3(E)- and 3(Z)-PEB served as standards. The HPLC analyses confirmed

the findings of the UV-Vis spectroscopy and proved that  $\Phi$ PcyX yields 15,16-DHBV and 3(*E*)- and 3(*Z*)-PEB. Hence,  $\Phi$ PcyX and PebS catalyze the same reaction. However, in the  $\Phi$ PcyX-mediated reaction a significant amount of the intermediate 15,16-DHBV is still present after a total reaction time of 30 min. In comparison, the reaction products of PebS only comprise traces of 15,16-DHBV after a reaction time of 10 min. These results indicate that the reaction rate is slower compared to the PebS-mediated reaction. Besides, it seems that the rate-limiting step of the  $\Phi$ PcyX reaction is the second reduction from 15,16-DHBV to PEB.

To rule out any influence of the purification system on the reaction rate, the experiments were repeated using a Strep-tagged  $\Phi$ PcyX protein. Yet, the velocity of the reaction as well as the reaction products were the same as for the GST-tagged construct (data not shown).

### 3.2.3 The reaction proceeds via a substrate radical

The time-resolved UV-Vis spectroscopy of the  $\Phi$ PcyX activity assays revealed that intermediates with absorbance maxima at  $\sim 450$  nm and  $\sim 750$  nm occur in the course of the reaction. To clarify, whether these intermediates are substrate radicals, freeze-quench EPR spectroscopy experiments were carried out. For that, a 3 ml anaerobic FDBR-assay was prepared. Samples were taken before and 2, 6 and 8 min after the start of the reaction. Subsequent EPR-measurements showed that no paramagnetic species had been present before the reaction was started (Figure 22;  $t = 0$  min). In contrast, 2 min after the addition of the NADPH-regenerating system a paramagnetic species giving an intensive EPR signal was detected. The signal intensity quickly decreased during the course of the reaction and the kinetic of the decay followed the decline of the absorbance at  $\sim 750$  nm (see Figure 21 A).

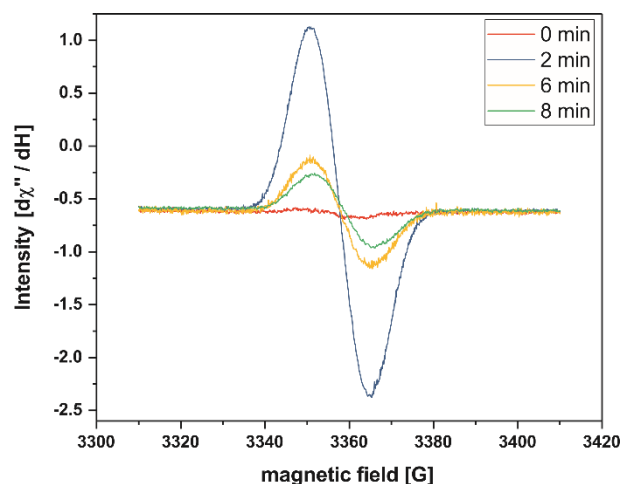


**Figure 22. EPR measurements of substrate radicals occurring during the  $\Phi$ PcyX mediated reduction of BV.** EPR spectroscopy experiments were conducted at 77 K, 20  $\mu$ W power and a field modulation of 10 Gauss. Samples were taken before the start of the reaction as well as 2, 6 and 8 min after the addition of the NADPH-regenerating system. The EPR experiments were conducted in a cooperation with Antonio Pierik and Dominique Bechtel (Biochemistry group - TU Kaiserslautern).

Hence, the  $\Phi$ PcyX reaction proceeds via a radical mechanism as it has been described for other FDBRs (Tu *et al.*, 2008; Busch *et al.*, 2011b).

### 3.2.4 The reaction rate is highly dependent on the redox partner

The FDBR-assays employing the purified  $\Phi$ PcyX revealed that the turnover is rather slow compared to the PebS-mediated reaction of BV to PEB. In order to optimize the assay conditions and to investigate the influence of the electron donor on the reaction rate, several ferredoxin concentrations, as well as several types of ferredoxins were evaluated in anaerobic  $\Phi$ PcyX activity tests. The effect of the electron donor on the PEB formation was quantified by subsequent HPLC analyses comparing the peak areas of PEB and DHBV. The evaluation of the HPLC analyses showed that the raise of the Fd<sub>P-SSM2</sub> concentration from 1  $\mu$ M to 4  $\mu$ M led to an almost 9-fold increase of the PEB to DHBV ratio. Furthermore, the increase of the Fd<sub>P-SSM2</sub> concentration to 20  $\mu$ M and the doubling of the FNR concentration to 0.02  $\mu$ M led to a PEB to DHBV ratio that was 55-fold higher compared to the assay conducted with 1  $\mu$ M Fd<sub>P-SSM2</sub>. Another possible influence on the reaction rate is the compatibility of the electron donor to  $\Phi$ PcyX. Thus, activity assays using a [2Fe-2S]-ferredoxin from *Spinacia oleracea* (Fd<sub>spinach</sub>), as well as a vertebrate-like [2Fe-2S]-ferredoxin from *Pseudomonas putida* (putidaredoxin; Pd) were conducted. The concentration of the ferredoxins was set to 4  $\mu$ M and in the assays with Pd the FNR from *Synechococcus* sp. PCC7002 was replaced with the corresponding reductase from *P. putida* (putidaredoxin reductase; PdR). The subsequent analyses of the HPLC data (Figure 23) showed that the PEB to DHBV ratio decreased by almost 50% when Fd<sub>spinach</sub> was used instead of Fd<sub>P-SSM2</sub>. Additionally, in the assays employing Pd and PdR, no PEB formation was visible in neither the time-resolved UV-Vis spectroscopy, nor the HPLC analyses. After a total reaction time

of 30 min still large quantities of BV were detectable and only small amounts of 15,16-DHBV were visible in the chromatogram (Figure 23).

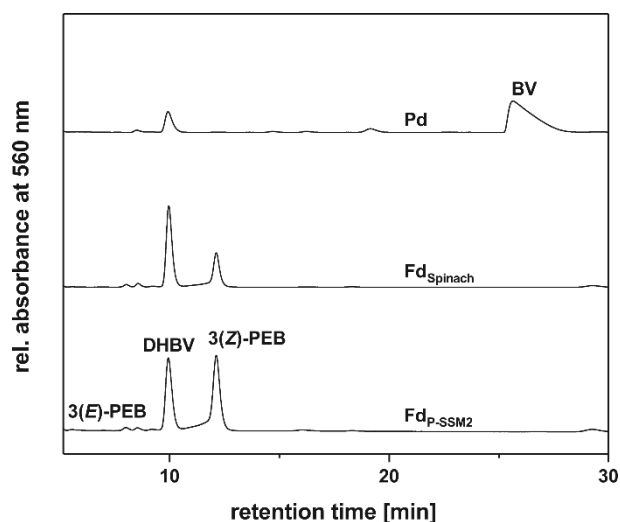


**Figure 23. HPLC analyses of the reaction products of anaerobic  $\Phi$ PcyX activity tests with different ferredoxins as electron donors.** The analyses were performed with a Luna 5  $\mu$ m reversed phase C18 column (Phenomenex) as stationary phase. The mobile phase consisted of a mixture of 50% (v/v) acetone and 50% (v/v) 20 mM formic acid. The products were detected at a wavelength of 560 nm. The single chromatograms are labeled with the employed electron donor. BV = Residual substrate.

These findings underline the significance of the compatibility between the redox partners. Based on these results, the ferredoxin from the cyanophage P-SSM2 is thus far the most suitable electron donor for  $\Phi$ PcyX.

### 3.2.5 Several side products occur under the chosen assay conditions

A closer inspection of the reaction products of the  $\Phi$ PcyX-mediated *in vitro* reaction of BV to PEB revealed several other products in addition to 15,16-DHBV and 3(*E*)- and 3(*Z*)-PEB. These products were mostly visible in the 380 nm and 680 nm channels of the UV-Vis detector, when large amounts of the  $\Phi$ PcyX reaction products were analyzed on the HPLC system (680 nm channel shown in Figure 24 A).

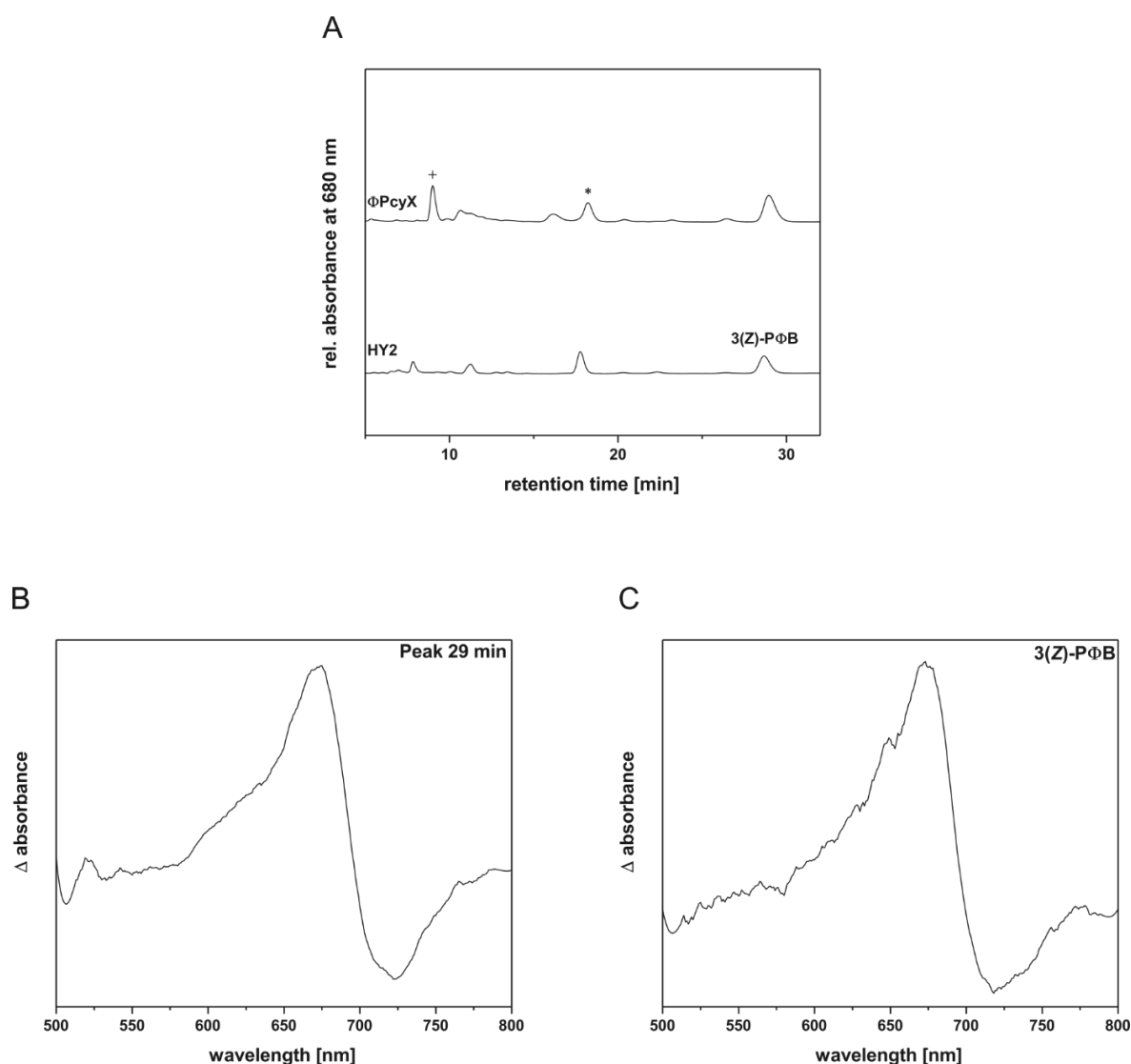


**Figure 24. HPLC analyses of side products and subsequent coupled phytochrome assembly assays.** **A.** HPLC analyses of side products in the  $\Phi$ PcyX-mediated turnover of BV. The analyses were conducted with a Luna 5  $\mu$ m reversed phase C18 column (Phenomenex) as stationary phase. The mobile phase consisted of a mixture of 50% (v/v) acetone and 50% (v/v) 20 mM formic acid. The products were monitored at a wavelength of 680 nm. The outcome of an anaerobic turnover of BV mediated by HY2 from *A. thaliana* served as standards. \* = Impurity of the BV stock; + = Unknown compound. **B.** Difference spectrum of a coupled phytochrome assembly assay using Cph1 and the isolated side product of  $\Phi$ PcyX with a retention time of ~ 29 min. **C.** Difference spectrum of a coupled phytochrome assembly assay employing Cph1 and 3(Z)-PΦB. The calculated difference spectra were smoothed using a 25 point Savitzky-Golay filter.

The compound with a retention time of ~ 18.5 min (labeled with an asterisk in Figure 24 A) was identified as an impurity of the BV IX $\alpha$  stock. Unfortunately, the nature of the product eluting after ~ 9.5 min (marked with a cross in Figure 24 A; designated as “Product 9.5 min”) was not revealed and therefore, remains enigmatic. The retention time is almost identical to 15,16-DHBV (~9.8 min), but an assessment of the peak absorbance ruled out the possibility that it is in fact 15,16-DHBV. Further comparison of the  $\Phi$ PcyX side products with the products of other FDBRs revealed that one of the products elutes with the same retention time as 3(Z)-PΦB. To verify the nature of this product as 3(Z)-PΦB, it was isolated via HPLC, freeze-dried and employed in coupled phytochrome assembly assays with Cph1 (Figure 24 B). This cyanobacterial phytochrome forms photoactive adducts with bilins that

possess an ethylidene group at their A-ring C3<sup>1</sup> and C3<sup>2</sup> atoms. Upon the incubation of these with red and far-red light, characteristic difference spectra can be calculated. As standard served 3(Z)-PΦB obtained from an anaerobic HY2 activity test (Figure 24 C). The conducted assays revealed that both compounds form photoactive adducts with Cph1. The calculated difference spectra showed both maxima (675 nm / 674 nm) and minima (722 nm / 717 nm) at approximately the same wavelengths. Together with the HPLC analyses, these results confirm that one of the side products of the ΦPcyX-mediated reaction is 3(Z)-PΦB.

To gain further insights into the ΦPcyX-mediated reaction, product formation was analyzed via HPLC in a time-resolved manner. Therefore, an anaerobic ΦPcyX activity test was performed in a total volume of 30 ml. Samples were taken every 3 min and were subsequently analyzed via HPLC. The course of the product formation was visualized by plotting the percentage of the peak area of the compounds in relation to the total peak area against the reaction time (Figure 25).

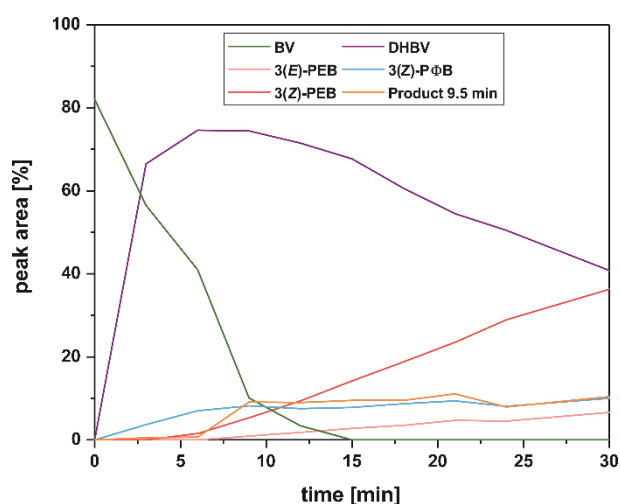


**Figure 25. Time-course experiment examining the product formation during the ΦPcyX reaction based on HPLC data.** In a 30 ml anaerobic ΦPcyX activity test, every 3 min a 2 ml sample was taken, dried and subsequently analyzed via HPLC. The total reaction time was 30 min. The percentage of the total peak area for the single compounds was plotted against the reaction time. BV, 3(Z)-PΦB and “Product 9.5 min” were detected at 680 nm. 15,16-DHBV, as well as 3(E)- and 3(Z)-PEB were detected at 560 nm.

The time-course experiments revealed that the amount of BV rapidly declined after the start of the reaction and was totally consumed after a reaction time of 15 min. In contrast, the amount of 15,16-DHBV increased until a reaction time of 6 min. Afterwards, the percentage of 15,16-DHBV decreased, as it was converted to PEB. Consequently, the two PEB isomers (i.e. 3(E)- and 3(Z)-PEB) were detected in reasonable amounts after a reaction time of 6 min. From this point on, the peak area of these products increased until the reaction was stopped after 30 min. These results confirm the findings of the time-resolved UV-Vis spectroscopy (Figure 21 A). The side products (i.e. 3(Z)-PΦB and “Product 9.5 min”) of the ΦPcyX-mediated reaction were immediately formed after the start of the reaction. Their

amount increased during the first 9 min of the assay and from then on remained stable. This result suggests that the formation of these products is directly linked to the abundance of BV in the reaction mixture. Moreover, the absolute peak areas of the compounds are approximately 20 times lower than the peak area of 3(Z)-PEB (~ 150 mAU\*s vs ~ 3000 mAU\*s). These findings raise the hypothesis that the side products are artifacts of the *in vitro* assay conditions and are not relevant for the biological function of  $\Phi$ PcyX.

### 3.2.6 The molecular structure of $\Phi$ PcyX

Although the sequence identity between the groups of PcyX and PebS reductases is rather low (~ 9% in the “core region”; Ledermann *et al.*, 2016), both catalyze the same reaction. To acquire further information about the reaction mechanism underlying this unexpected turnover, the X-ray structure of  $\Phi$ PcyX was solved. The determination of an X-ray structure requires a single crystal of the respective protein. Moreover, for the screening of the adequate crystallization conditions extra pure  $\Phi$ PcyX was needed. Therefore, the GST-tagged protein was purified via two affinity chromatography steps including an on-column protease treatment, followed by a size exclusion chromatography. Western Blot analyses were performed to rule out a contamination of  $\Phi$ PcyX with residual GST-tag (Figure 26 A & B). The analyses revealed that no residual GST-tag was present after the affinity chromatography. The SDS-PAGE performed after the SEC revealed that the protein was purified to homogeneity (Figure 26 C).

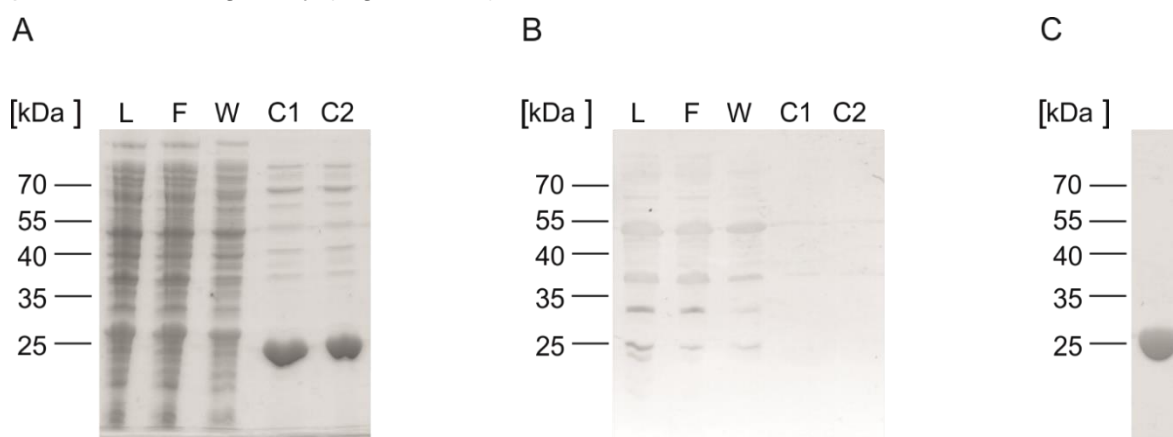


**Figure 26. Preparation of  $\Phi$ PcyX for crystallization experiments.** **A.** SDS-PAGE of the initial purification steps. **B.** Corresponding Western Blot analysis of the SDS-PAGE shown in (A) to detect residual GST-tag. SDS-PAGE of  $\Phi$ PcyX after size exclusion chromatography. L = Lysate; F = Flow-through; W = Washing fraction; C1 = Flow-through of the first affinity chromatography column after the on-column cleavage of the GST-tag. C2 = Flow-through of the second affinity chromatography column. **C.** SDS-PAGE of  $\Phi$ PcyX protein after preparative size exclusion chromatography.

The screening for suitable crystallization conditions was performed using the sitting drop vapor diffusion method with 100/100 nl mixtures of protein and reservoir solution. The best initial crystals were obtained at 4°C with 0.1 M Tris/HCl pH 8.5, 0.2 M Trimethylamine N-oxide (TMAO) and 20% (w/v) PEG MME 2000 as the reservoir solution (Figure 27 A; Qiagen

crystallization suite JCSG+, G4). In the next step, the crystallization conditions were refined by varying the pH value, the TMAO as well as the PEG MME 2000 concentrations. As a result, the final crystals were grown at 4°C in a 1/1  $\mu$ l hanging drop with 0.1 M Tris/HCl pH 8.5, 0.05 M TMAO and 15% (w/v) PEG MME 2000 as the reservoir solution. The diffraction patterns for the acquired crystals were recorded at the “European Synchrotron Radiation Facility” (ESRF) using beamline ID30B. The data allowed the solution of a  $\Phi$ PcyX crystal structure with a resolution of 2.2 Å.

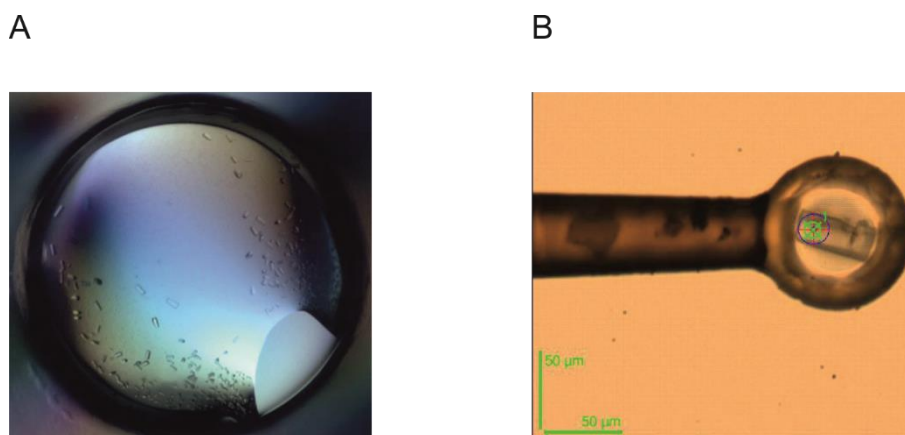


**Figure 27. Crystallized  $\Phi$ PcyX protein.** **A.** Initial crystals obtained in the crystallization suite JCSG+ condition G4. **B.**  $\Phi$ PcyX crystal in a nylon loop mounted on the synchrotron beamline. The crosshair marks the region of the crystal on which the synchrotron radiation was focused. Scale bar: 50  $\mu$ m. The data at the synchrotron were collected by Johannes Sommerkamp and Eckhard Hofmann (Protein Crystallography Group, Ruhr University Bochum).

Several attempts to solve the phase problem by molecular replacement using crystal structures of other FDBRs as templates failed. Therefore, the crystallographic phase problem was solved by experimental phasing using the “single-wavelength anomalous dispersion of sulfur atoms” technique (Dauter *et al.*, 1999). This led to the correct identification of the positions of 11 sulfur atoms. The initial model obtained by Phenix.autobuild (Adams *et al.*, 2010) was incomplete and comprised 153 residues in 10 fragments. Subsequently, the model was refined using Phenix.refine (Adams *et al.*, 2010) and Coot (Emsley and Cowtan, 2004). Nevertheless, 19 residues located at the N- and C-terminus, as well as the residues 62-63; 104-106; 116-147; 198-200 were not modeled due to missing or weak density. Statistics regarding data collection, phasing and model refinement are given in the table below.

**Table 13. Data collection and refinement statistics for the  $\Phi$ PcyX dataset leading to the solution of the crystal structure.** Data in parenthesis represent values for the highest resolution shell unless stated otherwise. The crystallization, data collection and the model refinement was performed in a cooperation with Eckhard Hofmann and Johannes Sommerkamp (Protein Crystallography Group; Ruhr University Bochum; modified after Ledermann *et al.*, 2017b).

Data collection		Phasing	
Beamline	ESRF ID30B	Resolution for phasing [Å]	48.45 – 3.0
No. of scaled datasets	15	Sulphur sites	11
Resolution [Å]	48.45 2.2 (2.26 2.2)	Figure of merit	0.352
Cell parameters		Refinement	
<i>a</i> , <i>b</i> , <i>c</i> [Å]	78.71 78.71 68.87		
$\alpha$ , $\beta$ , $\gamma$	90° 90° 120°		
Space group	P3 <sub>2</sub> 21 (No. 154)	R <sub>work</sub> / R <sub>free</sub>	30.23% / 31.84%
Wavelength	2.0664 Å	Root mean square deviation bond length [Å]	0.003
No. of observations	2918724 (64988)	Root mean square deviation angles [°]	0.546
No. of unique reflections	24230 (1787)	Ramachandran favored	94.74%
Completeness	100% (99.9%)	Ramachandran outlier	0
Multiplicity	120.459 (36.367)	Mean isotropic <i>B</i> -factor (maximum)	65.67 (116.17)
Average <i>I</i> / $\sigma$ <i>I</i>	24.4 (0.51)	No. of atoms (without riding hydrogens)	
CC(1/2)	100% (32.2%)	Protein	1492
R <sub>sym</sub>	21.3% (324.3%)	Water	13
R <sub>meas</sub>	21.4% (328.9%)		

The solution of the structure revealed that  $\Phi$ PcyX adopts the typical  $\alpha/\beta/\alpha$  sandwich fold, where a central antiparallel  $\beta$ -sheet is flanked by  $\alpha$ -helices (Figure 28), like it has been described for several other FDBRs.

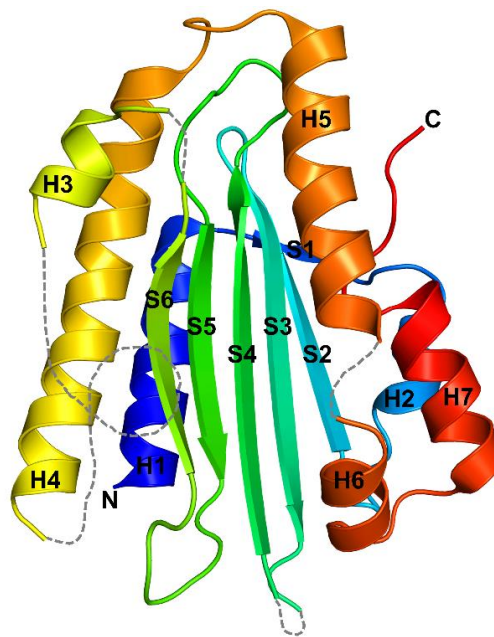


**Figure 28. Overview of the solved  $\Phi$ PcyX X-ray structure.** The structure of  $\Phi$ PcyX is shown in cartoon representation and is colored from blue (N-terminus) to red (C-terminus). Secondary structure elements are continuously numbered and labeled accordingly (H = helix; S = strand). Missing parts of the structure are indicated by dashed lines. The structure was solved in a cooperation with Eckhard Hofmann and Johannes Sommerkamp (Protein Crystallography Group, Ruhr University Bochum). The final model was deposited at the PDB with the accession code 5OWG. Adapted from Ledermann *et al.*, 2017b.

To identify the reasons for the gap in the  $\Phi$ PcyX structure between helix 3 and helix 4 (residues 116-147), this part of the structure was compared with solved structures from other FDBRs. This assessment showed that the large missing part of the structure lies in a region, where for example, PcyA and PebS possess mostly a disordered loop with only short secondary structure elements. Hence, it is very likely that in  $\Phi$ PcyX this region is similarly folded and cannot be modeled due to different conformations present in the crystal, leading to a weak electron density. The gaps between strand 3/ strand 4 (residues 62 - 63) and strand 6/ helix 3 (residues 104 - 106) are obviously disordered loop regions connecting the secondary structure elements. The gap between helix 5 and helix 6 (residues 198 - 200) is also most likely a disordered loop. Interestingly, the same region was also not modeled in a substrate-free PebS structure (PDB 2VCL; Dammeyer *et al.*, 2008b). Only upon the binding of the substrate, the region between the distal  $\alpha$ -helices could be modeled in PebS (PDB 2VCK; Dammeyer *et al.*, 2008b). A remarkable difference of  $\Phi$ PcyX in comparison to other FDBRs is the orientation of the helix H6, a structural element of the substrate binding site. Homologs to this helix are tilted for approximately 30° in PebA, PebS and PcyA (Hagiwara *et al.*, 2006b; Dammeyer *et al.*, 2008b; Busch *et al.*, 2011a).

#### *Insights into the binding pocket*

To gain insights into the structural arrangement within the substrate binding pocket, the  $\Phi$ PcyX model was superimposed with the crystal structure of the substrate-free form of PcyA (PDB 2DKE; Hagiwara *et al.*, 2006b) from *Synechocystis* sp. PCC 6803 (Figure 29).

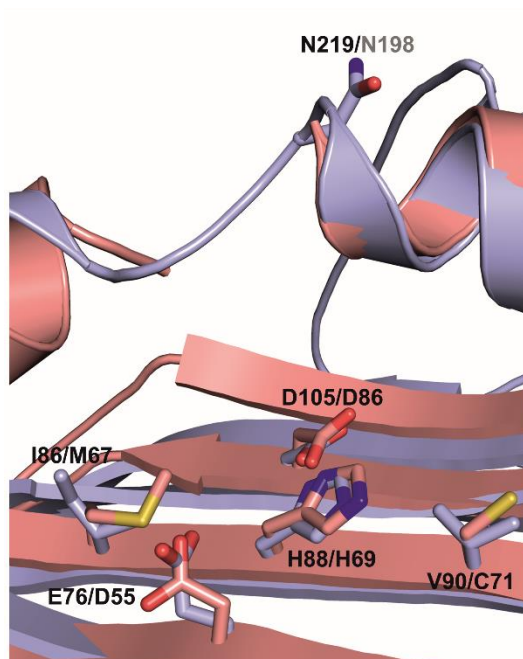


**Figure 29.** Overlay of the solved  $\Phi$ PcyX crystal structure with the substrate-free form of PcyA from *Synechocystis* sp. PCC 6803. Both structures are shown in cartoon representation. Important amino acid residues are shown as sticks and are labeled on the left for PcyA and on the right for  $\Phi$ PcyX. Not modeled residues (i.e. N198 in  $\Phi$ PcyX) are labeled in grey color. The  $\Phi$ PcyX structure is colored in salmon, PcyA (PDB 2DKE; Hagiwara *et al.*, 2006b) is shown in blue.

The comparison revealed that both active sites share a high similarity. On the central  $\beta$ -sheet, the conserved, essential His/Asp pair (i.e. His88 and Asp105) of PcyA can be found at almost the same position in the  $\Phi$ PcyX structure. In conclusion, it is very likely that His69 and Asp86 play the same crucial role in  $\Phi$ PcyX like in PcyA. The essential residue Glu76 of PcyA is substituted by Asp55 in  $\Phi$ PcyX. This amino acid exchange maintains the ability to function as a proton donor via the carboxyl moiety. Nevertheless, it also reduces the flexibility of the side chain, which could lead to an increased distance to the substrate. The hydrophobic residue Ile86 in PcyA, located in close proximity to the BV D-ring (see Figure 30 A), is replaced by Met67 in  $\Phi$ PcyX. Furthermore, PcyA possesses with Val90 a hydrophobic residue located next to the A-ring of BV that has been replaced with Cys71 in  $\Phi$ PcyX. As the distal side of the active site could not be modeled completely due to low electron density, the  $\Phi$ PcyX structure lacks the residues Asn198, Pro199 and His200 located between the distal  $\alpha$ -helices.

As mentioned in 1.2.4, BV can be bound in the active site in different conformations depending on the type of FDBR. In order to gain information about the substrate binding in  $\Phi$ PcyX, several attempts were undertaken to crystallize the FDBR in a complex with BV. No crystals were obtained in all of these experiments. Consequently, BV was manually positioned into the  $\Phi$ PcyX binding pocket (Figure 30 B), based on its conformation found in PcyA from *Synechocystis* sp. PCC 6803 (PDB 2D1E; Hagiwara *et al.*, 2006b). The model was idealized to avoid stereochemical clashes by the application of harmonic restraints.

Because the active sites of both reductases are highly similar, only minor changes to the substrate free structure of  $\Phi$ PcyX were needed to harbor the substrate. An obvious difference is the orientation of the residue Asp86 which required to be rotated upon binding of the substrate, like it is described for PcyA (Hagiwara *et al.*, 2006b). In this orientation, Asp86 is perfectly positioned to coordinate the nitrogen atoms of the BV pyrrole rings. Moreover, the binding of the substrate in PcyA leads to a rotary movement of the loop region between the distal  $\alpha$ -helices towards the binding pocket. The same rotary movement can be expected for the corresponding region in  $\Phi$ PcyX. Interestingly, this would position the potential proton donor His200 in close proximity to the substrate.

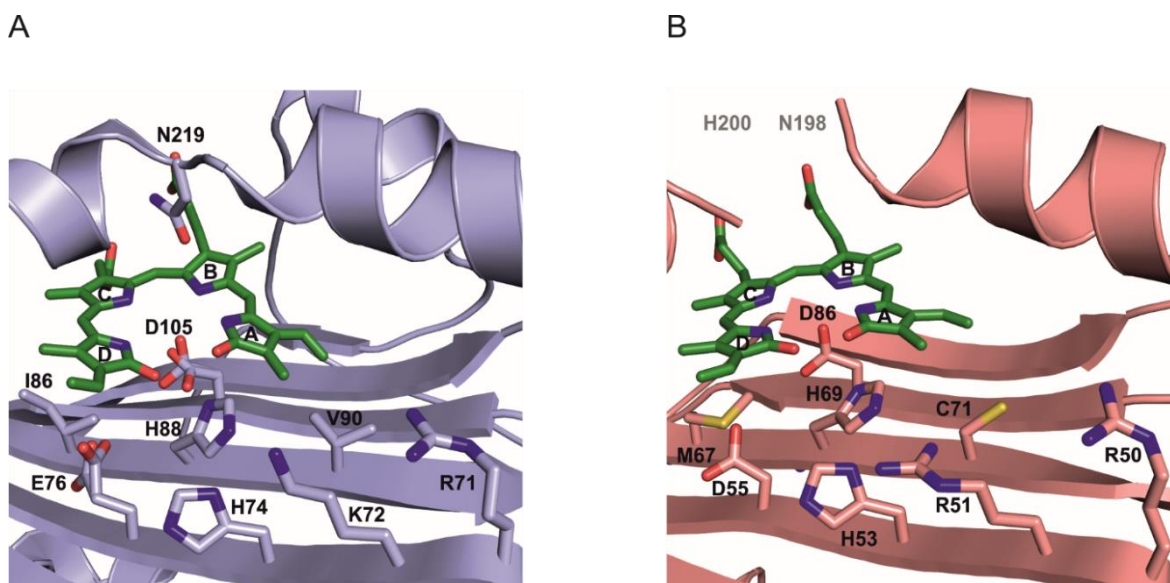


**Figure 30. Comparison of the substrate binding pockets of  $\Phi$ PcyX and PcyA with bound BV.** **A.** Close-up view of the active site of PcyA from *Synechocystis* sp. PCC 6803 (PDB 2D1E; Hagiwara *et al.*, 2006a). **B.** Close-up view of the substrate binding pocket of  $\Phi$ PcyX with manually positioned substrate. For both reductases important amino acid residues are shown as sticks and are labeled accordingly. Residues that are not represented in the  $\Phi$ PcyX structure are labeled in grey. In both cases the substrate is shown as green sticks and the pyrrole rings are labeled from A to D. The substrate-bound model of  $\Phi$ PcyX was constructed in a cooperation with Eckhard Hofmann and Johannes Sommerkamp (Protein Crystallography Group, Ruhr University Bochum).

### 3.2.7 Insights into the $\Phi$ PcyX reaction mechanism

Based on the solved  $\Phi$ PcyX structure and the model with the manually positioned substrate, several interesting amino acid residues that potentially play a direct role in the reaction mechanism were identified. These residues were further investigated with regard to their contribution to the  $\Phi$ PcyX activity by site-directed mutagenesis. The putative proton donor Asp55, a homolog to Glu76 in PcyA, was replaced with Asn55 creating the variant  $\Phi$ PcyX\_D55N. Moreover, His69 and Asp86 are homologs to the conserved His-Asp pair of PcyA (i.e. His88 and Asp105) that was proven to be essential for the catalytic activity. Thus, His69 was exchanged with Gln69 (creating  $\Phi$ PcyX\_H69Q) and Asp86 with Asn86 (creating  $\Phi$ PcyX\_D86N) in accordance to experiments already performed for PcyA by Tu and coworkers (Tu *et al.*, 2006).

All  $\Phi$ PcyX variants were produced and purified with yields comparable to the WT protein. To test the activity of the variants, they were employed in anaerobic FDBR assays. The incubation with the substrate revealed that all variants are still able to form complexes with BV, as the binding spectra were similar to WT (initial spectra marked as "BV" in Figure 31). The variant  $\Phi$ PcyX\_D55N displayed almost WT-like activity (Figure 31 B). Immediately after the start of the reaction, the BV absorbance decreased and furthermore, the formation and the decay of radical intermediates were observed. The product formation was comparable to WT  $\Phi$ PcyX. First, the formation of 15,16-DHBV with an absorbance maximum at 560 nm was visible. During later stages, this maximum shifted to shorter wavelengths due to the reduction of 15,16-DHBV to PEB. In contrast, the variant  $\Phi$ PcyX\_H69Q (Figure 31 C) displayed a different activity compared to WT. After the reaction was started, the BV absorbance decreased and the formation of radical intermediates with absorbance maxima at 450 nm and 750 nm were detected. The decay of the absorbance caused by the radical species is drastically slower compared to WT, suggesting that the variant stabilizes a radical intermediate. During later stages of the reaction, the formation of 15,16-DHBV with an absorbance maximum at 560 nm was visible. In contrast to the assay employing the WT protein, this maximum did not shift to shorter wavelengths, indicating that the formation of PEB from 15,16-DHBV is impaired in the  $\Phi$ PcyX\_H69Q variant. The activity tests with  $\Phi$ PcyX\_D86N (Figure 31 D) showed that this variant of the  $\Phi$ PcyX protein is unable to form either 15,16-DHBV or PEB. Though the absorbance related to BV declined immediately after the assay was started, it rose again as the reaction proceeded. Furthermore, the absorbance at ~ 750 nm showed an unusual double peak, suggesting the formation of an atypical radical. The absorbance at ~ 450 nm quickly increased after the reaction was started and remained stable until the end. A possible reason for this observation could be the stabilization of a substrate radical intermediate.

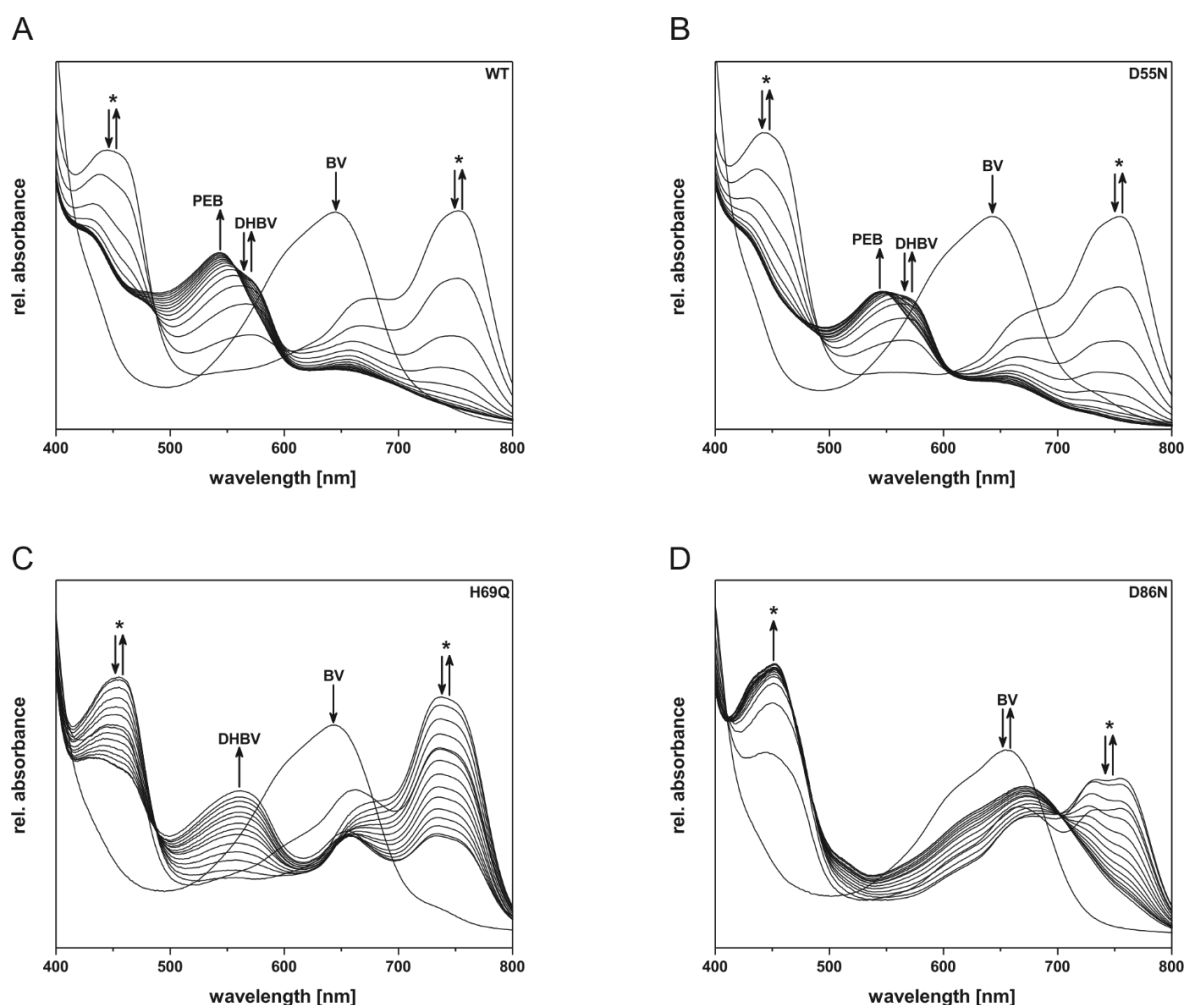


**Figure 31. Overview of time-resolved UV-Vis spectra of anaerobic FDBR activity tests.** The assays were conducted with different variants of  $\Phi$ PcyX using equimolar amounts of BV as the substrate. **A.**  $\Phi$ PcyX\_WT; **B.**  $\Phi$ PcyX\_D55N; **C.**  $\Phi$ PcyX\_H69A; **D.**  $\Phi$ PcyX\_D86N. The total reaction time for each assay was 30 min and spectra were taken every 30 s. In order to maintain clarity, only the spectra of every 2 min are shown. The arrows indicate the course of the absorbance during the reaction. Radical intermediates are labeled with asterisks and peak absorbance related to a specific bilin are marked accordingly. Adapted from Ledermann *et al.*, 2017b.

Intensive studies of the solved X-ray structure highlighted several other residues that were suspected to be important for the catalytic activities of  $\Phi$ PcyX. Residue Met67 was selected for site-directed mutagenesis, as it is located close to the D-ring of BV (see Figure 30 B). Moreover, Hagiwara and coworkers were able to show that Ile86, the PcyA homolog to Met67, is essential for the activity of PcyA (Hagiwara *et al.*, 2016). To investigate the role of Met67, it was exchanged with Ile67 creating the variant  $\Phi$ PcyX\_M67I. Another residue that was chosen for site-directed mutagenesis experiments was Cys71. In the substrate bound model of  $\Phi$ PcyX (Figure 30 B) this residue is located in proximity of the A-ring of BV, the site where the second reduction takes place. To elucidate, if Cys71 has an influence on this reduction, it was replaced with an Ala residue generating the variant  $\Phi$ PcyX\_C71A. Residue Asn198, located on the disordered loop between the distal  $\alpha$ -helices, was exchanged with Asp generating  $\Phi$ PcyX\_N198D. This variant was constructed to reconstitute the PebS arrangement with an acidic residue on the distal side of the binding

pocket. His200 is also located on the non-modeled loop between helix 5 and helix 6. As this residue is a potential proton donor in close proximity to the substrate, it was exchanged with the non-protonating residue Gln, yielding the variant  $\Phi$ PcyX\_H200Q.

The FDBR assays showed that all variants except for  $\Phi$ PcyX\_N198D showed BV binding spectra similar to WT, suggesting that they were correctly folded and able to form complexes with BV (Figure 32 A-D). The assays employing  $\Phi$ PcyX\_M67I (Figure 32 A) revealed that the variant is still capable to facilitate the formation of radical intermediates with absorbance maxima at ~ 450 nm and 750 nm. Despite this fact, no product formation was observed during a reaction time of 30 min. The activity assay with the  $\Phi$ PcyX\_C71A variant (Figure 32 B) revealed that it possesses almost WT-like activity. Hence, a direct involvement of Cys71 in the reduction of BV or 15,16-DHBV can be ruled out. The assays employing  $\Phi$ PcyX\_N198D (Figure 32 C) showed that this variant is not able to form a characteristic BV complex with an absorbance maximum at ~ 660 nm. Nevertheless, UV-Vis spectroscopy showed the formation of radicals, but no formation of 15,16-DHBV or PEB was detected. On the contrary, variant  $\Phi$ PcyX\_H200Q (Figure 32 D) displayed a faster turnover compared to WT. The substrate radical absorbance at 450 nm and 750 nm rose and declined quickly. After a total reaction time of 30 min, a distinct PEB absorbance at ~ 540 nm was visible.

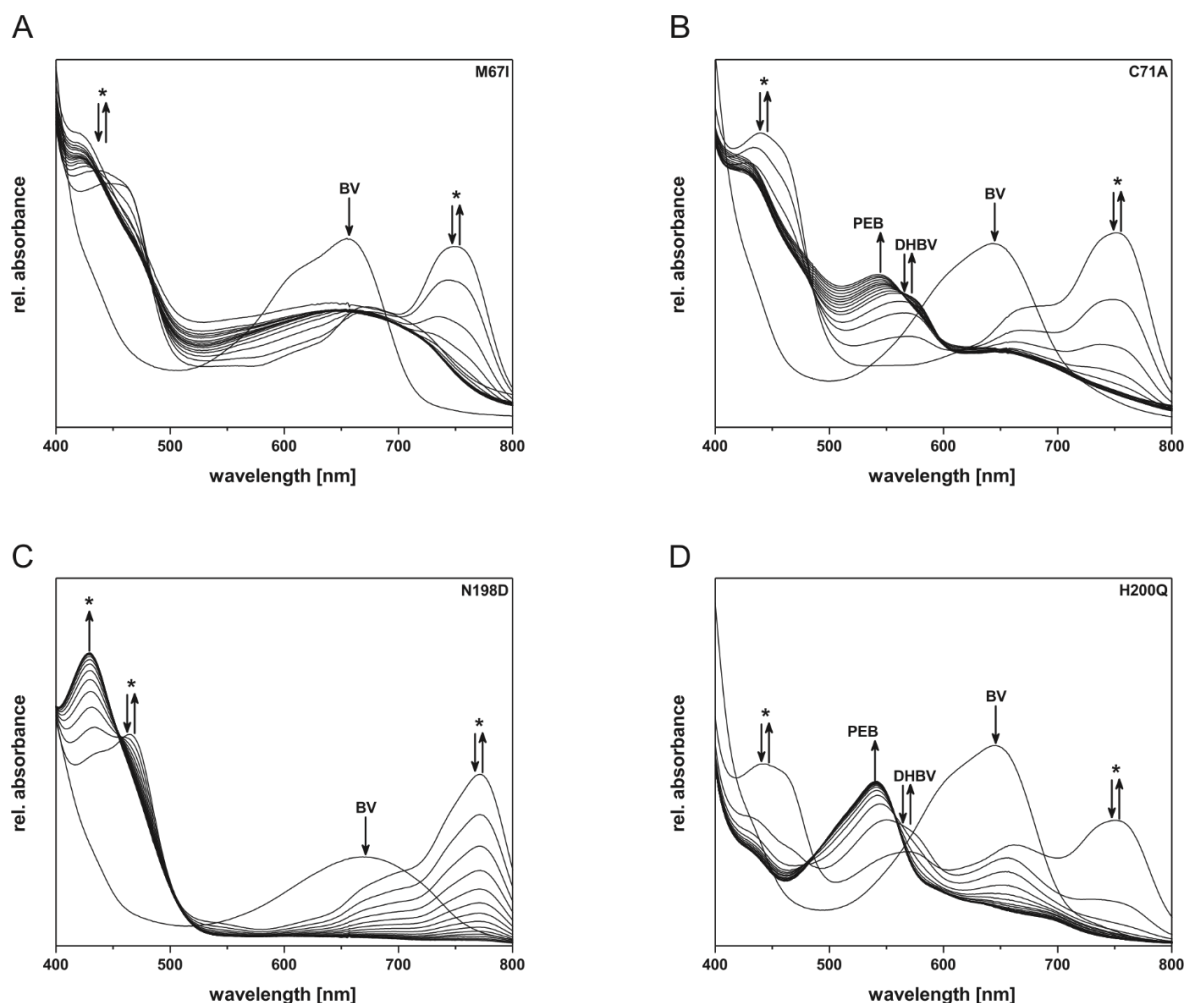


**Figure 32. Overview of time-resolved UV-Vis spectra of anaerobic FDBR activity tests performed with different variants of  $\Phi$ PcyX.** The assays were carried out with equimolar amounts of reductase and substrate. **A.**  $\Phi$ PcyX\_M67I; **B.**  $\Phi$ PcyX\_C71A; **C.**  $\Phi$ PcyX\_N198D; **D.**  $\Phi$ PcyX\_H200Q. The total reaction time for each assay was 30 min, spectra were taken every 30 s. For reasons of clarity only the spectra of every 2 min are shown. The arrows indicate the course of the absorbance over the reaction time. Absorbance related to radical intermediates are labeled with asterisks and peak absorbance linked to a specific bilin are marked accordingly. Adapted from Ledermann *et al.*, 2017b.

The reaction products of the assays conducted with the different variants of  $\Phi$ PcyX were subsequently analyzed via HPLC. The relative activities of the variants were determined by comparing the ratio of the peak areas of 15,16-DHBV and BV after a reaction time of 10 min in assays that were performed with 1  $\mu$ M Fd<sub>P-SSM2</sub> as the electron donor. The ratio of the WT was set to 100%. The results of these examinations are summarized in Table 14

**Table 14. Overview of the product formation and the activities of the examined  $\Phi$ PcyX variants.**

$\Phi$ PcyX variants	Activity (% of WT)	Products
WT	100	DHBV, PEB
D55N	76	DHBV, PEB
M67I	4	only radical intermediate; traces of DHBV
H69Q	6	DHBV, traces of PEB
C71A	38	DHBV, PEB
D86N	-	-
N198D	-	-
H200Q	153	DHBV, PEB

### 3.2.8 Biochemical characterization of PcyX\_actino and PcyA\_Brady

To gain further insights into the catalytic activity of the PcyX-family, two other FDBRs were characterized: PcyX\_actino, a member of the PcyX family, obtained by single-cell genomics on uncultured actinobacteria (WP\_029636740) that is to date the most distant member of the PcyX-clade. The second enzyme is PcyA\_Brady, a FDBR from *Bradyrhizobium* sp. ORS278, which groups between the PcyA- and the PcyX-group of reductases in the phylogenetic tree shown in Figure 15.

#### *Characterization of PcyX\_actino*

PcyX\_actino is the most distant member of the PcyX reductases in a phylogenetic tree. In order to find out, if this circumstance has an effect on the catalytic activity or the regiospecificity, the reductase was recombinantly produced in *E. coli* and subsequently purified by affinity chromatography (Figure 33 A).

Activity of the purified protein was examined in anaerobic tests employing equimolar amounts of reductase and BV (Figure 33 B). The assays were performed using 20  $\mu$ M Fd<sub>P</sub>-SSM<sub>2</sub> as the electron donor, because initial tests with a concentration of 4  $\mu$ M showed only a slow turnover of BV. The monitoring of the assays via time-resolved UV-Vis spectroscopy revealed that PcyX\_actino formed a BV complex with an absorbance maximum at ~ 660 nm (Figure 33 – initial spectrum labeled with “BV”). Immediately after the reaction was started, the BV absorbance started to decrease. Furthermore, the formation and the decay of substrate radical intermediates with absorbance maxima at 450 nm and 750 nm were detected. After a reaction time of 2 min, the formation of a product with an absorbance maximum at ~ 545 nm was observed, which is most likely due to the formation of PEB. Subsequent HPLC analyses (Figure 33 C) with the reaction products of PebS as standards confirmed the results of the time-resolved UV-Vis spectroscopy. After a total reaction time of 30 min, PcyX-actino yields mostly 3(Z)-PEB, as well as traces of 3(E)-PEB and 15,16-

DHBV. Hence, PcyX\_actino possesses the same activity as  $\Phi$ PcyX and is therefore, a “true” PcyX reductase.

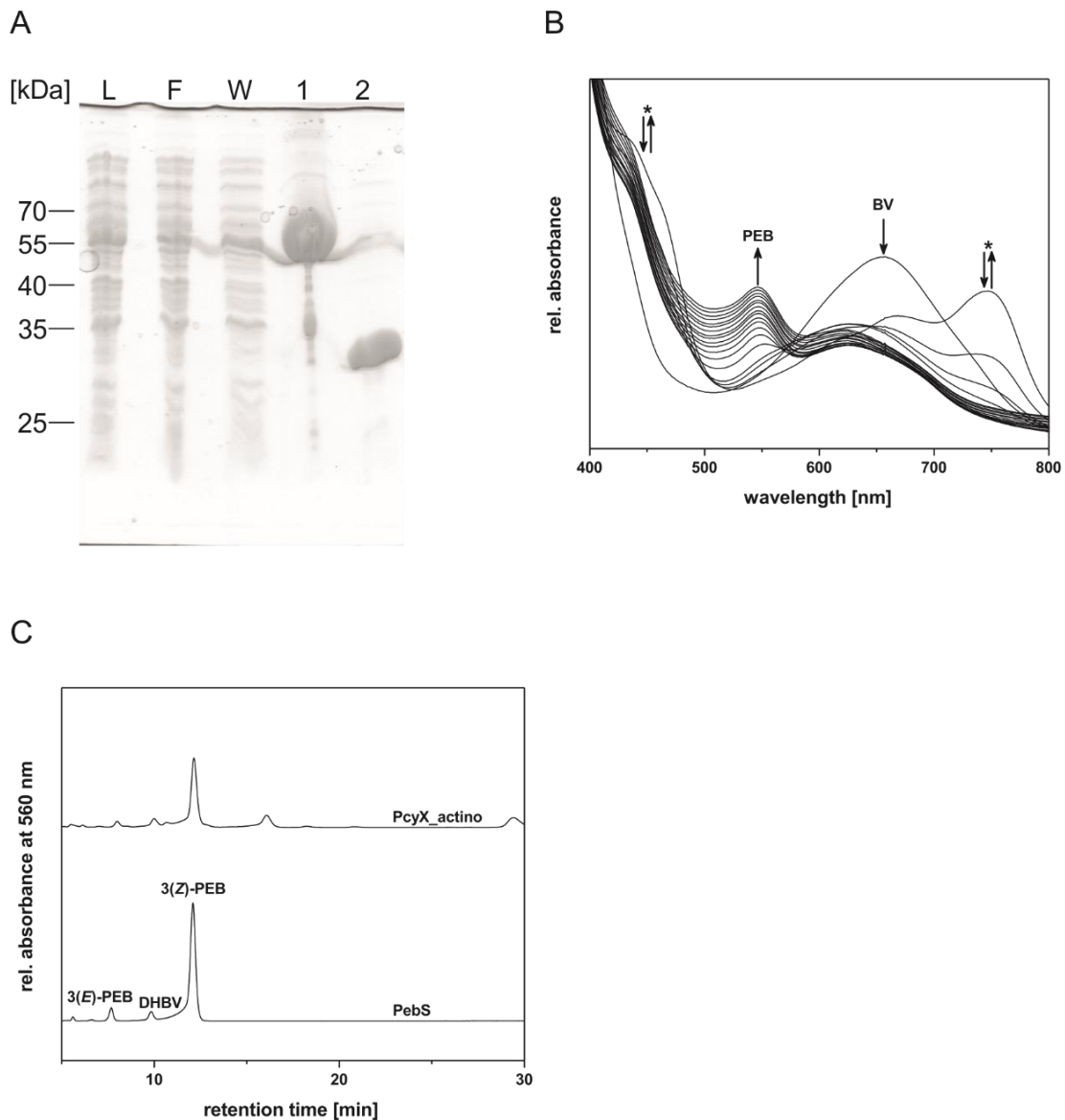


**Figure 33. Overview of the purification, activity assays and the characterization of the reaction products of PcyX\_actino.** **A.** SDS-PAGE showing a purification of GST-tagged PcyX\_actino protein (MW = 52.7 kDa) followed by a digest with PreScission Protease. L = Lysate; F = Flow-through; W = Washing fraction; 1 = Elution fraction before protease digest; 2 = Elution fraction after digest with PreScission Protease (MW PcyX\_actino without tag = 26.3 kDa). PageRuler™ Prestained Protein Ladder (Thermo Fisher) served as size standard. **B.** Time-resolved UV-Vis spectroscopy of an anaerobic activity test with equimolar amounts of PcyX\_actino and BV. The total reaction time was 30 min and spectra were recorded every 30 s. For the first two minutes of the reaction every spectrum is shown, from that point on the increment between the spectra is 2 min. The course of the absorbance is marked with arrows. Radical intermediates are labeled with asterisks and peak absorbance related to a specific bilin is labeled accordingly. **C.** HPLC-analyses of the PcyX\_actino reaction products using a Luna 5  $\mu$ m reversed phase C18 column (Phenomenex) as stationary phase. The products were detected at a wavelength of 560 nm and the reaction products of an anaerobic activity test of PebS from the cyanophage P-SSM2 served as standards.

#### Characterization of PcyA\_Brady

In order to answer the question of the biochemical properties of PcyA\_Brady, it was recombinantly produced in *E. coli* and subsequently purified by affinity chromatography (Figure 34 A). The catalytic activity of the purified protein was assayed in anaerobic tests using equimolar amounts of PcyA\_Brady and BV (Figure 34 B). The activity tests revealed

that PcyA\_Brady is an active FDBR. Interestingly, the initial spectrum of the assay showed not only an absorbance maximum related to a PcyA\_Brady:BV complex ( $\lambda_{\text{max}} \sim 660$  nm; marked as “BV” in Figure **34 B**), but also displayed an absorbance maximum at  $\sim 735$  nm. This absorbance can be related to a protonated BV species (i.e. BVH<sup>+</sup>), as it has been described for PcyA (Tu *et al.*, 2004). The absorbance of the BV complex rapidly declined after the reaction was started. Additionally, the formation and the decay of substrate radical intermediates with absorbance maxima at  $\sim 450$  nm and  $\sim 750$  nm was observed. During later stages of the reaction, the product formation became visible with a raise of the absorbance at  $\sim 650$  and  $715$  nm. These absorbance characteristics are indicative for the formation of PCB, as the formation of PEB would lead to an absorbance with a maximum at shorter wavelengths. The products of the activity assay were subsequently analyzed via HPLC using the products of PcyA from *Nostoc* sp. PCC 7120 as standards. Comparison of the elution profiles of the reaction products showed that both reductases form 3(*E*)- and 3(*Z*)-PCB as their reaction products. Therefore, PcyA\_Brady is a typical PcyA reductase despite clustering outside the PcyA clade in the phylogenetic comparison of the FDBRs. This result confirms the findings of Jaubert and coworkers who already showed the formation of PCB by PcyA\_Brady in an indirect setting (Jaubert *et al.*, 2007).

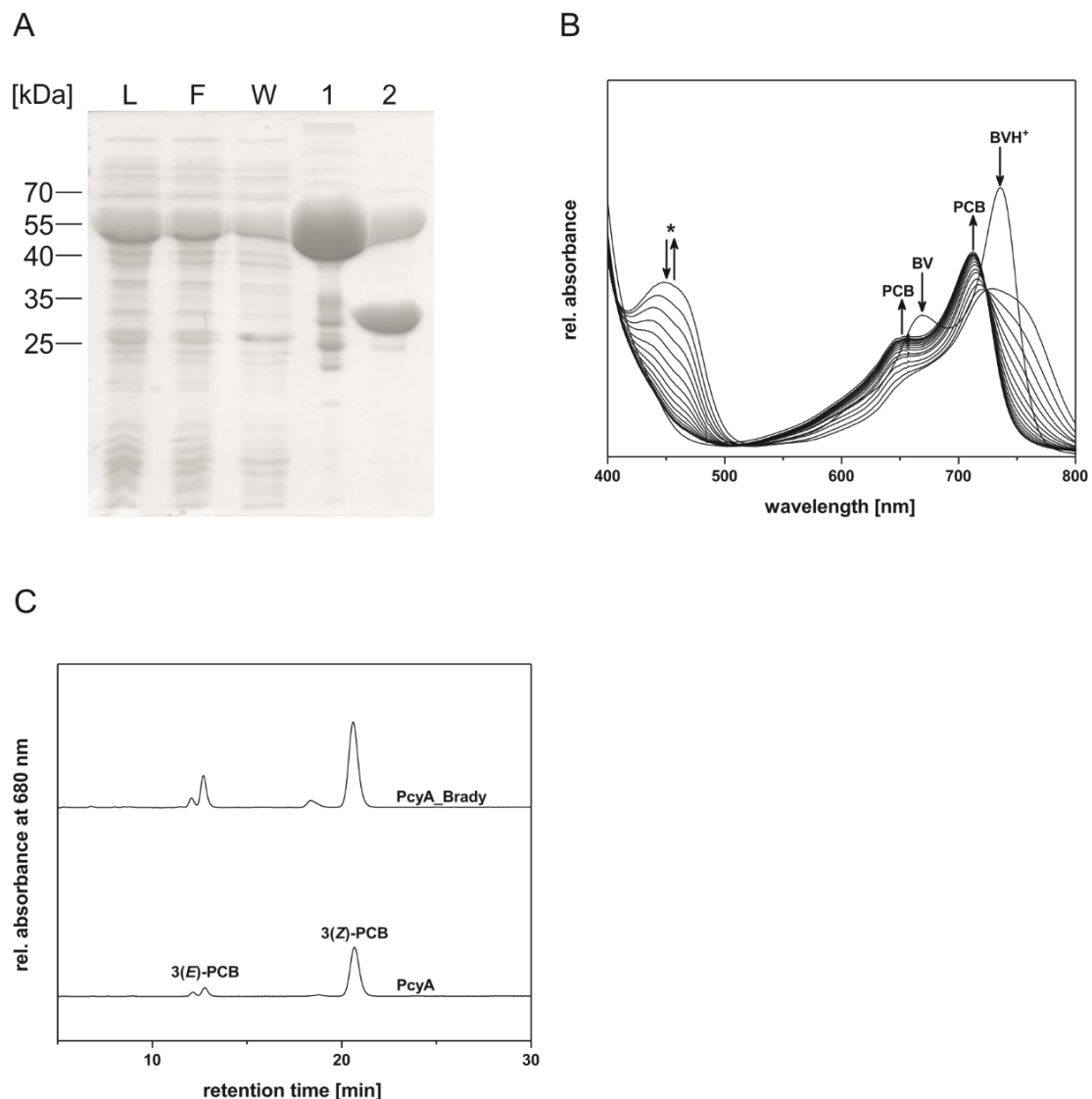


**Figure 34. Overview of the purification, activity assays and the characterization of the reaction products of PcyA\_Brady.** **A.** SDS-PAGE showing a typical purification of GST-tagged PcyA\_Brady protein (MW = 55.1 kDa). L = Lysate; F = Flow-through; W = Washing fraction; 1 = Elution fraction before protease digest; 2 = Elution fraction after protease digest (MW PcyA\_Brady without tag = 28.7 kDa). PageRuler™ Prestained Protein Ladder (Thermo Fisher) was used as size marker. **B.** Time-resolved UV-Vis spectroscopy of an anaerobic activity test with equimolar amounts of PcyA\_Brady and BV. The total reaction time was 30 min and spectra were recorded every 30 s. For reasons of clarity the increment between the shown spectra is 2 min. The course of the absorbance is marked with arrows. Radical intermediates are labeled with asterisks and peak absorbance related to a specific bilin are marked accordingly. BVH<sup>+</sup> symbolizes an absorbance most likely related to a protonated BV species. **C.** HPLC analyses of the PcyA\_Brady reaction products using a Luna 5 μm reversed phase C18 column (Phenomenex) as stationary phase. The mobile phase consisted of a mixture of 50% (v/v) acetone and 50% (v/v) 20 mM formic acid. The products were detected at a wavelength of 680 nm and the reaction products of an anaerobic activity test of PcyA from *Nostoc* sp. PCC 7120 served as standards.

The investigations regarding the biochemical activity of PcyX\_actino and PcyA\_Brady unraveled that both are “true” members of either the PcyX- or the PcyA-reductases. Hence, their positioning in the phylogenetic tree shown in 1.6 was experimentally confirmed.

### 3.3 Characterization of KflaHY2

As highlighted in the section before, the examination of ΦPcyX revealed that it possesses the same activity as PebS despite their low overall sequence identity (Ledermann *et al.*, 2016). This underlines the fact that the catalytic activity of FDBRs cannot solely be predicted

based on phylogenetic analyses. Another example for this circumstance is the FDBR KflaHY2 derived from the streptophyte alga *Klebsormidium flaccidum* (Rockwell *et al.*, 2017). Despite being phylogenetically a member of the HY2-family, this reductase was shown to be involved in the formation of the blue pigment PCB. This activity was demonstrated in an indirect system reconstituting the bilin biosynthesis and the attachment to a phytochrome in *E. coli* (Rockwell *et al.*, 2017).

To directly investigate the catalytic activity and to obtain more detailed insights into the mechanism of KflaHY2, it was recombinantly produced in *E. coli* with an N-terminal fusion to a His<sub>6</sub>-tag. It was purified via affinity chromatography using an Äkta Pure FPLC system with a 1 ml HisTrap FF column (Figure 35 A). The subsequently performed SDS-PAGE revealed that His<sub>6</sub>-KflaHY2 (MW = 36.1 kDa) was produced and purified in reasonable amounts to almost homogeneity (Figure 35 B).

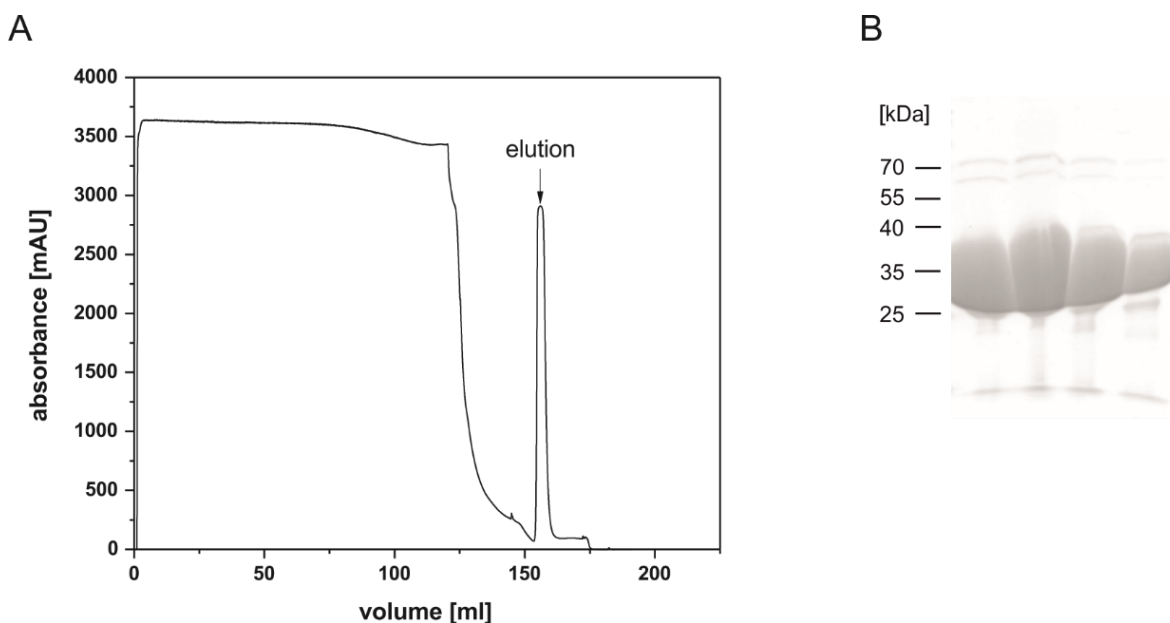


**Figure 35. Purification of recombinantly produced His<sub>6</sub>-KflaHY2 fusion protein.** **A.** Chromatogram of the purification by affinity chromatography performed on an Äkta Pure system using a 1 ml HisTrap FF column. **B.** SDS-PAGE showing the elution fractions of the His<sub>6</sub>-KflaHY2 purification. PageRuler™ Prestained Protein Ladder (Thermo Fisher) was used as size marker.

### 3.3.1 Determination of the oligomerization state

As described in chapter 1.2.4 all known members of the FDBR-family act as monomeric enzymes. To investigate, whether this is also true for KflaHY2, analytic size exclusion experiments employing the purified His<sub>6</sub>-KflaHY2 were performed. His<sub>6</sub>-KflaHY2 eluted at a volume of ~ 11.1 ml (Figure 36 A). Based on the calibration curve this corresponds to a relative MW of ~ 42.9 kDa (Figure 36 B). The slight difference between the calculated (36.1 kDa) and the determined MW is most likely related to the shape of the protein. Nevertheless, it can be concluded that KflaHY2 is present as a monomeric enzyme after purification.

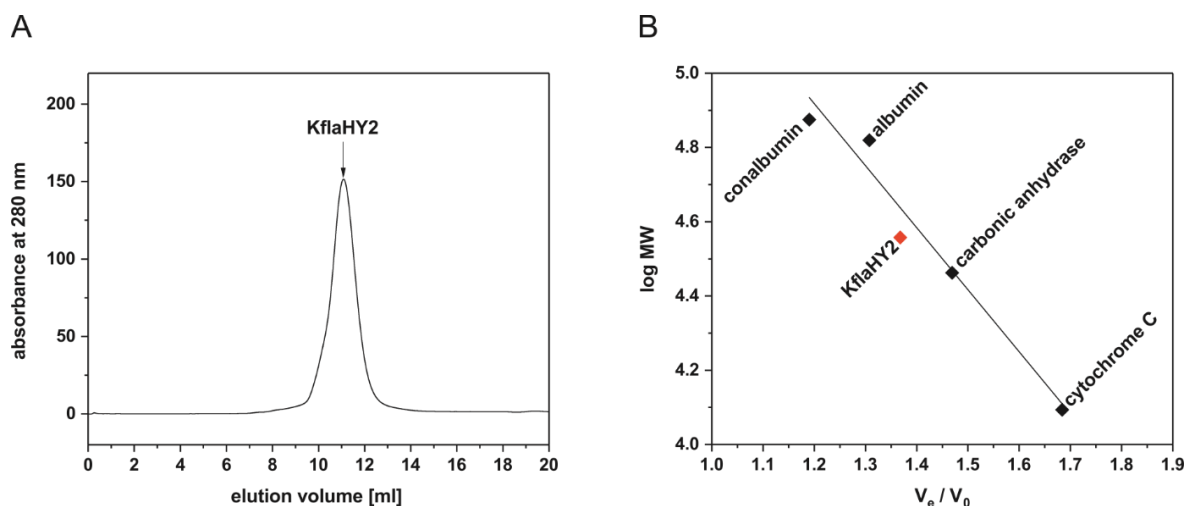


**Figure 36. Determination of the oligomerization state of purified His<sub>6</sub>-KflaHY2.** **A.** Size exclusion chromatography with purified His<sub>6</sub>-KflaHY2 protein. The experiment was performed with a Superdex® 75 10/300 GL equilibrated with TES buffer pH 7.5 and affinity chromatography purified His<sub>6</sub>-KflaHY2. Eluting proteins were detected using their absorbance at 280 nm. **B.** Calibration curve of the Superdex® 75 10/300 GL column. The standards used for calibration were: Conalbumin (MW = 75 kDa), albumin (MW = 66 kDa), carbonic anhydrase (MW = 29 kDa) and cytochrome C (MW = 12.4 kDa). The column was calibrated by plotting (black squares) the log of the MW (log MW) of the standards against the quotient of the elution volume and the void volume ( $V_e/V_0$ ). The calibration curve was calculated using a linear regression in Origin. The red square shows the position of His<sub>6</sub>-KflaHY2 in the calibration plot.

### 3.3.2 KflaHY2 catalyzes the reduction of BV to PCB

To clarify whether the unexpected outcome of the experiments performed by Rockwell and coworkers (Rockwell *et al.*, 2017) is due to an intrinsic PcyA-like activity of KflaHY2, the activity of the purified protein was tested in anaerobic bilin reductase activity assays (Figure 37).

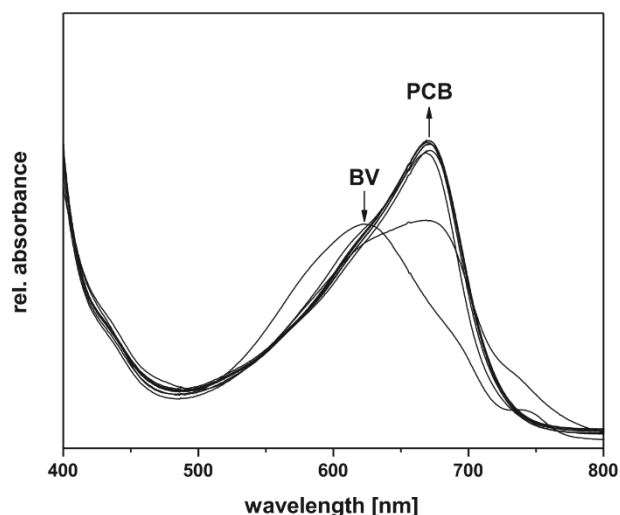


**Figure 37. Time-resolved UV-Vis spectra of an anaerobic bilin reductase activity test of KflaHY2 and BV.** The total reaction time was 5 min and spectra were recorded every 30 s. The course of the spectra is marked by arrows. Peak absorbance maxima are labeled with the corresponding bilin.

The reductase and the substrate formed an intensive turquoise colored complex upon incubation with an absorbance maximum at ~ 622 nm (Figure 37; initial spectrum marked with “BV”). This observation implicates that the reductase was folded correctly, as it was able to bind BV. After the reaction was started, the BV absorbance declined instantly.

Interestingly, no substrate radical related absorbance maxima at 450 nm and 750 nm were visible in the UV-Vis spectra. Nevertheless, a rapid formation of a product with an absorbance maximum at ~ 670 nm was observed, which can be linked to the formation of PCB. Subsequent HPLC analyses employing the reaction products of PcyA as standards confirmed that KflaHY2 forms 3(Z)-PCB as the main reaction product (Figure 38).

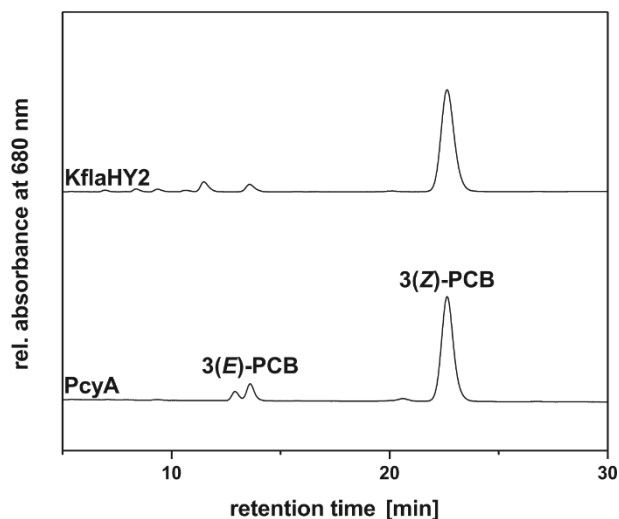


**Figure 38. HPLC analyses of the reaction products of KflaHY2 with BV as substrate.** The products were analyzed using a reversed-phase 5  $\mu$ m C18 Luna column (Phenomenex) as stationary phase. The mobile phase consisted of 50% (v/v) acetone and 50% (v/v) 20 mM formic acid. Products of an anaerobic turnover of BV to PCB mediated by PcyA served as standards.

### 3.3.3 Insights into the KflaHY2 reaction mechanism

The next part of the project was the identification of the intermediates that are formed in the reaction mediated by KflaHY2. The intermediates were isolated using the products of an anaerobic bilin reductase activity test, conducted with one electron equivalent of NADPH. HPLC analyses of the products showed that KflaHY2 forms two intermediates during the reaction (Figure 39 marked as “Inter 1” and “Inter 2”).

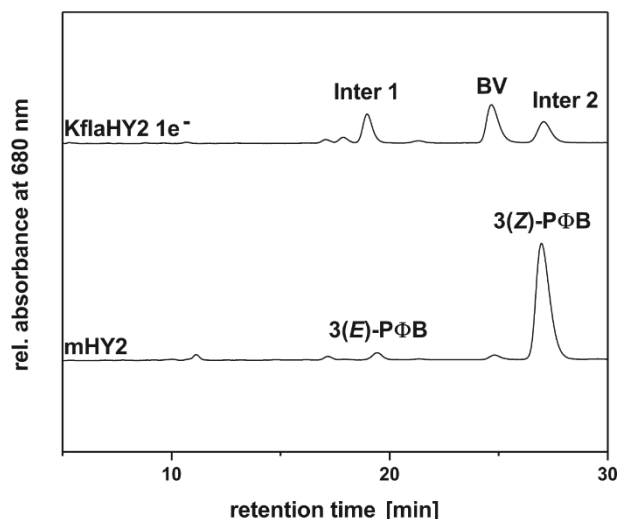


**Figure 39.** HPLC analyses of the reaction products of an anaerobic activity tests employing equimolar amounts of KflaHY2 and BV with one electron equivalent of NADPH. Products were resolved using a reversed-phase 5  $\mu\text{m}$  C18 Luna column (Phenomenex) as stationary phase and a mixture of 50% (v/v) acetone and 50% (v/v) 20 mM formic acid as mobile phase. The compounds were monitored at a wavelength of 680 nm. The products of an anaerobic turnover of BV to PΦB mediated by HY2 derived from *A. thaliana* were used as standards.

The intermediates revealed the same retention times as the products 3(*E*)-PΦB (~ 19 min) and 3(*Z*)-PΦB (~ 27 min) of the reductase HY2 derived from *A. thaliana*.

To clarify the nature of the intermediates identified by HPLC analyses, they were collected, freeze-dried and employed in coupled phytochrome assembly assays with the phytochrome Cph1 (Figure 40 A). Cph1 incubated with “Intermediate 1” did not produce a photoactive adduct, indicating that the A-ring of the intermediate does not possess an ethylidene group. Thus, no characteristic difference spectrum was obtained (Figure 40 A – blue curve). Incubation of Cph1 with “Intermediate 2” (Figure 40 A– red curve) led to a difference spectrum, like it was obtained for the incubation of Cph1 with 3(*Z*)-PΦB (Figure 40 A – yellow curve). These results, as well as the outcome of the HPLC analyses (Figure 39) indicate that “Intermediate 2” is 3(*Z*)-PΦB.

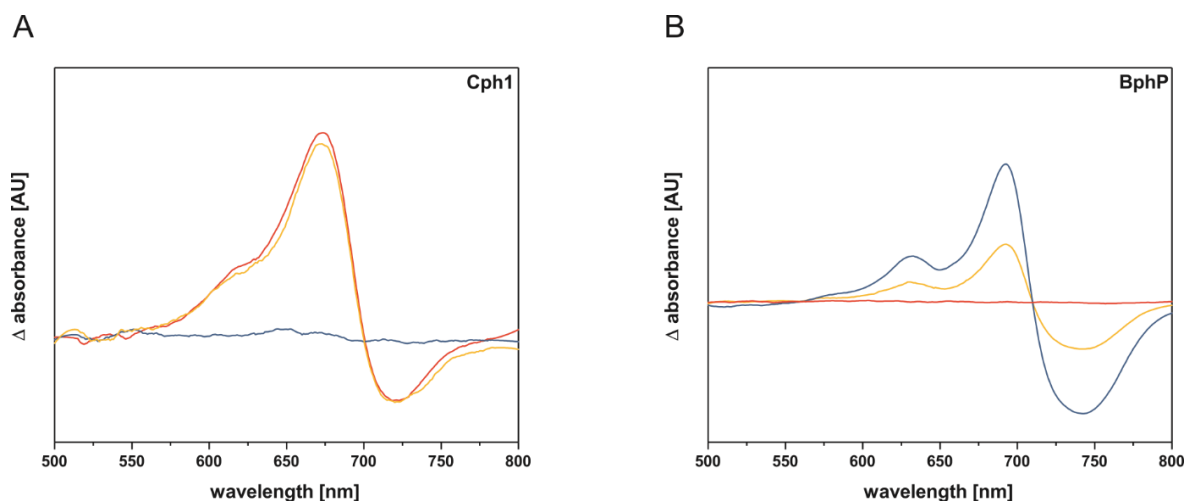


**Figure 40. Difference spectra of coupled phytochrome assembly assays employing the intermediates of the KflaHY2 reaction.** All calculated difference spectra were smoothed applying a 20 pt. Savitzky-Golay filter. **A.** Coupled phytochrome assembly assays employing apo-Cph1 and “Intermediate 1” (blue); apo-Cph1 and “Intermediate 2” (red); apo-Cph1 and 3(Z)-PΦB (yellow) **B.** Coupled phytochrome assembly assay employing apo-BphP and “Intermediate 1” (blue); apo-BphP and “Intermediate 2” (red); apo-BphP and 18<sup>1</sup>,18<sup>2</sup>-DHBV (yellow).

To identify “Intermediate 1”, coupled phytochrome assembly assays were conducted employing the bacterial phytochrome BphP from *P. aeruginosa* and the isolated intermediates. Interestingly, “Intermediate 1” formed a photoactive adduct with apo-BphP that possesses a difference spectrum (Figure 40 B – blue curve) similar to the difference spectrum obtained by the incubation of BphP with purified 18<sup>1</sup>,18<sup>2</sup>-DHBV (Figure 40 B – yellow curve). Moreover, “Intermediate 2” failed to form a photoactive adduct with apo-BphP (Figure 40 B – red curve). These results suggest that KflaHY2 forms both 18<sup>1</sup>,18<sup>2</sup>-DHBV and 3(Z)-PΦB as intermediates in the reduction of BV to PCB.

In the next step of this study, investigations whether the intermediates are only artifacts of the *in vitro* assay, or if both are suitable as substrates were performed. Therefore, both compounds were tested as substrates for His<sub>6</sub>-KflaHY2 in anaerobic bilin reductase activity tests. Subsequent HPLC analyses revealed that KflaHY2 converts both, 18<sup>1</sup>,18<sup>2</sup>-DHBV and 3(Z)-PΦB to mostly 3(Z)-PCB (Figure 41).

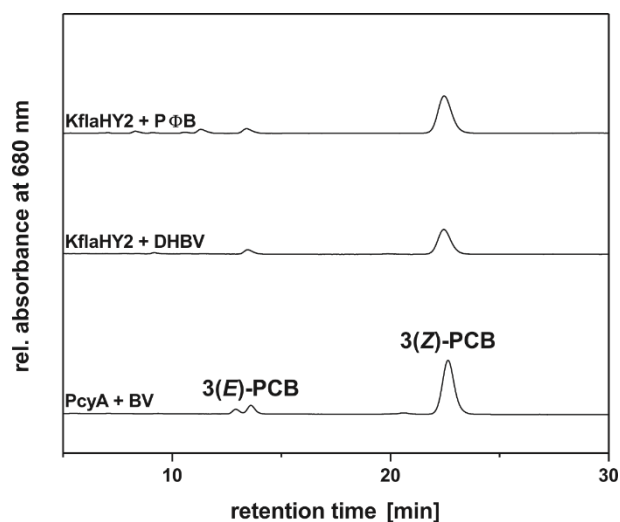


**Figure 41. HPLC analyses of the reaction products of activity tests employing 3(Z)-PΦB and 18<sup>1</sup>,18<sup>2</sup>-DHBV as substrates for KflaHY2.** Products were analyzed using a 5 μm reversed-phase C18 Luna column (Phenomenex) as stationary phase. The mobile phase consisted of 50% (v/v) acetone and 50% (v/v) 20 mM formic acid. The compounds were monitored at a wavelength of 680 nm. Reaction products of a PcyA mediated reduction of BV to PCB were used as standards

## 4 Discussion

The results of this study show that marine metagenomics are an important tool in the discovery of novel biocatalysts, as they proof that the newly found genes related to bilin biosynthesis actually encode for active enzymes. Nevertheless, it also turned out that the specific activity of the enzymes cannot solely be predicted based on phylogenetic analyses. Whereas the recently discovered member of the HO-family showed the expected turnover of heme to BV IX $\alpha$ , the PcyX reductases revealed a surprising activity. Despite their similarity to the PcyA reductases, which catalyze the formation of PCB, they reduce BV to PEB via the intermediate 15,16-DHBV. Hence, they possess the same catalytic activity as PebS, another phage-derived FDBR. Moreover, the recombinant production and purification of KflaHY2 showed that it directly catalyzes the four-electron reduction from BV to PCB *in vitro*, confirming the results of the *in vivo* approaches performed by Rockwell and coworkers (Rockwell *et al.*, 2017).

### 4.1 Characterization of the novel bilin biosynthesis enzymes

#### 4.1.1 $\Phi$ HemO - A “classic” heme oxygenase

The activity assays employing recombinantly produced  $\Phi$ HemO revealed that it is an active HO, yielding BV IX $\alpha$ . This bilin is accepted as substrate for all FDBRs except for PebB. This circumstance, as well as the fact that the discovered HO and FDBR genes are in most cases arranged in “mini-cassettes” on the genomic scaffolds of the metagenomics datasets, suggest that both enzymes act as a functional unit. Consequently, the next step in the course of this study was the biochemical characterization of a member of the PcyX subgroup of the FDBRs.

#### 4.1.2 $\Phi$ PcyX - An enzyme with an unexpected activity

The recombinant expression of the different variants of the  $\phi$ pcyX genes in *E. coli* revealed an interesting phenomenon: The expression of synthetic genes that were optimized for the *E. coli* codon usage did not yield reasonable amounts of soluble  $\Phi$ PcyX protein. Moreover, the purified  $\Phi$ PcyX did not possess any activity in the performed assays. Unexpectedly, the overexpression of the native sequence like it is found on the metagenomics scaffold massively increased the yield of soluble protein. Additionally, the purified  $\Phi$ PcyX showed a turnover of BV in FDBR activity tests. One possible explanation for this phenomenon could be that the overexpression of an optimized sequence leads to a translation process that is too fast to allow the correct folding of the protein. The algorithms employed in the optimization process alter the sequence of the gene to avoid the usage of rare tRNAs in the

expression host (Puigbo *et al.*, 2007). Therefore, they change the employed codons of the target gene so that they reflect the codon usage of the host (Gustafsson *et al.*, 2004). As the speed of the translation process is codon dependent, the usage of an adapted sequence should theoretically improve protein production (Sorensen *et al.*, 1989; Deng, 1997; Mitarai *et al.*, 2008). On the other hand, proteins are folded while they are produced, a process that is called co-translational folding (Wruck *et al.*, 2017). As a consequence, the codon composition of a gene has a direct influence on the efficiency of the protein folding (Yu *et al.*, 2015). Obviously, for  $\Phi pcyX$  this results in massive differences in the solubility and the activity of the protein. In this case, the usage of a non-optimized sequence is highly beneficial and leads to an improved folding of the protein during the translation process.

Improvements in the  $\Phi pcyX$  expression conditions allowed the biochemical characterization of the protein. The determination of the oligomerization state showed that after the purification process,  $\Phi PcyX$  is present as a monomeric enzyme, as it has been described for other FDBRs (Frankenberg and Lagarias, 2003). The anaerobic activity testing of the affinity purified protein revealed that  $\Phi PcyX$  catalyzes the reduction of BV to PEB via the intermediate 15,16-DHBV. Therefore, it possesses the same catalytic activity like PebS. This result was unexpected, as the PcyX reductases are closely related to the PcyA reductases and share only little sequence identity with PebS reductases (Ledermann *et al.*, 2016). For this reason,  $\Phi PcyX$  was expected to catalyze the reduction of BV to PCB via 18<sup>1</sup>,18<sup>2</sup>-DHBV. These findings highlight the importance of actual biochemical assaying of enzymes derived from metagenomics data, as the activity of the proteins cannot only be predicted based on phylogenetic analyses.

#### 4.1.3 Comparison of essential, conserved amino acid residues among PcyX, PcyA and PebS

The unexpected turnover catalyzed by  $\Phi PcyX$  raises the question, what actually determines the regiospecificity of a FDBR. A major factor is the presence of catalytically active amino acid residues in close proximity to the substrate. They are responsible for the site specific transfer of the protons involved in the reduction of BV. In order to highlight the differences between PcyX, PcyA and PebS, a multiple sequence alignment including several members of the reductases was constructed using the T-COFFEE webserver (Notredame *et al.*, 2000; <http://tcoffee.crg.cat/>). The comparison of the conserved essential amino acid residues (Figure 42 Blue arrows – PcyA *Synechocystis* sp. PCC 6803 numbering; red arrow – PebS P-SSM2 numbering) shows that the PcyX reductases indeed are very similar to PcyA. The PcyX Asp55 is a homolog to the essential Glu76 in PcyA which was shown to be crucial for the reduction of BV to 18<sup>1</sup>,18<sup>2</sup>-DHBV (Tu *et al.*, 2007). Moreover, PcyX possesses with His69 and Asp86 also the essential His88/Asp105 pair that is conserved among the PcyA

reductases (Tu *et al.*, 2006). In contrast, His88 is replaced by Asn88 in PebS. Additionally, PcyX lacks an acidic homolog to Asp206, a proton donor on the distal  $\alpha$ -helices that was shown to be critical for the second reduction from 15,16-DHBV to PEB in PebS (Busch *et al.*, 2011b).

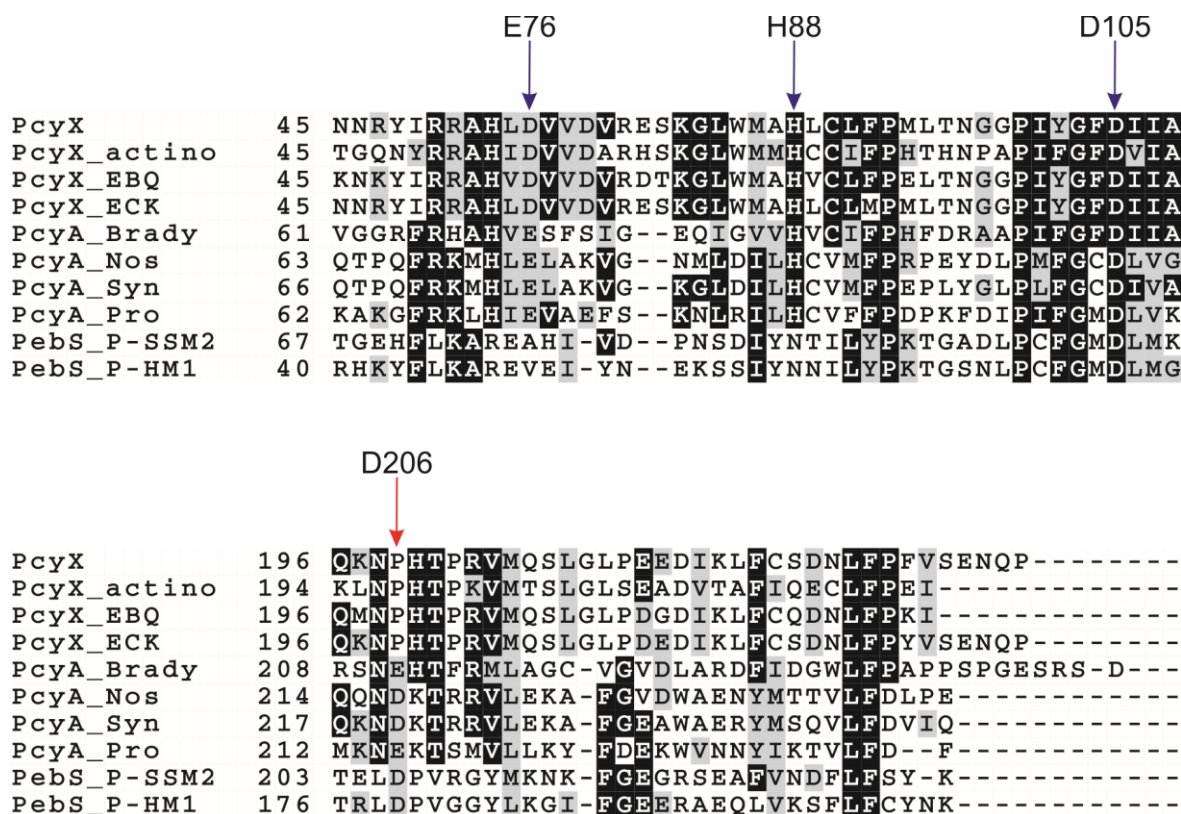


**Figure 42. Excerpt of an alignment of different PcyX, PcyA and PebS reductases.** The alignment was constructed using the T-COFFEE webserver (<http://tcoffee.org.cat/>) and visualized using the BoxShade server ([https://www.ch.embnet.org/software/BOX\\_form.html](https://www.ch.embnet.org/software/BOX_form.html)). The amino acid residues that were shown to be essential for the activities of either PcyA or PebS are marked with arrows and are labeled accordingly. Blue arrows = PcyA from *Synechocystis* sp. PCC 6803 numbering; red arrow = PebS from P-SSM2 numbering. The reductases employed for the constructions are: PcyX =  $\Phi$ PcyX = PcyX\_EBK42635 - GOS\_8734801; PcyX\_actino = PcyX from single cell genomics actinobacterium SCGC AAA041 L13; PcyX\_EBQ = PcyX\_EBQ35476 - GOS\_7763903; PcyX\_ECK = PcyX\_ECK49855 - GOS\_3623672; PcyA\_Brady = PcyX from *Bradyrhizobium* sp. ORS 278; PcyA\_Nos = PcyA from *Nostoc* sp. PCC 7120; PcyA\_Syn = PcyA from *Synechocystis* sp. PCC 6803; PcyA\_Pro = PcyA from *Prochlorococcus marinus*; PebS\_P-SSM2 = PebS from the *Prochlorococcus* phage P-SSM2; PebS\_P-HM1 = PebS from the *Prochlorococcus* phage P-HM1.

Based on sequence alignments, as well as a comparisons of the solved  $\Phi$ PcyX crystal structure with a PcyA structure, different variants of  $\Phi$ PcyX were chosen to be constructed. Overexpression and subsequent biochemical characterization allow the following assumptions.

#### *PcyX and PcyA act via different mechanisms*

The analyses regarding the activities of the variants showed that Asp55, the homolog to the PcyA Glu76, is not involved in the first reduction from BV to DHBV. In PcyA this residue was shown to be essential for the reduction of the D-ring exovinyl group, as the corresponding PcyA\_E76Q variant only yielded P $\Phi$ B (Tu *et al.*, 2007). In contrast to these findings, the  $\Phi$ PcyX\_D55N variant displays WT-like activity, yielding 15,16-DHBV and PEB

(Figure **31 B**). Consequently, it can be ruled out that Asp55 in  $\Phi$ PcyX fulfills the same role as Glu76 in PcyA. One possible explanation for this effect could be the shorter length and the reduced flexibility of the Asp55 side chain compared to the Glu residue. This could increase the distance between the carboxyl moiety and the substrate, preventing a proton transfer onto the substrate. In order to investigate this circumstance and to eventually create a  $\Phi$ PcyX that has a PcyA-like activity, the variant  $\Phi$ PcyX\_D55E was generated. Unfortunately, the purified  $\Phi$ PcyX\_D55E protein was relatively unstable compared to the WT protein. Nevertheless, a preliminary activity test and subsequent HPLC analyses showed that the variant still forms PEB (data not shown). Therefore, it can be concluded that the different regiospecificity of the first reduction in PcyX and PcyA is not only based on the exchange of a single amino acid.

#### *His69 and Asp86 are critical for the activity*

The FDBR assays employing the variants  $\Phi$ PcyX\_H69Q and  $\Phi$ PcyX\_D86N unraveled that this conserved His-Asp pair plays also an essential role for the activity of  $\Phi$ PcyX (Figure **31 C & D**). The exchange of His69 with Gln69 leads to an enzyme that is still able to form 15,16-DHBV. Hence, His69 is not directly involved in the first reduction step. Yet, the formation of 15,16-DHBV proceeds very slow, as the variant stabilizes a radical intermediate. Thus, His69 might be involved in a proton transport chain to Asp86. The variant  $\Phi$ PcyX\_D86N is not capable to form either 15,16-DHBV or PEB. As  $\Phi$ PcyX\_D86N is still able to facilitate an electron transfer onto the substrate, but fails to produce a reduced product, it is very likely that Asp86 is a protonating residue in the  $\Phi$ PcyX reaction. Moreover, the differences in the substrate radical-related absorbance at  $\sim 450$  nm and  $\sim 750$  nm compared to WT also support this suggestion. Interestingly, the same can be observed for the corresponding PcyA\_D105N variant (Tu *et al.*, 2006).

#### *$\Phi$ PcyX lacks a proton donor on the distal helices*

In contrast to the PebS reductases, PcyX does not possess an obvious acidic proton donor on the distal side of the active site (Figure **42**). The only residue that could be involved in the donation of a proton from this side of the binding pocket is His200. This hypothesis can be ruled out, as the variant  $\Phi$ PcyX\_H200Q led to an enzyme that actually showed a faster turnover compared to WT (Figure **32 D**). This unexpected result is probably caused by an improved electron transfer from the ferredoxin onto the bilin. A reason for this could be a better hydrogen bonding network to the substrate or an increase in the affinity of the ferredoxin and the FDBR. In order to reconstitute the PebS-like arrangement with an acidic amino acid residue located on one of the  $\alpha$ -helices,  $\Phi$ PcyX\_N198D was created. This variant is able to facilitate an electron transfer to BV, as it accumulates a radical intermediate but no product formation was observed (Figure **32 C**). A possible explanation is that Asn198

is involved in the coordination of BV in the binding pocket. Therefore, the exchange with Asp198 might result in a wrong positioning of the substrate in the active site.

#### *Met67 is critical for the $\Phi$ PcyX activity*

The activity tests employing the variant  $\Phi$ PcyX\_M67I exposed that Met67 is crucial for the activity of  $\Phi$ PcyX (Figure **32 A**). The variant is still able to transfer an electron onto the substrate, as the formation of radical intermediates were visible in the time-resolved UV-Vis spectroscopy. Nevertheless, the variant is not capable to facilitate the transfer of a second electron, leading to the formation of 15,16-DHBV. A possible explanation for this is the fact that the exchange of Met67 with Ile67 alters the hydrogen bonding network of the residues or water molecules that are involved in the proton transfer onto the bilin. Interestingly, the corresponding PcyA variant PcyA\_I86D has lost all of its activity (Hagiwara *et al.*, 2016). The PcyA\_I86D crystal structure revealed a reduced flexibility of Asp105 which is thought to be an important feature of this residue in the catalytic cycle of PcyA (Unno *et al.*, 2015; Hagiwara *et al.*, 2016). As a consequence, it can be concluded that the catalytic activity is not only determined by the presence or absence of amino acids with reactive side chains. Moreover, the interplay of residues that are directly involved in the catalysis, as well as water molecules and residues that are important for the arrangement of the active site control the activity of a FDBR. Assays employing  $\Phi$ PcyX\_C71A revealed that the enzyme possesses almost WT activity (Figure **32 B**). As a result it can be excluded that Cys71 is directly involved in the reduction of the A-ring.

#### *Conclusions for the PcyX reaction mechanism*

The postulation of a proper reaction mechanism is not possible in regard to the data gathered during the course of this project. Yet, some conclusions can be drawn: His69 and Asp86 play also a crucial role for the PcyX activity like they do in PcyA. Based on the activity test of the different variants, the initial protonation of the substrate seems to be performed by either Asp86 or a water molecule. The initial proton transfer creates a positively charged BVH<sup>+</sup> which accepts the first electron donated from Fd<sub>red</sub>. PcyA employs Glu76 as the proton donor in the next reaction step. In contrast, Asp55 is not crucial for the PcyX activity. Hence, at this stage of the reaction, the mechanisms of PcyX and PcyA must differ. The data of the activity assays suggest that His69 is not essential for the formation of 15,16-DHBV. As other obvious proton donors on the central  $\beta$ -sheet are missing, the site specific reduction at C16 most likely involves a proton transfer from Asp86 like it is expected for PebS (Busch *et al.*, 2011b). The necessary reprotonation of Asp86 is presumably facilitated by a proton channel leading from His69, over His53, Arg51 and Arg50 to the solvent (Figure **30**). The same arrangement of basic amino acid residues can also be found in PcyA (Figure **29**; Hagiwara *et al.*, 2006a; Tu *et al.*, 2007). The activity tests employing  $\Phi$ PcyX\_H200Q revealed that

PcyX lacks a proton donor on the distal side of the active site, like it was described for PebS (Busch *et al.*, 2011b). Therefore, the A-ring reduction most likely involves the same residues like the first reduction step. Based on the proposed mechanism for PcyA, the DHBV intermediate is possibly protonated by Asp86, leading to the formation of DHBVH<sup>+</sup> (Kohler *et al.*, 2010). The subsequent electron transfer from Fd<sub>red</sub> forms a neutral, semi-reduced bilin radical. A proton donated either from a water molecule or His69, followed by a second electron transfer from Fd<sub>red</sub> then would lead to the formation of PEB. The overall reaction is visualized in Figure 43.

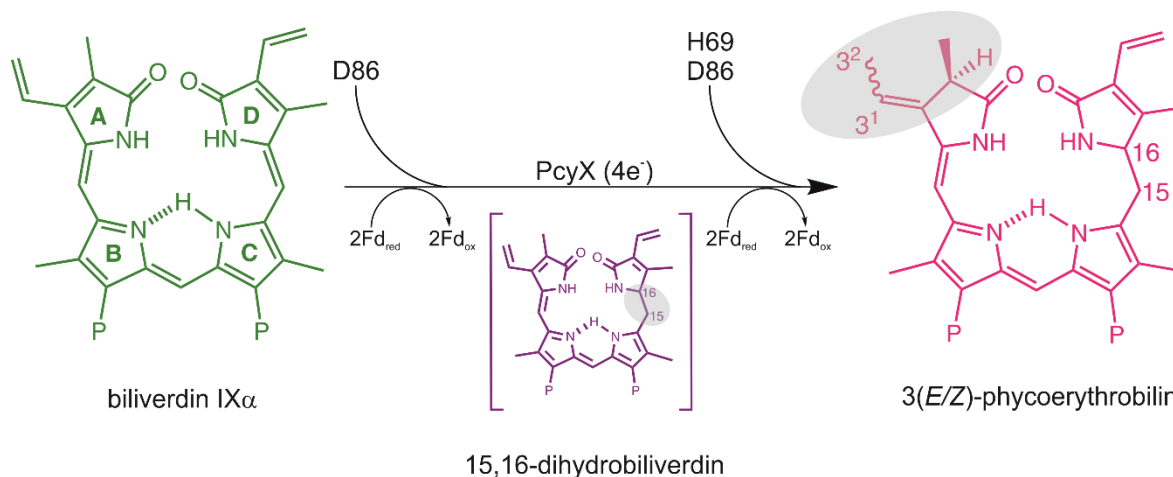


**Figure 43. Overview of the reaction mediated by the PcyX reductases.** The substrate BV is reduced in a first two-electron reduction to 15,16-DHBV. This involves a protonation from Asp86 and eventually a water molecule. The second two-electron reduction from 15,16-DHBV at the A-ring yields 3(E/Z)-PEB. This reduction step involves most likely protons from His69, Asp86 or a water molecule. The sites of the individual reduction steps are highlighted in light-blue. The pyrrole rings of BV are consecutively labeled from A to D; P = propionate side chains; 3(E/Z)-phycoerythrobilin = 3(E)- and 3(Z)-phycoerythrobilin. Amino acid residues that are thought to be involved in the reduction steps are shown in single letter code.

Another attribute of the PcyX reductases is the slow reaction rate in the currently used assay setup. Especially when the rate of the product formation is compared to other members of the FDBR-family that were assayed employing the same reaction conditions, it became clear that the reaction is rather slow. In particular the second reduction step from 15,16-DHBV to PEB seems to be the rate limiting step of the  $\Phi$ PcyX-mediated reaction, as the intermediate is formed relatively fast and is only slowly converted to the final product (Figure 25). The results of the activity assays performed with different concentrations of ferredoxin revealed that the velocity of the reaction is strongly dependent on the concentration of the used ferredoxin. Moreover, the gathered data show that the origin of the redox partner has an impact on the reaction rate (Figure 23). Based on these results it is very likely that the affinity of the reductase and the corresponding ferredoxin is a parameter that has an influence on the rate of the reaction. Chemical crosslinking experiments showed that HY2, PcyA, PebA, PebB and PebS form 1:1 complexes with Fd. The protein-protein interaction between the FDBR and the Fd is mediated by electrostatic interactions via surface-charged residues (Chiu *et al.*, 2010). In case of the reductase these residues are located on the

surface of the binding pocket (Hagiwara *et al.*, 2006b; Tu *et al.*, 2007; Dammeyer *et al.*, 2008b; Chiu *et al.*, 2010). A possible explanation for the not ideal interaction of  $\Phi$ PcyX and the ferredoxins might be due to the composition of the contact patch of the reductase. Results that support this assumption are the activity tests performed with the variant  $\Phi$ PcyX\_H200Q. This variant showed a significantly increased reaction rate compared to WT, even though it lacks the potential proton donor His200 on the distal side of the  $\alpha$ -helices. Thus, a possible explanation for the increased reaction rate could be the improved interaction of FDBR and ferredoxin. A study by Chiu and coworkers highlights the influence of the electron donor on the activity of the FDBRs (Chiu *et al.*, 2010). Six Fds from *A. thaliana* were tested for their suitability as electron donor for the corresponding HY2 reductase. All employed Fds led to highly different enzyme activities. Interestingly, the two most suitable ferredoxins share about 90% sequence identity and a similar redox potential. Nevertheless, even between these two ferredoxins a difference in the activity of approximately ~ 25% was observed. These findings support the theory that the interaction of  $\Phi$ PcyX with the ferredoxin is the limiting factor in the current reaction setup. In this context it needs to be stressed that on one of the metagenomics scaffolds carrying a *pcyX* gene, a putative [2Fe-2S] ferredoxin was discovered. This suggests that maybe a special redox partner is needed for the PcyX reductases. Unfortunately, several approaches to produce this ferredoxin in *E. coli* only yielded unstable, inactive protein.

Another phenomenon of the  $\Phi$ PcyX-mediated reduction is the occurrence of several side products during the reaction (see section 3.2.5). Based on the findings of the time-course experiment regarding the product formation, it is very likely that the compounds that are formed besides 15,16-DHBV and 3(*E/Z*)-PEB are artifacts of the *in vitro* assay conditions. Their abundance only increases while reasonable amounts of BV are still present in the reaction mixture and remains stable during later stages of the reaction. As the assay is carried out in a highly reductive environment with large amounts of NADPH present in the reaction mixture, the formation of unspecific side or decay products is not unlikely. The unknown compound as well as 3(*Z*)-P $\Phi$ B are presumably unspecific decay products of BV caused by the slow reaction rate of the  $\Phi$ PcyX-mediated reaction. Another possible explanation for the occurrence of P $\Phi$ B in the reaction mixture could be the function as an intermediate in the formation of PEB. This would require a reaction mechanism in which the A-ring reduction takes place, before the C15-C16 double bond between the C- and the D-ring is reduced. A result that rejects this hypothesis is the fact that P $\Phi$ B is not accepted as a substrate by the PcyX reductases (Meike Schwan; Master Thesis; 2017; not published). This explains, why the P $\Phi$ B concentration remains stable during the later stages of the assay. In conclusion, it can be ruled out that P $\Phi$ B functions as an intermediate in the formation of PEB and is most likely an *in vitro* artifact caused by suboptimal assay

conditions. Nevertheless, the occurrence of these side products shows that the proton and electron flow in the FDBRs needs to be tightly controlled to avoid the formation of unwanted products. Therefore, the formation of side-products in the FDBRs assays is not totally uncommon, as the same was described in assays employing PUBS (Chen *et al.*, 2012).

## 4.2 The biological function of $\Phi$ PcyX

The characterization of the new HOs and FDBRs derived from metagenomics data revealed that they are active enzymes. As they most likely originate from phages that infect alphaproteobacteria (see chapter 1.6) this raises questions regarding their biological functions. The screening of metatranscriptomic datasets revealed that *pcyX* genes are actually transcribed in both the Atlantic and the Pacific Ocean (Ledermann *et al.*, 2017b). This is a strong hint that the genes actually play an important role during infection.

AMGs related to photosynthesis are rather common among cyanophages (Puxty *et al.*, 2015). Despite their potential disadvantage by expanding the size of the phage genome, they are thought to improve phages fitness during infection events (Sharon *et al.*, 2009; Puxty *et al.*, 2015). For example, the FDBR PebS was discovered in phages that infect marine *Prochlorococcus* species. Moreover, the gene was shown to be expressed during the infection of the host (Dammeyer *et al.*, 2008a).

Studies on the genes that are located in close proximity to the *hemO* and *pcyX* sequences revealed that they originate from phages that most likely infect alphaproteobacteria rather than cyanobacteria (Ledermann *et al.*, 2016). To date there are no known members of the alphaproteobacteria that perform oxygenic photosynthesis. The phototrophic members of the alphaproteobacteria use anoxygenic photosynthesis to convert light energy into chemical energy. They possess only one type of photosystem and employ bacteriochlorophylls instead of chlorophylls (Isaacs *et al.*, 1995; Croce and van Amerongen, 2014). Moreover, they do not enhance their light-harvesting machinery with phycobilisomes or phycobiliproteins, respectively (Nowicka and Kruk, 2016). Thus, the occurrence of bilin biosynthesis genes in phages that are thought to infect these organisms, is enigmatic.

Possible functions for these genes in the infection of alphaproteobacteria could be related to the phytochrome-based sensing of light. The FDBR PcyA\_Brady, which is closely related to the PcyX reductases, was discovered in *Bradyrhizobium* sp. ORS278. This photosynthetic alphaproteobacterium possesses a bacteriophytochrome (i.e. BrBphP3) that was acquired by lateral gene transfer together with a heme oxygenase and PcyA\_Brady (Jaubert *et al.*, 2007). BrBphP3 was shown to bind PCB as its chromophore, a unique feature among bacteriophytochromes which typically employ BV IX $\alpha$  as their light-sensing chromophore. Moreover, BrBphP3 possesses unusual photochemical properties. Its dark-adapted form absorbs at relatively short wavelengths (~ 610 nm) and the light intensity required to photoconvert significant amounts of the phytochrome is relatively high (Jaubert

*et al.*, 2007). Therefore, it is speculated, whether BrBphP3 functions as a sensor for light-intensity, rather than for light-quality (Jaubert *et al.*, 2007). The biological function of phytochromes in anoxygenic photosynthetic alphaproteobacteria is the regulation of the synthesis of the photosystem (Giraud and Vermeglio, 2008). BrBphP1 for example, was shown to control the synthesis of the complete photosynthetic apparatus in *Bradyrhizobium* sp. ORS278 (Giraud *et al.*, 2002).

Hence, one could hypothesize that the function of the newly discovered bilin biosynthesis genes is related to the phytochrome-dependent regulation of the abundance of the photosynthetic system in the hosts during the infection. The expression of *hemO* and *pcyX* would allow the synthesis of PEB. One of the intrinsic properties of a phytochrome is the photoisomerization at the C15-C16 double bond (Rockwell and Lagarias, 2010). This bond between the C- and the D-ring is reduced in PEB. As a result, it was shown to bind to plant-type phytochromes, resulting in the formation of a phytofluor (Murphy and Lagarias, 1997). Phytofluors are fluorescent phytochromes that are not able to photoconvert and are usually not observed in nature. Yet, one could speculate that the binding of PEB could lock a phytochrome in a specific conformation. This could either result in the total loss of its signaling function or could even fix it in an "always on" state. Another possible function of PEB in the host is being a precursor for other bilins. The isomerization of open-chain tetrapyrroles upon the attachment to PBPs or phytochromes is not unusual in nature. The PBP-lyase RpcG from *Synechococcus* sp. WH8102 was shown to catalyze both the attachment of PEB to a PBP subunit as well as its subsequent isomerization to PUB (Blot *et al.*, 2009). Studies performed by Beale and Cornejo moreover revealed that PEB is a precursor for PCB in the red alga *Cyanidium caldarium* (Beale and Cornejo, 1991a).

Interestingly, the FDBR PUBS, that catalyzes the reduction of BV to PUB, is redundant to HY2 in the moss *Physcomitrella patens* (Chen *et al.*, 2012). The *hy2* and *pubs* single mutants showed light-dependent, WT-like phenotypes, whereas the double mutant showed a clear growth deficiency especially under red light illumination. Therefore, the authors of this study concluded that the *hy2* mutant still showed phytochrome-mediated responses even though only PUB was available as the chromophore for the phytochromes. This result is surprising, as PUB does neither possess an ethyliden group at the A-ring nor a C15-C16 double bond. A reason for the maintenance of the photochemical activity could be the stabilization of phytochrome upon transient binding of PUB. Furthermore, the authors speculate whether PUB is further isomerized to yield a reduced A-ring 2,3,3<sup>1</sup>,3<sup>2</sup>-diene system and a C15-C16 double bond by either "unknown factors in the moss cell or by the apo-phytochrome itself" (Chen *et al.*, 2012). The same could apply for PEB formed by the PcyX reductases in the host cell after infection.

A possibility that cannot be ruled out completely is that the host phytochrome and PEB actually form a *bona fide* phytochrome, as the photoisomerization of the bilin could also take place at another double bond of the tetrapyrrolic system. The advantage of a chromophore absorbing at shorter wavelengths (unbound PEB  $\lambda_{\max} \sim 540$  nm) in marine environments could be the adaptation to deeper habitats. Green light is able to penetrate deeper into the water column, whereas red and far-red light is more quickly absorbed (Clarke, 1936). Therefore, a phytochrome that employs PEB could provide a functional photosensor in deep waters. In this context it should be mentioned that Ulijasz and coworkers described a light-induced rotation of the PCB A-ring (i.e. a Z/E-isomerization at the C4-C5 double bond) in a cyanobacterial phytochrome from *Synechococcus* OSB' (Ulijasz *et al.*, 2010). But these results were later proven to be wrong (Song *et al.*, 2014).

Recent studies on *Chlamydomonas reinhardtii* gave hints that there is a bilin-related light sensing beyond the classic phytochromes. *C. reinhardtii* possesses two genes encoding for heme oxygenases (*HMOX1* and *HMOX2*) as well as a gene encoding for a FDBR (i.e. *PCYA*) but no phytochrome. It was shown that a *hmox1* mutant fails to grow photoautotrophically and only adapts poorly to increased illumination (Wittkopp *et al.*, 2017). These effects are related to a reduced accumulation of PSI. The mutant can be rescued by exogenous BV IX $\alpha$  and is dependent on blue-light. Hence, Wittkopp and coworkers propose the existence of a "bilin-based blue-light sensing system" designated as chlorochrome (Wittkopp *et al.*, 2017). The chlorochrome is thought to be a phycobiliprotein that employs either BV IX $\alpha$  or PCB as the light-sensing chromophore. As the distribution and the mechanisms underlying this system still need to be elucidated, it cannot be ruled out that HemO, PcyX and their products might play a role in chlorochrome-related light-sensing.

Another role of the bilin biosynthesis genes in the genome of the phages could also be related to the iron metabolism during the infection of the host. Many HOs were described to play important roles during iron depletion, as the cleavage of heme also releases iron from the macrocycle (Poss and Tonegawa, 1997; Richaud and Zabulon, 1997). This could be advantageous for phages in aquatic environments, because the concentration of iron in the ocean is rather low. It can fall below 1 nmol/kg of seawater in regions far away from continental margins and moreover, it has been shown that iron is the limiting factor for the growth of phytoplankton in nutrient rich areas of the ocean (Martin *et al.*, 1989; Martin *et al.*, 1991). Therefore, it is possible that some phages have developed a system to utilize and redirect the iron "stored" in the heme of the host during the infection event. In human heme oxygenase-1 the rate determining step in absence of biliverdin reductase is the release of biliverdin from the active site of the enzyme (Liu and de Montellano, 2000). In presence of biliverdin reductase, an enzyme that reduces BV to bilirubin, the release of biliverdin is accelerated, making the conversion of Fe<sup>2+</sup>-verdoheme to the Fe<sup>3+</sup>-biliverdin the rate-

determining step of the overall reaction (Liu and de Montellano, 2000). Hence, the physical role of PcyX in iron scavenging might also be to foster the HemO-reaction by shifting the equilibrium towards the product side (Frankenberg *et al.*, 2001).

### 4.3 KflaHY2 - A new type of HY2 enzyme

Another part of this study was the characterization of the FDBR from KflaHY2 derived from the streptophyte alga *K. flaccidum*. The enzyme was shown in indirect *in vivo* assays to synthesize the reduction of BV to PCB, resembling PcyA-like activity (Rockwell *et al.*, 2017). This unexpected turnover is new to the HY2 family. To rule out any influences of the heterologous *in vivo* system on the product formation the protein was purified after heterologous production in *E. coli* and further tested in anaerobic bilin reductase assays. These experiments confirmed that KflaHY2 mediates the reduction of BV to PCB. This raises the question, what causes the difference in the activity of the reductases in the HY2 FDBR family. To investigate this phenomenon, an amino acid sequence alignment employing several PcyA as well as HY2 sequences was constructed using the T-COFFEE webserver (Notredame *et al.*, 2000; <http://tcoffee.crg.cat/>). The analysis of the sequences revealed that the main difference between KflaHY2 and the other members of the HY2 family is Asp122 (red arrow - Figure 44), a homolog to Asp105 from PcyA (PcyA from *Synechocystis* sp. PCC 6803 numbering) that can be found in KflaHY2. This acidic residue is conserved among all FDBRs except in HY2 from land plants. Asp105 is essential for the catalytic activity in PcyA, PebA, PebB, PebS and PcyX (Tu *et al.*, 2006; Busch *et al.*, 2011a; Busch *et al.*, 2011b; Ledermann *et al.*, 2017b). This acidic residue is typically located on the central  $\beta$ -sheet of the substrate binding pocket and is thought to be the initial proton donor involved in the formation of BVH<sup>+</sup> in PcyA (Unno *et al.*, 2015). Therefore, it is very likely that in KflaHY2 Asp122 is also involved in the protonation of the substrate and/or intermediates that occur during the reaction. Moreover, the sequence analysis showed that KflaHY2 lacks a homolog to the PcyA Glu76, which is essential for the formation of 18<sup>1</sup>,18<sup>2</sup>-DHBV in PcyA (Tu *et al.*, 2007). Another interesting feature of KflaHY2 is the residue Asn105, the homolog to PcyA His88. The substitution of this His residue with an Asn can also be found in PebS, PebA and PebB. Land-plant HY2 enzymes possess an Asp residue at this position which is thought to be involved in the positioning of the substrate in the active site (Tu *et al.*, 2008). Moreover, KflaHY2 possesses with Asp242 still a homolog to Asp256 from *A. thaliana* HY2 located on the distal side of the binding pocket. This residue was shown to be involved in the reduction at the A-ring of the substrate and is most likely the initial proton donor of the reaction (Tu *et al.*, 2008). KflaHY2 Asp242 is also a homolog to PebS Asp206, which is essential for the reduction at the A-ring 2,3,3<sup>3</sup>,3<sup>2</sup>-diene system. Hence, it is very likely, that it is also involved in the A-ring reduction in the reaction mediated by KflaHY2. Based on these findings it is very plausible that the ability of KflaHY2 to form PCB originates from the

presence of Asp122. The arrangement of potentially important, acidic residues is comparable to PebS which also possesses protonating residues both on the proximal  $\beta$ -sheet and the distal  $\alpha$ -helices.

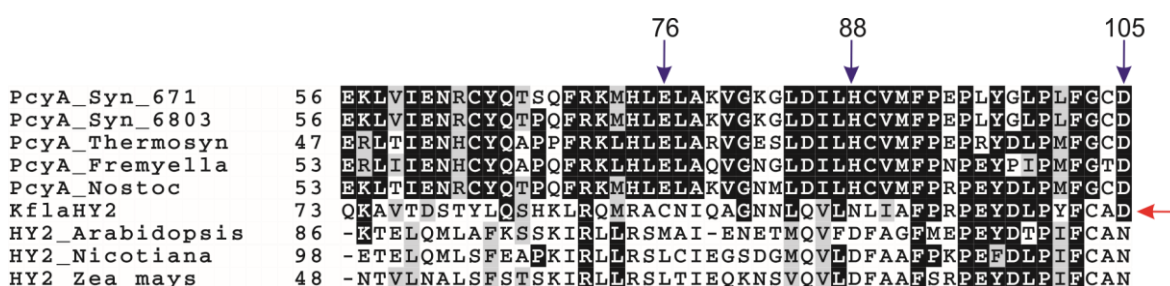


**Figure 44. Excerpt of an alignment of different ferredoxin-dependent bilin reductases.** The alignment was constructed using the T-COFFEE webserver (<http://tcoffee.crg.cat/>) and visualized with the BoxShade server ([https://www.ch.embnet.org/software/BOX\\_form.html](https://www.ch.embnet.org/software/BOX_form.html)). The amino acid residues discussed in the text are marked with blue arrows and labeled according to the numbering of PcyA from *Synechocystis* sp. PCC 6803. The red arrow highlights Asp122 the main difference between KflaHY2 and the other members of the HY2 family. The reductases employed for the constructions are: PcyA\_Syn\_671 = PcyA from *Synechocystis* sp. PCC 6714; PcyA\_Syn\_6803 = PcyA from *Synechocystis* sp. PCC 6803; PcyA\_Thermosyn = *Thermosynechococcus* sp. NK55a; PcyA\_Fremyella = PcyA from *Fremyella diplosiphon* Fd33; PcyA\_Nostoc = PcyA from *Nostoc* sp. PCC 7120; KflaHY2 = HY2 from *Klebsormidium flaccidum*; HY2\_Arabidopsis = HY2 from *Arabidopsis thaliana*; HY2\_Nicotiana = HY2 from *Nicotiana attenuata*; HY2\_Zea\_mays = HY2 from *Zea mays*.

The findings of the alignment were validated by a structure model that was constructed using the PHYRE2 webserver (Kelley *et al.*, 2015; <http://www.sbg.bio.ic.ac.uk/phyre2>). To gain insights about the possible positioning of BV in the substrate binding pocket, a structural overlay with a solved PebS structure from the cyanophage P-SSM2 (PDB 2VCK; Dammeyer *et al.*, 2008b) was performed using the molecular visualization software PyMOL.

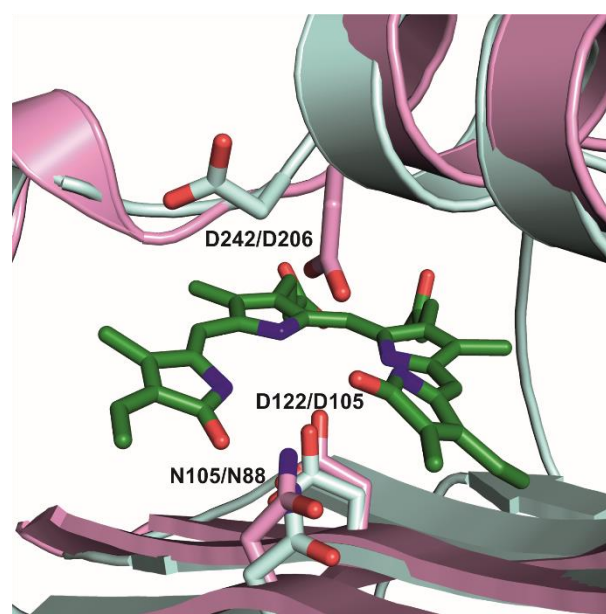


**Figure 45. Close-up view of an overlay of the active sites of a KflaHY2 structural model and PebS from the cyanophage P-SSM2.** The KflaHY2 model was constructed using the PHYRE2 webserver (Kelley *et al.*, 2015) with the sequence of His<sub>6</sub>-KflaHY2 as input. The KflaHY2 model is shown in cartoon representation and is colored in light-blue. The structure of PebS (PDB 2VCK) is shown as pink cartoon. The substrate of the PebS structure is represented as green sticks. The structures were aligned using PyMOL. Important amino acid residues are shown as sticks and are labeled on the left for KflaHY2 and on the right for PebS.

Even based on this rough model, it is obvious that Asp122 is indeed located on one of the central  $\beta$ -strands and is positioned in close proximity to the substrate. The residue Asp242

is located on a flexible loop between two of the distal helices. Interestingly this is one of the loops that could not be modeled in the structures of PebS and  $\Phi$ PcyX that were crystallized without substrate. It is very likely that also in KflaHY2 this region is flexible and able to change its conformation upon binding of BV. This could swing the loop towards the  $\beta$ -sheets, enabling an efficient proton transfer from Asp242 onto the substrate. The structural model suggests that KflaHY2 employs a mechanism like it can be found in the PebS reductases. In PebS, Asp105 was shown to be crucial for the first reduction of BV to 15,16-DHBV. In the overlay shown in Figure 45, KflaHY2 Asp122 and PebS Asp105 superimpose perfectly. Thus, it is very likely that in KflaHY2 Asp122 is also involved in the formation of the 18<sup>1</sup>,18<sup>2</sup>-DHBV intermediate. The difference in the regiospecificity of the first reduction may be due to a slightly altered conformation of the substrate in the binding pocket of KflaHY2. This could tilt the D-ring exovinyl group towards the Asp residue, enabling a proton transfer from the carboxyl moiety. Moreover, in PebS the proton donor Asp206 was proven to be essential for the second reduction at the A-ring 2,3,3<sup>1</sup>,3<sup>2</sup>-diene system. In the structural model the KflaHY2 homolog Asp242 is located at almost the same position. Based on this arrangement it can be expected that it serves the same function as in PebS.

#### 4.3.1 KflaHY2 – An enzyme with two pathways

In theory, PCB biosynthesis can proceed via two different routes depending on the site where the first reduction takes place (Figure 46). The PcyA reductases first reduce the D-ring exovinyl group yielding the intermediate 18<sup>1</sup>,18<sup>2</sup>-DHBV before the A-ring is reduced to create PCB. Another possible way to synthesize PCB, is the reduction of BV at the A-ring 2,3,3<sup>1</sup>,3<sup>2</sup>-diene system to P $\Phi$ B, followed by a second reduction step at the D-ring exovinyl group.

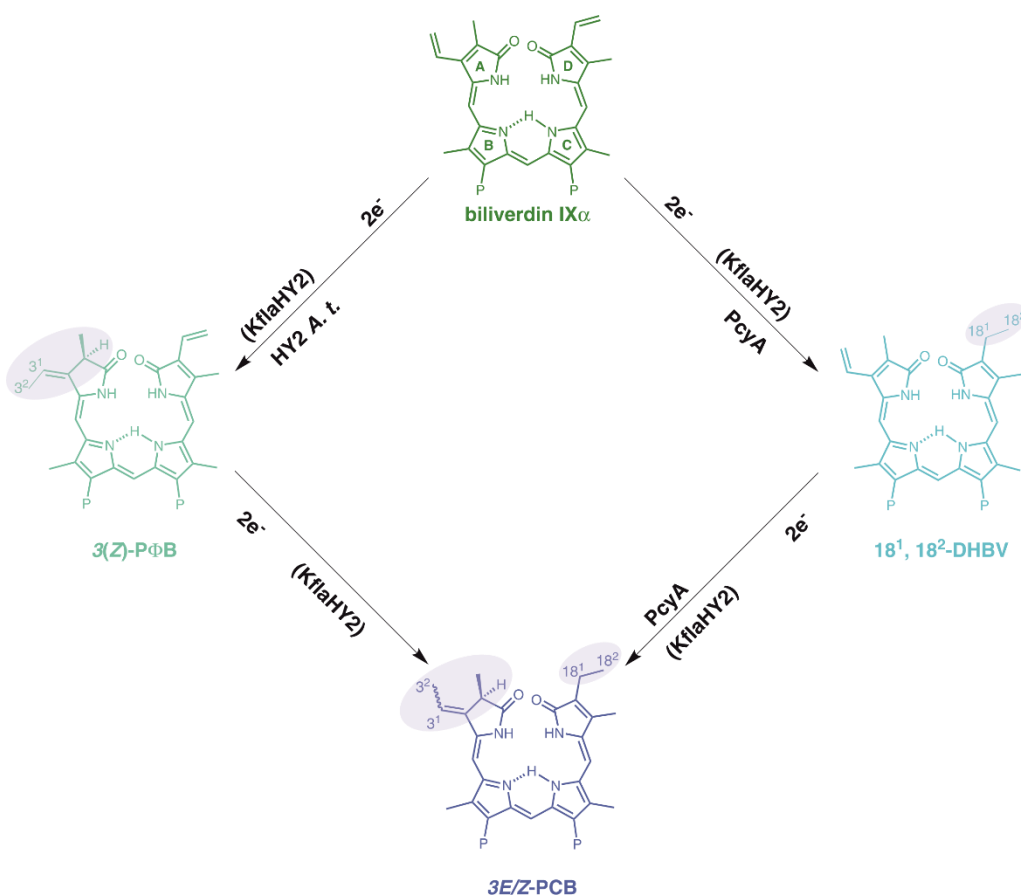


**Figure 46. Overview of the two possible pathways to yield phycocyanobilin from biliverdin.** Depending on the site of the first reduction step the reaction can follow two different ways: The first possibility is to start with the reduction at the A-ring, yielding PΦB, resembling the reaction mediated by HY2 reductases from land plants. A subsequent two-electron reduction at the D-ring exovinyl group yields the product PCB. The second option is the pathway like it is employed by PcyA reductases. This involves the initial reduction at the D-ring exovinyl group to yield 18<sup>1</sup>,18<sup>2</sup>-DHBV. A second reduction at the A-ring leads to the formation of the product PCB.

KflaHY2 is a member of the HY2 enzyme family which are known to catalyze the A-ring reduction of BV to PΦB. This raises the question, if the reaction proceeds via PΦB or via 18<sup>1</sup>,18<sup>2</sup>-DHBV as the intermediate. Experiments with defined electron equivalents showed that under the current *in vitro* assay conditions, KflaHY2 forms two different intermediates. These intermediates were identified as 18<sup>1</sup>,18<sup>2</sup>-DHBV and 3(Z)-PΦB. Thus, it seems that KflaHY2 is able to proceed via the two possible ways to produce PCB. A reason for this phenomenon could be the external delivery of the substrate to the reductase in the *in vitro* assay. It is possible that the substrate is bound in two different conformations leading to the formation of two different intermediates. An interaction of KflaHY2 with the corresponding heme oxygenase KflaHY1 *in vivo* might result in a channeling of the substrate to the active site of the reductase, locking it in a defined conformation.

Experiments with the isolated intermediates exposed that KflaHY2 is able to accept both molecules as externally delivered substrates, which are both successfully converted to PCB. Thus, the substrate selectivity of this reductase is rather low. This circumstance is not unusual among the FDBRs, as for example PebS accepts “its” intermediate 15,16-DHBV

as a substrate, successfully converting it to PEB (Dammeyer *et al.*, 2008a). Another example for the promiscuous substrate recognition of some FDBRs is PebA. This enzyme is capable to use P $\Phi$ B as a substrate, transforming it to PEB (Dammeyer and Frankenberg-Dinkel, 2006). The same was shown for a member of the PcyA reductases that is also able to convert P $\Phi$ B to PCB (Frankenberg and Lagarias, 2003). Another substrate that is accepted by PcyA is 18<sup>1</sup>,18<sup>2</sup>-DHBV. In contrast, PcyA does not accept 15,16-DHBV as a substrate. Moreover, the reductase PebB shows a strict substrate specificity towards 15,16-DHBV and is to date the only known member of the FDBR family that does not recognize BV as its substrate (Dammeyer and Frankenberg-Dinkel, 2006). There are different substrate specificities among the FDBR family and based on these findings the vinyl group at the A-ring seems not to play an essential role in the recognition process. Furthermore, the changed planarity or the loss of flexibility that is accompanied by the reduction of the C15-C16 methine bridge seems to have an effect on the accommodation of the substrate.

## 5 Summary

The screening of metagenomic datasets led to the identification of new phage-derived members of the heme oxygenase and the ferredoxin-dependent bilin reductase enzyme families.

The novel bilin biosynthesis genes were shown to form mini-cassettes on metagenomic scaffolds and further form distinct clusters in phylogenetic analyses (Ledermann *et al.*, 2016). In this project, it was demonstrated that the discovered sequences actually encode for active enzymes. The biochemical characterization of a member of the heme oxygenases ( $\Phi$ HemO) revealed that it possesses a regioselectivity for the  $\alpha$ -methine bridge in the cleavage of the heme macrocycle. The reaction product biliverdin IX $\alpha$  was shown to function as the substrate for the novel ferredoxin-dependent bilin reductases (PcyX reductases), which catalyze its reduction to PEB via the intermediate 15,16-DHBV. While it was demonstrated that  $\Phi$ PcyX, a phage-derived member of the PcyX reductases, is an active enzyme, it also became clear that the rate of the reaction is highly dependent on the employed redox partner. It turned out that the ferredoxin from the cyanophage P-SSM2 is to date the most suitable redox partner for the reductases of the PcyX group. Furthermore, the solution of the  $\Phi$ PcyX crystal structure revealed that it adopts an  $\alpha/\beta/\alpha$ -sandwich fold, typical for the FDBR-family. Activity assays and subsequent HPLC analyses with different variants of the  $\Phi$ PcyX protein demonstrated that, despite their similarity, PcyX and PcyA reductases must act via different reaction mechanisms.

Another part of this project focused on the biochemical characterization of the FDBR KflaHY2 from the streptophyte alga *Klebsormidium flaccidum*. Experiments with recombinant KflaHY2 showed that it is an active FDBR which produces 3(Z)-PCB as the main reaction product, like it can be found in reductases of the PcyA group. Moreover, it was shown that under the employed assay conditions the reaction of BV to PCB proceeds in two different ways: Both 3(Z)-P $\Phi$ B and 18<sup>1</sup>,18<sup>2</sup>-DHBV occur as intermediates. Activity assays with the purified intermediates yielded PCB. Hence, both compounds are suitable substrates for KflaHY2.

The results of this work highlight the importance of the biochemical experiments, as catalytic activity cannot solely be predicted by sequence analysis.

## 6 Zusammenfassung

Die Analyse metagenomischer Daten führte zur Entdeckung neuartiger Mitglieder der Enzymfamilien der Hämoxygenasen und der Ferredoxin-abhängigen Bilinreduktasen.

In phylogenetischen Untersuchungen zeigte sich, dass diese Proteine abgegrenzte Cluster in phylogenetischen Stammbäumen formen. Im Laufe dieser Arbeit konnte nachgewiesen werden, dass die entdeckten Sequenzen für funktionelle Enzyme codieren. Die biochemische Charakterisierung eines Mitglieds der neuen Hämoxygenasen ( $\Phi\text{HemO}$ ) ergab, dass das Enzym die Reaktion von Häm zu Biliverdin IX $\alpha$  katalysiert. Weiterhin fungiert Biliverdin IX $\alpha$  als Substrat für die neuen Ferredoxin-abhängigen Bilinreduktasen (PcyX-Reduktasen). Diese katalysieren die Umsetzung des Biliverdins in das pinke Pigment PEB (Phycoerythrobilin) über das Zwischenprodukt 15,16-Dihydrobiliverdin. Untersuchungen an einem Mitglied der PcyX-Reduktasen ( $\Phi\text{PcyX}$ ) zeigten, dass die Reaktionsgeschwindigkeit in großem Maße von dem verwendeten Redoxpartner abhängig ist. Es stellte sich heraus, dass das Ferredoxin aus dem Cyanophagen P-SSM2 der geeignetste Redoxpartner für  $\Phi\text{PcyX}$  ist. Die Röntgenstrukturanalyse an  $\Phi\text{PcyX}$  ergab, dass das Enzym eine  $\alpha/\beta/\alpha$ -Faltung einnimmt. Dieses Strukturmerkmal ist charakteristisch für alle Ferredoxin-abhängigen Bilinreduktasen. Mit Hilfe von ortsspezifischer Mutagenese wurden verschiedene Varianten des  $\Phi\text{PcyX}$ -Proteins erzeugt. Untersuchungen bezüglich der Aktivität dieser Mutanten zeigten, dass die Reduktasen der PcyX- und PcyA-Gruppen verschiedene Reaktionsmechanismen aufweisen müssen. Dies war unerwartet, da die PcyA- und PcyX-Reduktasen eine große Ähnlichkeit innehaben.

Ein weiterer Aspekt dieser Arbeit war die Charakterisierung der Ferredoxin-abhängigen Bilinreduktase KflaHY2 aus der Alge *Klebsormidium flaccidum*. Experimente mit rekombinant produziertem Protein zeigten, dass das Enzym die Reaktion von Biliverdin IX $\alpha$  zu 3(Z)-Phycocyanobilin katalysiert. Untersuchungen zu den Zwischenprodukten ergaben, dass KflaHY2 unter den verwendeten Reaktionsbedingungen die Reaktion von Biliverdin IX $\alpha$  zu 3(Z)-Phycocyanobilin über zwei verschiedene Wege realisiert. Es konnten sowohl 18<sup>1</sup>,18<sup>2</sup>-Dihydrobiliverdin, als auch 3(Z)-Phytochromobilin als Intermediate identifiziert werden. Weiterhin wurde mit Hilfe der isolierten Intermediate gezeigt, dass beide Verbindungen von KflaHY2 zu 3(Z)-PCB umgesetzt werden.

Die Ergebnisse dieser Arbeiten unterstreichen die Notwendigkeit der biochemischen Charakterisierung von putativen Enzymen aus Metagenomdaten, da Sequenzanalysen für eine genaue Vorhersage der Enzymaktivität nicht hinreichend sind.

---

## References

- Aaij, C., and Borst, P.** (1972) The gel electrophoresis of DNA. *Biochim Biophys Acta* **269**: 192-200.
- Adams, P.D., Afonine, P.V., Bunkoczi, G., Chen, V.B., Davis, I.W., Echols, N. et al.** (2010) PHENIX: a comprehensive Python-based system for macromolecular structure solution. *Acta Crystallogr D Biol Crystallogr* **66**: 213-221.
- Aft, R.L., and Mueller, G.C.** (1984) Hemin-mediated oxidative degradation of proteins. *J Biol Chem* **259**: 301-305.
- Angly, F.E., Felts, B., Breitbart, M., Salamon, P., Edwards, R.A., Carlson, C. et al.** (2006) The marine viromes of four oceanic regions. *Plos Biol* **4**: 2121-2131.
- Apt, K.E., Collier, J.L., and Grossman, A.R.** (1995) Evolution of the phycobiliproteins. *J Mol Biol* **248**: 79-96.
- Beale, S.I., and Cornejo, J.** (1984a) Enzymic Transformation of Biliverdin to Phycocyanobilin by Extracts of the Unicellular Red Alga *Cyanidium caldarium*. *Plant Physiol* **76**: 7-15.
- Beale, S.I., and Cornejo, J.** (1984b) Enzymatic heme oxygenase activity in soluble extracts of the unicellular red alga, *Cyanidium caldarium*. *Arch Biochem Biophys* **235**: 371-384.
- Beale, S.I., and Cornejo, J.** (1991a) Biosynthesis of Phycobilins - 3(Z)-Phycoerythrobilin and 3(Z)-Phycocyanobilin Are Intermediates in the Formation of 3(E)-Phycocyanobilin from Biliverdin-IX-Alpha. *J Biol Chem* **266**: 22333-22340.
- Beale, S.I., and Cornejo, J.** (1991b) Biosynthesis of phycobilins. Ferredoxin-mediated reduction of biliverdin catalyzed by extracts of *Cyanidium caldarium*. *J Biol Chem* **266**: 22328-22332.
- Bhoo, S.H., Davis, S.J., Walker, J., Karniol, B., and Vierstra, R.D.** (2001) Bacteriophytochromes are photochromic histidine kinases using a biliverdin chromophore. *Nature* **414**: 776-779.

- 
- Blot, N., Wu, X.J., Thomas, J.C., Zhang, J., Garczarek, L., Bohm, S. et al.** (2009) Phycourobilin in Trichromatic Phycocyanin from Oceanic Cyanobacteria Is Formed Post-translationally by a Phycoerythrobilin Lyase-Isomerase. *J Biol Chem* **284**: 9290-9298.
- Blumenstein, A., Vienken, K., Tasler, R., Purschwitz, J., Veith, D., Frankenberg-Dinkel, N., and Fischer, R.** (2005) The *Aspergillus nidulans* phytochrome FphA represses sexual development in red light. *Curr Biol* **15**: 1833-1838.
- Brandt, S., Von Stetten, D., Gunther, M., Hildebrandt, P., and Frankenberg-Dinkel, N.** (2008) The Fungal Phytochrome FphA from *Aspergillus nidulans*. *J Biol Chem* **283**: 34605-34614.
- Breitbart, M., Salamon, P., Andresen, B., Mahaffy, J.M., Segall, A.M., Mead, D. et al.** (2002) Genomic analysis of uncultured marine viral communities. *Proc Natl Acad Sci USA* **99**: 14250-14255.
- Bryant, D.A., Cohenbazire, G., and Glazer, A.N.** (1981) Characterization of the Biliproteins of *Gloeobacter-Violaceus* Chromophore Content of a Cyanobacterial Phycoerythrin Carrying Phycourobilin Chromophore. *Arch Microbiol* **129**: 190-198.
- Burgie, E.S., Bussell, A.N., Walker, J.M., Dubiel, K., and Vierstra, R.D.** (2014) Crystal structure of the photosensing module from a red/far-red light-absorbing plant phytochrome. *Proc Natl Acad Sci USA* **111**: 10179-10184.
- Busch, A.W., Reijerse, E.J., Lubitz, W., Frankenberg-Dinkel, N., and Hofmann, E.** (2011a) Structural and mechanistic insight into the ferredoxin-mediated two-electron reduction of bilins. *Biochem J* **439**: 257-264.
- Busch, A.W., Reijerse, E.J., Lubitz, W., Hofmann, E., and Frankenberg-Dinkel, N.** (2011b) Radical mechanism of cyanophage phycoerythrobilin synthase (PebS). *Biochem J* **433**: 469-476.
- Butler, W.L., Norris, K.H., Siegelman, H.W., and Hendricks, S.B.** (1959) Detection, Assay, and Preliminary Purification of the Pigment Controlling Photoresponsive Development of Plants. *Proc Natl Acad Sci USA* **45**: 1703-1708.
- Chen, Y.R., Su, Y.S., and Tu, S.L.** (2012) Distinct phytochrome actions in nonvascular plants revealed by targeted inactivation of phytyl biosynthesis. *Proc Natl Acad Sci USA* **109**: 8310-8315.

- 
- Chiu, F.Y., Chen, Y.R., and Tu, S.L.** (2010) Electrostatic interaction of phytochromobilin synthase and ferredoxin for biosynthesis of phytochrome chromophore. *J Biol Chem* **285**: 5056-5065.
- Chory, J., Peto, C.A., Ashbaugh, M., Saganich, R., Pratt, L., and Ausubel, F.** (1989) Different Roles for Phytochrome in Etiolated and Green Plants Deduced from Characterization of *Arabidopsis thaliana* Mutants. *Plant Cell* **1**: 867-880.
- Chu, G.C., Katakura, K., Zhang, X.H., Yoshida, T., and Ikeda-Saito, M.** (1999) Heme degradation as catalyzed by a recombinant bacterial heme oxygenase (Hmu O) from *Corynebacterium diphtheriae*. *J Biol Chem* **274**: 21319-21325.
- Clarke, G.L.** (1936) Light penetration in the western North Atlantic and its application to biological problems. *Rapp Cons Explor Mer* **101**.
- Cornejo, J., and Beale, S.I.** (1988) Algal heme oxygenase from *Cyanidium caldarium*. Partial purification and fractionation into three required protein components. *J Biol Chem* **263**: 11915-11921.
- Croce, R., and Van Amerongen, H.** (2014) Natural strategies for photosynthetic light harvesting. *Nat Chem Biol* **10**: 492-501.
- Dammeyer, T., and Frankenberg-Dinkel, N.** (2006) Insights into phycoerythrobilin biosynthesis point toward metabolic channeling. *J Biol Chem* **281**: 27081-27089.
- Dammeyer, T., Bagby, S.C., Sullivan, M.B., Chisholm, S.W., and Frankenberg-Dinkel, N.** (2008a) Efficient phage-mediated pigment biosynthesis in oceanic cyanobacteria. *Curr Biol* **18**: 442-448.
- Dammeyer, T., Hofmann, E., and Frankenberg-Dinkel, N.** (2008b) Phycoerythrobilin synthase (PebS) of a marine virus. Crystal structures of the biliverdin complex and the substrate-free form. *J Biol Chem* **283**: 27547-27554.
- Dauter, Z., Dauter, M., De La Fortelle, E., Bricogne, G., and Sheldrick, G.M.** (1999) Can anomalous signal of sulfur become a tool for solving protein crystal structures? *J Mol Biol* **289**: 83-92.
- Davydov, R.M., Yoshida, T., Ikeda-Saito, M., and Hoffman, B.M.** (1999) Hydroperoxy-heme oxygenase generated by cryoreduction catalyzes the formation of alpha-meso-hydroxyheme as detected by EPR and ENDOR. *J Am Chem Soc* **121**: 10656-10657.

- 
- Deng, T.** (1997) Bacterial expression and purification of biologically active mouse c-Fos proteins by selective codon optimization. *FEBS Lett* **409**: 269-272.
- Duarte, C.M.** (2015) Seafaring in the 21st century: the Malaspina 2010 Circumnavigation Expedition. *Limnol Oceanogr* **24**: 11-14.
- Emsley, P., and Cowtan, K.** (2004) Coot: model-building tools for molecular graphics. *Acta Crystallogr D Biol Crystallogr* **60**: 2126-2132.
- Enomoto, G., Nomura, R., Shimada, T., Ni Ni, W., Narikawa, R., and Ikeuchi, M.** (2014) Cyanobacteriochrome SesA is a diguanylate cyclase that induces cell aggregation in *Thermosynechococcus*. *J Biol Chem* **289**: 24801-24809.
- Fairchild, C.D., and Glazer, A.N.** (1994) Nonenzymatic Bilin Addition to the Gamma-Subunit of an Apophytoerythrin. *J Biol Chem* **269**: 28988-28996.
- Foyer, C.H., Lelandais, M., and Kunert, K.J.** (1994) Photooxidative Stress in Plants. *Physiol Plantarum* **92**: 696-717.
- Frankenberg-Dinkel, N.** (2004) Bacterial heme oxygenases. *Antioxid Redox Sign* **6**: 825-834.
- Frankenberg, N., Mukougawa, K., Kohchi, T., and Lagarias, J.C.** (2001) Functional genomic analysis of the HY2 family of ferredoxin-dependent bilin reductases from oxygenic photosynthetic organisms. *Plant Cell* **13**: 965-978.
- Frankenberg, N., and Lagarias, J.C.** (2003) Phycocyanobilin:ferredoxin oxidoreductase of *Anabaena* sp. PCC 7120. Biochemical and spectroscopic. *J Biol Chem* **278**: 9219-9226.
- Fromme, R., Ishchenko, A., Metz, M., Chowdhury, S.R., Basu, S., Boutet, S. et al.** (2015) Serial femtosecond crystallography of soluble proteins in lipidic cubic phase. *IUCrJ* **2**: 545-551.
- Gao, E.B., Huang, Y.H., and Ning, D.G.** (2016) Metabolic Genes within Cyanophage Genomes: Implications for Diversity and Evolution. *Genes* **7**.
- Gasper, R., Schwach, J., Hartmann, J., Holtkamp, A., Wiethaus, J., Riedel, N. et al.** (2017) Distinct Features of Cyanophage-encoded T-type Phycobiliprotein Lyase PhiCpeT: The role of auxiliary metabolic genes. *J Biol Chem* **292**: 3089-3098.

- 
- Gill, S.C., and Von Hippel, P.H.** (1989) Calculation of protein extinction coefficients from amino acid sequence data. *Anal Biochem* **182**: 319-326.
- Giraud, E., Fardoux, L., Fourrier, N., Hannibal, L., Genty, B., Bouyer, P. et al.** (2002) Bacteriophytochrome controls photosystem synthesis in anoxygenic bacteria. *Nature* **417**: 202-205.
- Giraud, E., and Vermeglio, A.** (2008) Bacteriophytochromes in anoxygenic photosynthetic bacteria. *Photosynth Res* **97**: 141-153.
- Gisk, B., Wiethaus, J., Aras, M., and Frankenberg-Dinkel, N.** (2012) Variable composition of heme oxygenases with different regiospecificities in *Pseudomonas* species. *Arch Microbiol* **194**: 597-606.
- Glazer, A.N.** (1977) Structure and molecular organization of the photosynthetic accessory pigments of cyanobacteria and red algae. *Mol Cell Biochem* **18**: 125-140.
- Grombein, S., Rudiger, W., and Zimmerman, H.** (1975) Structures of Phytochrome Chromophore in Both Photoreversible Forms. *H-S Z Physiol Chem* **356**: 1709-1714.
- Gunsalus, I.C., and Wagner, G.C.** (1978) Bacterial P-450cam methylene monooxygenase components: cytochrome m, putidaredoxin, and putidaredoxin reductase. *Methods Enzymol* **52**: 166-188.
- Gustafsson, C., Govindarajan, S., and Minshull, J.** (2004) Codon bias and heterologous protein expression. *Trends Biotechnol* **22**: 346-353.
- Hagiwara, Y., Sugishima, M., Takahashi, Y., and Fukuyama, K.** (2006a) Crystal structure of phycocyanobilin:ferredoxin oxidoreductase in complex with biliverdin IXalpha, a key enzyme in the biosynthesis of phycocyanobilin. *Proc Natl Acad Sci USA* **103**: 27-32.
- Hagiwara, Y., Sugishima, M., Takahashi, Y., and Fukuyama, K.** (2006b) Induced-fitting and electrostatic potential change of PcyA upon substrate binding demonstrated by the crystal structure of the substrate-free form. *FEBS Lett* **580**: 3823-3828.
- Hagiwara, Y., Wada, K., Irikawa, T., Sato, H., Unno, M., Yamamoto, K. et al.** (2016) Atomic-resolution structure of the phycocyanobilin:ferredoxin oxidoreductase I86D mutant in complex with fully protonated biliverdin. *FEBS Lett* **590**: 3425-3434.

- 
- Heirwegh, K.P., Blanckaert, N., and Van Hees, G.** (1991) Synthesis, chromatographic purification, and analysis of isomers of biliverdin IX and bilirubin IX. *Anal Biochem* **195**: 273-278.
- Hirose, Y., Narikawa, R., Katayama, M., and Ikeuchi, M.** (2010) Cyanobacteriochrome CcaS regulates phycoerythrin accumulation in *Nostoc punctiforme*, a group II chromatic adapter. *Proc Natl Acad Sci USA* **107**: 8854-8859.
- Hirose, Y., Rockwell, N.C., Nishiyama, K., Narikawa, R., Ukaji, Y., Inomata, K. et al.** (2013) Green/red cyanobacteriochromes regulate complementary chromatic acclimation via a protochromic photocycle. *Proc Natl Acad Sci USA* **110**: 4974-4979.
- Holmes, M.G., and Smith, H.** (1975) Function of Phytochrome in Plants Growing in Natural-Environment. *Nature* **254**: 512-514.
- Hörtensteiner, S., and Kräutler, B.** (2011) Chlorophyll breakdown in higher plants. *Biochim Biophys Acta* **1807**: 977-988.
- Ikeuchi, M., and Ishizuka, T.** (2008) Cyanobacteriochromes: a new superfamily of tetrapyrrole-binding photoreceptors in cyanobacteria. *Photoch Photobio Sci* **7**: 1159-1167.
- Isaacs, N.W., Cogdell, R.J., Freer, A.A., and Prince, S.M.** (1995) Light-harvesting mechanisms in purple photosynthetic bacteria. *Curr Opin Struct Biol* **5**: 794-797.
- Ishizuka, T., Kamiya, A., Suzuki, H., Narikawa, R., Noguchi, T., Kohchi, T. et al.** (2011) The cyanobacteriochrome, TePixJ, isomerizes its own chromophore by converting phycocyanobilin to phycoviolobilin. *Biochemistry* **50**: 953-961.
- Jaubert, M., Lavergne, J., Fardoux, J., Hannibal, L., Vuillet, L., Adriano, J.M. et al.** (2007) A singular bacteriophytochrome acquired by lateral gene transfer. *J Biol Chem* **282**: 7320-7328.
- Kabsch, W.** (2010) Xds. *Acta Crystallogr D Biol Crystallogr* **66**: 125-132.
- Kelley, L.A., Mezulis, S., Yates, C.M., Wass, M.N., and Sternberg, M.J.** (2015) The Phyre2 web portal for protein modeling, prediction and analysis. *Nat Protoc* **10**: 845-858.
- Keyse, S.M., and Tyrrell, R.M.** (1989) Heme Oxygenase Is the Major 32-Kda Stress Protein-Induced in Human-Skin Fibroblasts by Uva Radiation, Hydrogen-Peroxide, and Sodium Arsenite. *Proc Natl Acad Sci USA* **86**: 99-103.

- 
- Kohchi, T., Mukougawa, K., Frankenberg, N., Masuda, M., Yokota, A., and Lagarias, J.C.** (2001) The Arabidopsis HY2 gene encodes phytochromobilin synthase, a ferredoxin-dependent biliverdin reductase. *Plant Cell* **13**: 425-436.
- Kohler, A.C., Gae, D.D., Richley, M.A., Stoll, S., Gunn, A., Lim, S. et al.** (2010) Structural basis for hydration dynamics in radical stabilization of bilin reductase mutants. *Biochemistry* **49**: 6206-6218.
- Koornneef, M., Rolff, E., and Spruit, C.** (1980) Genetic control of light-inhibited hypocotyl elongation in Arabidopsis thaliana (L.) Heynh. *Z Pflanzenphysiol* **100**: 147-160.
- Krall, L., and Reed, J.W.** (2000) The histidine kinase-related domain participates in phytochrome B function but is dispensable. *Proc Natl Acad Sci USA* **97**: 8169-8174.
- Kumar, S., and Bandyopadhyay, U.** (2005) Free heme toxicity and its detoxification systems in human. *Toxicol Lett* **157**: 175-188.
- Kutty, R.K., and Maines, M.D.** (1981) Purification and characterization of biliverdin reductase from rat liver. *J Biol Chem* **256**: 3956-3962.
- Laemmli, U.K.** (1970) Cleavage of structural proteins during the assembly of the head of bacteriophage T4. *Nature* **227**: 680-685.
- Lagarias, J.C., and Rapoport, H.** (1980) Chromopeptides from Phytochrome - the Structure and Linkage of the Pr Form of the Phytochrome Chromophore. *J Am Chem Soc* **102**: 4821-4828.
- Lamparter, T., Esteban, B., and Hughes, J.** (2001) Phytochrome Cph1 from the cyanobacterium Synechocystis PCC6803. Purification, assembly, and quaternary structure. *Eur J Biochem* **268**: 4720-4730.
- Larsen, R., Gouveia, Z., Soares, M.P., and Gozzelino, R.** (2012) Heme cytotoxicity and the pathogenesis of immune-mediated inflammatory diseases. *Front Pharmacol* **3**: 77.
- Ledermann, B., Beja, O., and Frankenberg-Dinkel, N.** (2016) New biosynthetic pathway for pink pigments from uncultured oceanic viruses. *Environ Microbiol* **18**: 4337-4347.
- Ledermann, B., Aras, M., and Frankenberg-Dinkel, N.** (2017a) Biosynthesis of Cyanobacterial Light-Harvesting Pigments and Their Assembly into Phycobiliproteins. In *Modern Topics in the Phototrophic Prokaryotes*: Springer, pp. 305-340.

- 
- Ledermann, B., Schwan, M., Sommerkamp, J.A., Hofmann, E., Beja, O., and Frankenberg-Dinkel, N.** (2017b) Evolution and molecular mechanism of four-electron reducing ferredoxin-dependent bilin reductases from oceanic phages. *FEBS J.*
- Lindell, D., Sullivan, M.B., Johnson, Z.I., Tolonen, A.C., Rohwer, F., and Chisholm, S.W.** (2004) Transfer of photosynthesis genes to and from Prochlorococcus viruses. *Proc Natl Acad Sci USA* **101**: 11013-11018.
- Liu, Y., and De Montellano, P.R.O.** (2000) Reaction intermediates and single turnover rate constants for the oxidation of heme by human heme oxygenase-1. *J Biol Chem* **275**: 5297-5307.
- Maines, M.D.** (1988) Heme oxygenase: function, multiplicity, regulatory mechanisms, and clinical applications. *FASEB J* **2**: 2557-2568.
- Mann, N.H., Cook, A., Millard, A., Bailey, S., and Clokie, M.** (2003) Marine ecosystems: bacterial photosynthesis genes in a virus. *Nature* **424**: 741.
- Mannisto, R.H., Kivela, H.M., Paulin, L., Bamford, D.H., and Bamford, J.K.H.** (1999) The complete genome sequence of PM2, the first lipid-containing bacterial virus to be isolated. *Virology* **262**: 355-363.
- Martin, J.H., Gordon, R.M., Fitzwater, S., and Broenkow, W.W.** (1989) Vertex - Phytoplankton Iron Studies in the Gulf of Alaska. *Deep-Sea Res* **36**: 649-&.
- Martin, J.H., Gordon, R.M., and Fitzwater, S.E.** (1991) The Case for Iron. *Limnol Oceanogr* **36**: 1793-1802.
- Marx, A., and Adir, N.** (2013) Allophycocyanin and phycocyanin crystal structures reveal facets of phycobilisome assembly. *Biochim Biophys Acta* **1827**: 311-318.
- Mathews, S.** (2006) Phytochrome-mediated development in land plants: red light sensing evolves to meet the challenges of changing light environments. *Mol Ecol* **15**: 3483-3503.
- Matile, P., Hortensteiner, S., Thomas, H., and Krautler, B.** (1996) Chlorophyll breakdown in senescent leaves. *Plant Physiol* **112**: 1403-1409.
- Mcdaniel, L.D., Rosario, K., Breitbart, M., and Paul, J.H.** (2014) Comparative metagenomics: natural populations of induced prophages demonstrate highly unique, lower diversity viral sequences. *Environ Microbiol* **16**: 570-585.

- 
- Mcdowell, M.T., and Lagarias, J.C.** (2001) Purification and biochemical properties of phytochromobilin synthase from etiolated oat seedlings. *Plant Physiol* **126**: 1546-1554.
- Middelboe, M., Riemann, L., Steward, G.F., Hansen, V., and Nybroe, O.** (2003) Virus-induced transfer of organic carbon between marine bacteria in a model community. *Aquat Microb Ecol* **33**: 1-10.
- Millard, A.D., Zwirgmaier, K., Downey, M.J., Mann, N.H., and Scanlan, D.J.** (2009) Comparative genomics of marine cyanomyoviruses reveals the widespread occurrence of *Synechococcus* host genes localized to a hyperplastic region: implications for mechanisms of cyanophage evolution. *Environ Microbiol* **11**: 2370-2387.
- Mitarai, N., Sneppen, K., and Pedersen, S.** (2008) Ribosome collisions and translation efficiency: optimization by codon usage and mRNA destabilization. *J Mol Biol* **382**: 236-245.
- Moore, J.** (1964) Gel permeation chromatography. I. A new method for molecular weight distribution of high polymers. *J Polym Sci Pol Chem* **2**: 835-843.
- Mullis, K.B., and Faloona, F.A.** (1987) Specific synthesis of DNA in vitro via a polymerase-catalyzed chain reaction. *Methods Enzymol* **155**: 335-350.
- Muramoto, T., Kohchi, T., Yokota, A., Hwang, I., and Goodman, H.M.** (1999) The Arabidopsis photomorphogenic mutant *hy1* is deficient in phytochrome chromophore biosynthesis as a result of a mutation in a plastid heme oxygenase. *Plant Cell* **11**: 335-348.
- Murphy, J.T., and Lagarias, J.C.** (1997) The phytofluors: a new class of fluorescent protein probes. *Curr Biol* **7**: 870-876.
- Nagano, S.** (2016) From photon to signal in phytochromes: similarities and differences between prokaryotic and plant phytochromes. *J Plant Res* **129**: 123-135.
- Narikawa, R., Ishizuka, T., Muraki, N., Shiba, T., Kurisu, G., and Ikeuchi, M.** (2013) Structures of cyanobacteriochromes from phototaxis regulators AnPixJ and TePixJ reveal general and specific photoconversion mechanism. *Proc Natl Acad Sci USA* **110**: 918-923.

- 
- Narikawa, R., Nakajima, T., Aono, Y., Fushimi, K., Enomoto, G., Ni Ni, W. et al.** (2015) A biliverdin-binding cyanobacteriochrome from the chlorophyll d-bearing cyanobacterium *Acaryochloris marina*. *Sci Rep* **5**: 7950.
- Nealson, K.H., and Venter, J.C.** (2007) Metagenomics and the global ocean survey: what's in it for us, and why should we care? *Isme J* **1**: 185-187.
- Notredame, C., Higgins, D.G., and Heringa, J.** (2000) T-Coffee: A novel method for fast and accurate multiple sequence alignment. *J Mol Biol* **302**: 205-217.
- Nowicka, B., and Kruk, J.** (2016) Powered by light: Phototrophy and photosynthesis in prokaryotes and its evolution. *Microbiol Res* **186**: 99-118.
- Parks, B.M., and Quail, P.H.** (1991) Phytochrome-Deficient hy1 and hy2 Long Hypocotyl Mutants of Arabidopsis Are Defective in Phytochrome Chromophore Biosynthesis. *Plant Cell* **3**: 1177-1186.
- Perez Sepulveda, B., Redgwell, T., Rihtman, B., Pitt, F., Scanlan, D.J., and Millard, A.** (2016) Marine phage genomics: the tip of the iceberg. *FEMS Microbiol Lett* **363**.
- Pesant, S., Not, F., Picheral, M., Kandels-Lewis, S., Le Bescot, N., Gorsky, G. et al.** (2015) Open science resources for the discovery and analysis of Tara Oceans data. *Sci Data* **2**.
- Poss, K.D., and Tonegawa, S.** (1997) Heme oxygenase 1 is required for mammalian iron reutilization. *Proc Natl Acad Sci USA* **94**: 10919-10924.
- Puigbo, P., Guzman, E., Romeu, A., and Garcia-Vallve, S.** (2007) OPTIMIZER: a web server for optimizing the codon usage of DNA sequences. *Nucleic Acids Res* **35**: W126-131.
- Puxty, R.J., Millard, A.D., Evans, D.J., and Scanlan, D.J.** (2015) Shedding new light on viral photosynthesis. *Photosynth Res* **126**: 71-97.
- Ratliff, M., Zhu, W.M., Deshmukh, R., Wilks, A., and Stojiljkovic, I.** (2001) Homologues of neisserial heme oxygenase in gram-negative bacteria: Degradation of heme by the product of the pigA gene of *Pseudomonas aeruginosa*. *J Bacteriol* **183**: 6394-6403.
- Rhie, G., and Beale, S.I.** (1992) Biosynthesis of phycobilins. Ferredoxin-supported nadph-independent heme oxygenase and phycobilin-forming activities from *Cyanidium caldarium*. *J Biol Chem* **267**: 16088-16093.

- 
- Richaud, C., and Zabolon, G.** (1997) The heme oxygenase gene (pbsA) in the red alga *Rhodella violacea* is discontinuous and transcriptionally activated during iron limitation. *Proc Natl Acad Sci USA* **94**: 11736-11741.
- Rivera, M., and Zeng, Y.** (2005) Heme oxygenase, steering dioxygen activation toward heme hydroxylation. *J Inorg Biochem* **99**: 337-354.
- Rockwell, N.C., Njuguna, S.L., Roberts, L., Castillo, E., Parson, V.L., Dwojak, S. et al.** (2008) A second conserved GAF domain cysteine is required for the blue/green photoreversibility of cyanobacteriochrome Tlr0924 from *Thermosynechococcus elongatus*. *Biochemistry* **47**: 7304-7316.
- Rockwell, N.C., and Lagarias, J.C.** (2010) A brief history of phytochromes. *Chemphyschem* **11**: 1172-1180.
- Rockwell, N.C., Martin, S.S., Li, F.W., Mathews, S., and Lagarias, J.C.** (2017) The phycocyanobilin chromophore of streptophyte algal phytochromes is synthesized by HY2. *New Phytol* **214**: 1145-1157.
- Rodriguez, J.C., Zeng, Y., Wilks, A., and Rivera, M.** (2007) The hydrogen-bonding network in heme oxygenase also functions as a modulator of enzyme dynamics: chaotic motions upon disrupting the H-bond network in heme oxygenase from *Pseudomonas aeruginosa*. *J Am Chem Soc* **129**: 11730-11742.
- Römling, U., Galperin, M.Y., and Gomelsky, M.** (2013) Cyclic di-GMP: the first 25 years of a universal bacterial second messenger. *Microbiol Mol Biol Rev* **77**: 1-52.
- Rossmann, M.G., and Blow, D.M.** (1962) The detection of sub-units within the crystallographic asymmetric unit. *Acta Cryst* **15**: 24-31.
- Rusch, D.B., Halpern, A.L., Sutton, G., Heidelberg, K.B., Williamson, S., Yooseph, S. et al.** (2007) The Sorcerer II Global Ocean Sampling expedition: Northwest Atlantic through Eastern Tropical Pacific. *Plos Biol* **5**: 398-431.
- Sanger, F., Air, G.M., Barrell, B.G., Brown, N.L., Coulson, A.R., Fiddes, J.C. et al.** (1977) Nucleotide-Sequence of Bacteriophage Phichi174 DNA. *Nature* **265**: 687-695.
- Savakis, P., De Causmaecker, S., Angerer, V., Ruppert, U., Anders, K., Essen, L.O., and Wilde, A.** (2012) Light-induced alteration of c-di-GMP level controls motility of *Synechocystis* sp. PCC 6803. *Mol Microbiol* **85**: 239-251.

- 
- Schacter, B.A., Nelson, E.B., Marver, H.S., and Masters, B.S.** (1972) Immunochemical evidence for an association of heme oxygenase with the microsomal electron transport system. *J Biol Chem* **247**: 3601-3607.
- Scheer, H., and Zhao, K.H.** (2008) Biliprotein maturation: the chromophore attachment. *Mol Microbiol* **68**: 263-276.
- Schirmer, T., Huber, R., Schneider, M., Bode, W., Miller, M., and Hackert, M.L.** (1986) Crystal structure analysis and refinement at 2.5 Å of hexameric C-phycoerythrin from the cyanobacterium *Agmenellum quadruplicatum*. The molecular model and its implications for light-harvesting. *J Mol Biol* **188**: 651-676.
- Schmitt, M.P.** (1997) Utilization of host iron sources by *Corynebacterium diphtheriae*: Identification of a gene whose product is homologous to eukaryotic heme oxygenases and is required for acquisition of iron from heme and hemoglobin. *J Bacteriol* **179**: 838-845.
- Shan, J., Jia, Y., Clokie, M.R., and Mann, N.H.** (2008) Infection by the 'photosynthetic' phage S-PM2 induces increased synthesis of phycoerythrin in *Synechococcus* sp. WH7803. *FEMS Microbiol Lett* **283**: 154-161.
- Sharon, I., Alperovitch, A., Rohwer, F., Haynes, M., Glaser, F., Atamna-Ismaeel, N. et al.** (2009) Photosystem I gene cassettes are present in marine virus genomes. *Nature* **461**: 258-262.
- Sharon, I., Battchikova, N., Aro, E.M., Giglione, C., Meinel, T., Glaser, F. et al.** (2011) Comparative metagenomics of microbial traits within oceanic viral communities. *Isme J* **5**: 1178-1190.
- Sharrock, R.A.** (2008) The phytochrome red/far-red photoreceptor superfamily. *Genome Biol* **9**.
- Shen, G., Saunee, N.A., Williams, S.R., Gallo, E.F., Schluchter, W.M., and Bryant, D.A.** (2006) Identification and characterization of a new class of bilin lyase: the *cpcT* gene encodes a bilin lyase responsible for attachment of phycoerythrin to Cys-153 on the beta-subunit of phycoerythrin in *Synechococcus* sp. PCC 7002. *J Biol Chem* **281**: 17768-17778.
- Shin, M., and Oshino, R.** (1978) Ferredoxin-Sepharose 4B as a tool for the purification of ferredoxin-NADP<sup>+</sup> reductase. *J Biochem* **83**: 357-361.

- 
- Shukla, A., Biswas, A., Blot, N., Partensky, F., Karty, J.A., Hammad, L.A. et al.** (2012) Phycoerythrin-specific bilin lyase-isomerase controls blue-green chromatic acclimation in marine *Synechococcus*. *Proc Natl Acad Sci USA* **109**: 20136-20141.
- Smith, H., and Whitelam, G.C.** (1990) Phytochrome, a Family of Photoreceptors with Multiple Physiological Roles. *Plant Cell Environ* **13**: 695-707.
- Soldano, A., Klinke, S., Otero, L.H., Rivera, M., Catalano-Dupuy, D.L., and Ceccarelli, E.A.** (2017) Structural and mutational analyses of the *Leptospira interrogans* virulence-related heme oxygenase provide insights into its catalytic mechanism. *PLoS One* **12**: e0182535.
- Song, C., Psakis, G., Kopycki, J., Lang, C., Matysik, J., and Hughes, J.** (2014) The D-ring, not the A-ring, rotates in *Synechococcus* OS-B' phytochrome. *J Biol Chem* **289**: 2552-2562.
- Sorensen, M.A., Kurland, C.G., and Pedersen, S.** (1989) Codon usage determines translation rate in *Escherichia coli*. *J Mol Biol* **207**: 365-377.
- Stoll, S., Gunn, A., Brynda, M., Sughrue, W., Kohler, A.C., Ozarowski, A. et al.** (2009) Structure of the biliverdin radical intermediate in phycocyanobilin:ferredoxin oxidoreductase identified by high-field EPR and DFT. *J Am Chem Soc* **131**: 1986-1995.
- Studier, F.W., and Moffatt, B.A.** (1986) Use of bacteriophage T7 RNA polymerase to direct selective high-level expression of cloned genes. *J Mol Biol* **189**: 113-130.
- Sugishima, M., Omata, Y., Kakuta, Y., Sakamoto, H., Noguchi, M., and Fukuyama, K.** (2000) Crystal structure of rat heme oxygenase-1 in complex with heme. *FEBS Lett* **471**: 61-66.
- Sugishima, M., Migita, C.T., Zhang, X., Yoshida, T., and Fukuyama, K.** (2004) Crystal structure of heme oxygenase-1 from cyanobacterium *Synechocystis* sp. PCC 6803 in complex with heme. *Eur J Biochem* **271**: 4517-4525.
- Sullivan, M.B., Lindell, D., Lee, J.A., Thompson, L.R., Bielawski, J.P., and Chisholm, S.W.** (2006) Prevalence and evolution of core photosystem II genes in marine cyanobacterial viruses and their hosts. *Plos Biology* **4**: 1344-1357.
- Sullivan, M.B., Huang, K.H., Ignacio-Espinoza, J.C., Berlin, A.M., Kelly, L., Weigele, P.R. et al.** (2010) Genomic analysis of oceanic cyanobacterial myoviruses

- 
- compared with T4-like myoviruses from diverse hosts and environments. *Environ Microbiol* **12**: 3035-3056.
- Sun, J., Wilks, A., Ortiz De Montellano, P.R., and Loehr, T.M.** (1993) Resonance Raman and EPR spectroscopic studies on heme-heme oxygenase complexes. *Biochemistry* **32**: 14151-14157.
- Sun, S.L., Chen, J., Li, W.Z., Altintas, I., Lin, A., Peltier, S. et al.** (2011) Community cyberinfrastructure for Advanced Microbial Ecology Research and Analysis: the CAMERA resource. *Nucleic Acids Res* **39**: D546-D551.
- Suttle, C.A.** (2007) Marine viruses--major players in the global ecosystem. *Nat Rev Microbiol* **5**: 801-812.
- Tamoi, M., Miyazaki, T., Fukamizo, T., and Shigeoka, S.** (2005) The Calvin cycle in cyanobacteria is regulated by CP12 via the NAD(H)/NADP(H) ratio under light/dark conditions. *Plant J* **42**: 504-513.
- Tappel, A.L.** (1955) Unsaturated Lipide Oxidation Catalyzed by Hematin Compounds. *J Biol Chem* **217**: 721-733.
- Tasler, R., Moises, T., and Frankenberg-Dinkel, N.** (2005) Biochemical and spectroscopic characterization of the bacterial phytochrome of *Pseudomonas aeruginosa*. *FEBS J* **272**: 1927-1936.
- Tenhunen, R., Marver, H.S., and Schmid, R.** (1968) The enzymatic conversion of heme to bilirubin by microsomal heme oxygenase. *Proc Natl Acad Sci USA* **61**: 748-755.
- Tenhunen, R., Marver, H.S., and Schmid, R.** (1969) Microsomal heme oxygenase. Characterization of the enzyme. *J Biol Chem* **244**: 6388-6394.
- Terry, M.** (1997) Phytochrome chromophore-deficient mutants. *Plant Cell Environ* **20**: 740-745.
- Terry, M.J., and Lagarias, J.C.** (1991) Holophytochrome assembly. Coupled assay for phytochromobilin synthase in organello. *J Biol Chem* **266**: 22215-22221.
- Terry, M.J., Wahleithner, J.A., and Lagarias, J.C.** (1993) Biosynthesis of the plant photoreceptor phytochrome. *Arch Biochem Biophys* **306**: 1-15.

- 
- Terry, M.J., Mcdowell, M.T., and Lagarias, J.C.** (1995) (3Z)- and (3E)-phytochromobilin are intermediates in the biosynthesis of the phytochrome chromophore. *J Biol Chem* **270**: 11111-11118.
- Thompson, L.R., Zeng, Q., Kelly, L., Huang, K.H., Singer, A.U., Stubbe, J., and Chisholm, S.W.** (2011) Phage auxiliary metabolic genes and the redirection of cyanobacterial host carbon metabolism. *Proc Natl Acad Sci USA* **108**: E757-764.
- Towbin, H., Staehelin, T., and Gordon, J.** (1979) Electrophoretic transfer of proteins from polyacrylamide gels to nitrocellulose sheets: procedure and some applications. *Proc Natl Acad Sci USA* **76**: 4350-4354.
- Tu, S.-L., Rockwell, N.C., Lagarias, J.C., and Fisher, A.J.** (2007) Insight into the Radical Mechanism of Phycocyanobilin– Ferredoxin Oxidoreductase (PcyA) Revealed by X-ray Crystallography and Biochemical Measurements. *Biochemistry* **46**: 1484-1494.
- Tu, S.L., Gunn, A., Toney, M.D., Britt, R.D., and Lagarias, J.C.** (2004) Biliverdin reduction by cyanobacterial phycocyanobilin:ferredoxin oxidoreductase (PcyA) proceeds via linear tetrapyrrole radical intermediates. *J Am Chem Soc* **126**: 8682-8693.
- Tu, S.L., Sughrue, W., Britt, R.D., and Lagarias, J.C.** (2006) A conserved histidine-aspartate pair is required for exovinyl reduction of biliverdin by a cyanobacterial phycocyanobilin:ferredoxin oxidoreductase. *J Biol Chem* **281**: 3127-3136.
- Tu, S.L., Chen, H.C., and Ku, L.W.** (2008) Mechanistic studies of the phytochromobilin synthase HY2 from *Arabidopsis*. *J Biol Chem* **283**: 27555-27564.
- Ulijasz, A.T., Cornilescu, G., Cornilescu, C.C., Zhang, J.R., Rivera, M., Markley, J.L., and Vierstra, R.D.** (2010) Structural basis for the photoconversion of a phytochrome to the activated Pfr form. *Nature* **463**: 250-U143.
- Unno, M., Ishikawa-Suto, K., Kusaka, K., Tamada, T., Hagiwara, Y., Sugishima, M. et al.** (2015) Insights into the Proton Transfer Mechanism of a Bilin Reductase PcyA Following Neutron Crystallography. *J Am Chem Soc* **137**: 5452-5460.
- Venter, J.C., Remington, K., Heidelberg, J.F., Halpern, A.L., Rusch, D., Eisen, J.A. et al.** (2004) Environmental genome shotgun sequencing of the Sargasso Sea. *Science* **304**: 66-74.

- 
- Vieira, J., and Messing, J.** (1982) The pUC plasmids, an M13mp7-derived system for insertion mutagenesis and sequencing with synthetic universal primers. *Gene* **19**: 259-268.
- Weinbauer, M.G., and Rassoulzadegan, F.** (2004) Are viruses driving microbial diversification and diversity? *Environ Microbiol* **6**: 1-11.
- Wilhelm, S.W., and Suttle, C.A.** (1999) Viruses and Nutrient Cycles in the Sea - Viruses play critical roles in the structure and function of aquatic food webs. *BioScience* **49**: 781-788.
- Wilks, A., and Schmitt, M.P.** (1998) Expression and characterization of a heme oxygenase (Hmu O) from *Corynebacterium diphtheriae*. Iron acquisition requires oxidative cleavage of the heme macrocycle. *J Biol Chem* **273**: 837-841.
- Wilks, A.** (2002) Heme oxygenase: evolution, structure, and mechanism. *Antioxid Redox Signal* **4**: 603-614.
- Wilks, A., and Heinzl, G.** (2014) Heme oxygenation and the widening paradigm of heme degradation. *Arch Biochem Biophys* **544**: 87-95.
- Wittkopp, T.M., Schmollinger, S., Saroussi, S.I., Hu, W., Zhang, W., Fan, Q. et al.** (2017) Bilin-dependent photoacclimation in *Chlamydomonas reinhardtii*. *Plant Cell*.
- Wruck, F., Katranidis, A., Nierhaus, K.H., Buldt, G., and Hegner, M.** (2017) Translation and folding of single proteins in real time. *Proc Natl Acad Sci USA* **114**: E4399-E4407.
- Yeh, K.C., Wu, S.H., Murphy, J.T., and Lagarias, J.C.** (1997) A cyanobacterial phytochrome two-component light sensory system. *Science* **277**: 1505-1508.
- Yeh, K.C., and Lagarias, J.C.** (1998) Eukaryotic phytochromes: light-regulated serine/threonine protein kinases with histidine kinase ancestry. *Proc Natl Acad Sci USA* **95**: 13976-13981.
- Yoshida, T., Noguchi, M., and Kikuchi, G.** (1980) Oxygenated form of heme . heme oxygenase complex and requirement for second electron to initiate heme degradation from the oxygenated complex. *J Biol Chem* **255**: 4418-4420.
- Yoshihara, S., Katayama, M., Geng, X., and Ikeuchi, M.** (2004) Cyanobacterial phytochrome-like PixJ1 holoprotein shows novel reversible photoconversion between blue- and green-absorbing forms. *Plant Cell Physiol* **45**: 1729-1737.

- 
- Yu, C.H., Dang, Y.K., Zhou, Z.P., Wu, C., Zhao, F.Z., Sachs, M.S., and Liu, Y.** (2015) Codon Usage Influences the Local Rate of Translation Elongation to Regulate Co-translational Protein Folding. *Mol Cell* **59**: 744-754.
- Yu, M.H., Glazer, A.N., Spencer, K.G., and West, J.A.** (1981) Phycoerythrins of the Red Alga *Callithamnion* - Variation in Phycoerythrobilin and Phycourobilin Content. *Plant Physiol* **68**: 482-488.
- Zheng, Q., Jiao, N., Zhang, R., Chen, F., and Suttle, C.A.** (2013) Prevalence of psbA-containing cyanobacterial podoviruses in the ocean. *Sci Rep* **3**: 3207.
- Zhou, W., Ding, W.L., Zeng, X.L., Dong, L.L., Zhao, B., Zhou, M. et al.** (2014) Structure and mechanism of the phycobiliprotein lyase CpcT. *J Biol Chem* **289**: 26677-26689.
- Zhu, W.M., Wilks, A., and Stojiljkovic, I.** (2000) Degradation of heme in gram-negative bacteria: the product of the hemO gene of *Neisseriae* is a heme oxygenase. *J Bacteriol* **182**: 6783-6790.
- Zilinskas, B.A., and Greenwald, L.S.** (1986) Phycobilisome structure and function. *Photosynth Res* **10**: 7-35.
- Zouni, A., Witt, H.T., Kern, J., Fromme, P., Krauss, N., Saenger, W., and Orth, P.** (2001) Crystal structure of photosystem II from *Synechococcus elongatus* at 3.8 Å resolution. *Nature* **409**: 739-743.

---

## Appendix

DNA sequences of the synthetic genes used in this study:

>*ΦhemO\_optimizer* (EBK 42634 from GOS scaffold JCVI\_SCAF\_1101668336406: sequence adapted for the *E.coli* codon usage using the OPTIMIZER webtool)

```
ATGGACAACGAAAAAAAAATACAAAATCACCGAACTGACCTGGGAATACCACAAAAC
GCGGAACGTCAGGACTTCGTTAAAATCCTGCTGTCTGGTCAAATCGACGAACGTCTG
TACGCGACCTACCTGTACAACCAGCTGGCGTGCTACTCTAAACTGGAAGAATACTGC
CTGGAATCTTCTCTGTTTCATGGACACCAAAAACCTGCCGCGTGCGCCGCACATCCAC
TACGACTACACCCACCTGTGGACCGACATCGGTTCTCCGCCGGAAGTACCGAATCT
ACCAAAGCGTACGTTGAACACCTGGACACCATCCGTGGTCAAACGAAAACGAAACTGTAC
GCGCACGTTTACGTTTCGTCACCTGGGTGACCTGTCTGGTGGTCAAGATGATCATGCGT
AAAACCCCGGGTCCGAACCGTACTACATCTTCAAACACAAAGAAGTTAAAGAATACA
AACGTATCGTTAAAGAACGTGTTGAATCTTACCTGAACCTGTACGAAGTTAACGTTCT
GCCGGAAGCGATCTTCTGCTTCGAATCTGCGACCAAACCTGTTCAAAGAAATGTACGA
CCTGGGTAAAACCTACTAA
```

>*ΦpcyX* native sequence (EBK 42635 from GOS scaffold JCVI\_SCAF\_1101668336406)

```
ATGATTTGGGAAAGACTTATTAAGTGGAAAGATGAGACTATTGAAGTCTTAAACAATA
ATCTGGTTGAATACAATGAACCAGGTATGGAAAGATTCAATAATGAAAAGTTAGGTTG
GGTCAATAGAACCTGGAATAACAGATATATTAGAAGAGCTCATCTTGACGTAGTTGAT
GTTAGAGAATCTAAAGGTCTTTGGATGGCTCATCTATGTTTATTTCTATGTTGACAAA
TGGTGGACCGATTTACGGTTTTGATATTATTGCAGGTGAAAAAAGGTCACAGGCGC
CTTTCACGATTTTAGTCCTTTATTACAAAAGACCACCCATTAACAAAATGGTTCATAG
AAGAAAACAAGTGGTTTAAACCGAGTAAAGAGAGAGAGTTACCAGAGTGGGCAAAGG
CTATCTTTTCGGGAGGTATGATAGCCGCTGGTAACGTTAGAGAAGAAGACGAATTA
ATAAATCTGTACAATGGCAGTATCTAATTTAATAATTACATTGACAAGATAAGAAAT
CACGAAGGCGAGGCTGAAATGGCAGACGTAATTAAGGCACAAAATTACTACTCTGAA
CATCAACAAAAGAATCCTCACACGCCTAGAGTTATGCAATCACTTGGTTTGCCTGAAG
AGGATATCAAATTATTCTGCTCGGACAACCTATTTCCATTTGTTTCAGAAAACCAACC
TACTTGAAATAA
```

>*ΦpcyX\_optimizer* (*ΦpcyX* sequence adapted with the OPTIMIZER web tool for the *E.coli* codon usage)

```
ATGATCTGGGAACGTCTGATCAAATGGAAAGACGAAACCATCGAAGTTCTGAACAAC
AACCTGGTTGAATACAACGAACCGGGTATGGAACGTTTCAACAACGAAAACGTTGGT
TGGGTTAACCGTACCTGGAACAACCGTTACATCCGTGCGCACCTGGACGTTGTT
```

---

GACGTTTCGTGAATCTAAAGGTCTGTGGATGGCGCACCTGTGCCTGTTCCCGATGCTG  
ACCAACGGTGGTCCGATCTACGGTTTCGACATCATCGCGGGTGAAAAAAGTTACC  
GGTGC GTTCCACGACTTCTCTCCGCTGCTGCAGAAAGACCACCCGCTGACCAAATG  
GTTTCATCGAAGAAAACAAATGGTTCAAACCGTCTAAAGAACGTGAACTGCCGGAATG  
GGCGAAAGCGATCTTCTCTGGTGGTATGATCGCGGGGTAACGTTTCGTGAAGAAG  
ACGAACTGAACAAAATCTGCACCATGGCGGTTTCTAACCTGAACAACTACATCGACA  
AAATCCGTAACCACGAAGGTGAAGCGGAAATGGCGGACGTTATCAAAGCGCAGAAC  
TACTACTCTGAACACCAGCAGAAAAACCCGCACACCCCGCGTGTTATGCAGTCTCTG  
GGTCTGCCGGAAGAAGACATCAAATGTTCTGCTCTGACAACTGTTCCCGTTCGTT  
TCTGAAAACCAGCCGTACCTGAAATAA

>*pcyA\_Brady* (*PcyA* from *Bradyrhizobium* sp. ORS278)

ATGAGTGATGGGGACGACGGCGACGACTTGATCTGCGATCTGCAGCACGCGGCCG  
AAGACTTCGCGGCGGATTTGCGCGCCGTGCCGGCGCTGGAGCGCGTACGCGTACC  
CGATTTCCACGCTGCCGCGATCGCCGAGGGCACACTGCAGAAGGAGATCACCTGGC  
GCAACGACGTCTTCGTGCGCGGCCGCTTCCGCCACGCGCATGTGAGTCGTTCTCG  
ATCGGCGAGCAGATCGGCGTTCGTTTCATGTCTGCATCTTTCCGCATTTTCGACCGCGC  
GGCGCCGATTTTCGGCTTCGACATCATCGCCGGCCGCAAGAAGGCGACCGGTGCCT  
TTCTCGACCTGTCGCCAACGACTATGGCAGCGAACGCGATCATCGACGGCTGGTCC  
GAGGCGAGCGCTGCCCAAAGAGCAAATTTTCAGAGAGACGCGCATCCTGCCGGCCTG  
GGCGGCGTCGATTTTCTCGCGCAGCGCGCTCGCCATCCGCCCGGCATCCAGGCAC  
GAGGTCGCCAGCGTCGTGCGGCTCGGGCGTTCCGCTTTGGCGTACTATCTCGACGC  
GCACCTTGCACGGCGGCCGAGGCCGAGATGCAGGTCGCCCAGCGCAAATACATC  
GAGGCTCAGCGCAGCAATGAGCATACTGTTCCGGATGCTCGCCGGATGCGTCGGAGT  
CGATCTCGCCCGCGATTTTCATCGACGGCTGGCTCTTCCCGGCGCCGCCATCGCCTG  
GCGAAAGTCGCAGCGACGCTGCCGCCCGCGGCGCGCTCGCGCATGTGATTGA

>*pcyX\_actino* (*pcyX* from the uncultured actinobacterium SCGC AAA041-L13 obtained by single cell genomics)

ATGAATAGTGTGTGGGATAGTTTAATTCAGCTAGAACTTTCTTTGAAACAGCATTAA  
CGCATCCGGTACACTGATTAATGATCCTTCAATGGATCGATTTAATCAGCCCGGATG  
GGTTAATTTAGTATGGACAGGACAAAACACTACCGAAGAGCCCACATTGATGTCGTCGA  
TGCAAGACATTCAAAGGACTATGGATGATGCACTGCTGTATTTTCCCCATACTCAT  
AATCCTGCTCCAATTTTTGGATTTGATGTCATTGCTGGAAAGAGTAAAATTACTGGTT  
GTTTCTACGACTATAGTCCAGCAGGCGACGTTGAACATCCTATGCTAGATTGGTTTTTC  
CAGTGAAGCCGCTAAGTTGCAATGGAATAAACACGAAAACACTACCAGAATGGGCTGA  
ACGTATATTCAGCAGTAGTATGATCGCAGCCAGTAATGTAAGTAAACCAGAAGAAGTT

---

GAGCAAATTCTATCAATTGCAAAAAAAGGAATAGATCAATATCTAGTAGCAGTCGGCG  
AAACTAATAAACAGCTATCAGCACTGCCCATGAGCAAATTTCTATTGCGAGAATCA  
AAAATTAATCCCCATACACCTAAAGTAATGACCAGTTTGGGATTGAGTGAAGCTGAC  
GTGACTGCATTTATTCAAGAATGTTTGTTCAGAAATTAAGTAA

---

## Danksagung

Mein besonderer Dank gilt meiner Doktormutter Prof. Dr. Nicole Frankenberg-Dinkel für die Vergabe des interessanten Themas und für die Möglichkeit meine Doktorarbeit in ihrer Arbeitsgruppe anzufertigen. Ich danke ihr für die tolle Unterstützung und die stete Bereitschaft zur Diskussion.

Bei Prof. Dr. Johannes Herrmann bedanke ich mich für die Übernahme des Korreferats. Weiterhin danke ich Prof. Dr. Ekkehard Neuhaus für die Bereiterklärung den Vorsitz der Promotionskommission zu übernehmen.

Mein Dank gilt Prof. Dr. Oded Béjà vom Technion Israel Institute of Technology für die Kooperation im Rahmen unseres GIF-Projektes und für die Bereitstellung der Sequenzen und der synthetischen Gene.

Ebenso bedanke ich mich bei Prof. Eckhard Hoffmann und Johannes Sommerkamp von der Ruhr-Universität Bochum für die Zusammenarbeit bezüglich der Röntgenstrukturanalyse.

Weiterhin danke ich Prof. Dr. Antonio Pierik und Dominique Bechtel von der TU Kaiserslautern für die Hilfe bei den EPR-Messungen.

Außerdem möchte ich mich bei Prof. Dr. J. Clark Lagarias von der UC Davis für die Bereitstellung des KflaHY2-Konstrukts bedanken.

Den neuen und alten FKBlern danke ich für die tolle Zeit im Labor. Dank euch hat es sich meistens nicht nach Arbeit angefühlt. Vielen Dank den Bochumern Krissy, Sabrina, Julia, Basti und Co., dass ihr mich so gut in die FKB-Familie aufgenommen habt. Spezieller Dank geht an meinen Zimmergenossen Marco, mit dem ich stets eine gute Zeit auf Konferenzen hatte. Des Weiteren möchte ich mich bei meinen Laborkollegen Kerstin, Natascha, Anne, Lo und meiner ehemaligen Masterstudentin Meike für die gute Arbeitsatmosphäre bedanken.

Den größten Dank möchte ich an meine Familie richten, ohne die mein Studium und diese Arbeit nicht möglich gewesen wären. Danke Mama, Papa, Alisa und Oma! Herzlichster Dank gilt meiner Freundin Martina für ihre fortwährende Hilfe und Unterstützung.

---

# Curriculum Vitae

## PERSÖNLICHE DATEN

---

**Name** Benjamin Ledermann

## UNIVERSITÄTS- & SCHULAUSSBILDUNG

---

<b>Seit 04/2015</b>	<b>Doktorand in der Arbeitsgruppe „Mikrobiologie“ von Prof. Dr. Frankenberg-Dinkel an der TU Kaiserslautern</b>
02/2014 – 03/2015	Doktorand in der Arbeitsgruppe „Physiologie der Mikroorganismen“ von Prof. Dr. Frankenberg-Dinkel an der Ruhr-Universität Bochum
11/2012 - 10/2013	Masterarbeit am Fraunhofer-Institut für Angewandte Polymerforschung Potsdam
04/2011 – 10/2013	Masterstudium der Biochemie an der Heinrich Heine Universität Düsseldorf Abschluss: Master of Science
11/2010 – 03/2011	Bachelorarbeit am Institut für Toxikologie des Helmholtz Zentrum München
04/2007– 03/2011	Studium der Biologischen Chemie an der Hochschule Mannheim Abschluss: Bachelor of Science
10/2005 – 03/2007	Chemiestudium an der Universität Karlsruhe

---

---

## PUBLIKATIONEN

**Ledermann, B., Beja, O., and Frankenberg-Dinkel, N.** (2016) New biosynthetic pathway for pink pigments from uncultured oceanic viruses. *Environ Microbiol* **18**: 4337-4347.

**Ledermann, B., Schwan, M., Sommerkamp, J.A., Hofmann, E., Beja, O., and Frankenberg-Dinkel, N.** (2017) Evolution and molecular mechanism of four-electron reducing ferredoxin-dependent bilin reductases from oceanic phages. *FEBS J.*

---

# Eidesstattliche Erklärung

Ich erkläre hiermit an Eides statt, dass ich die vorliegende Dissertation selbstständig und ohne Benutzung anderer als der angegebenen Hilfsmittel angefertigt habe. Die aus fremden Quellen übernommenen Gedanken sind ausnahmslos als solche kenntlich gemacht. Die Promotionsordnung des Fachbereichs Biologie der TU Kaiserslautern ist mir in der derzeit gültigen Fassung bekannt. Die Ergebnisse anderer Mitarbeiter sowie anderer Autoren wurden klar gekennzeichnet. Die Dissertation oder Teile daraus wurden in keinem anderen Fachbereich oder keiner anderen Fakultät als Prüfungsarbeit eingereicht. Ich habe zu keinem früheren Zeitpunkt an einer anderen Universität ein Promotionsverfahren beantragt.

Kaiserslautern, 15.12.2017

Benjamin Ledermann